IntechOpen

State of the Art in Nano-bioimaging

Edited by Morteza Sasani Ghamsari

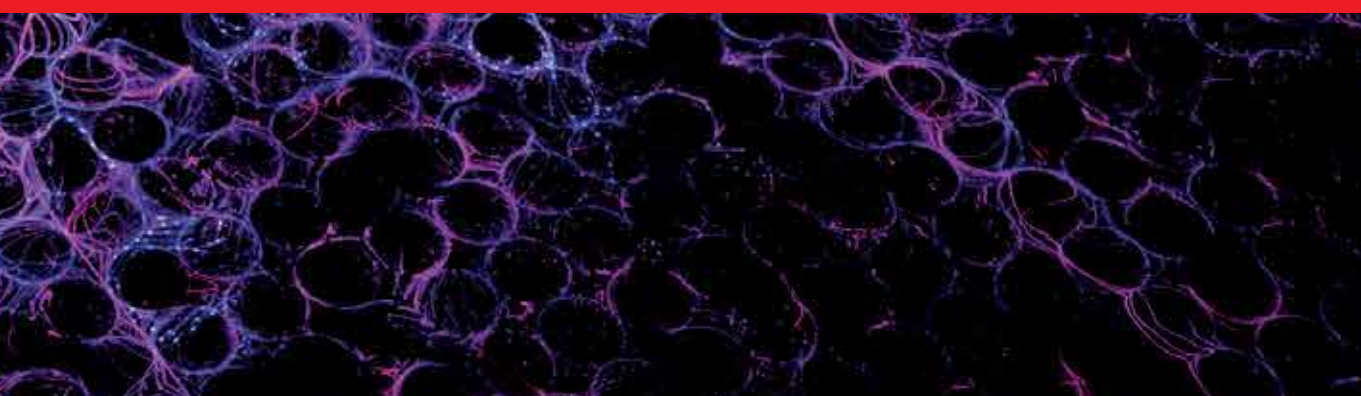

STATE OF THE ART IN NANO-BIOIMAGING

Edited by **Morteza Sasani Ghamsari**

State of the Art in Nano-bioimaging
http://dx.doi.org/10.5772/intechopen.70076
Edited by Morteza Sasani Ghamsari

Contributors

Mariadoss Asha Jhonsi, Lulu Wang, Eun-Kyung Lim, Jae-Woo Lim, Seong Uk Son, Anielle Silva, Lucas Ian Veloso Correia, Mariana Alves Pereira Zóia, Fernanda Van Petten Vasconcelos Azevedo, Marcelo Silva, Veridiana De Melo Ávila, Luiz Ricardo Goulart, Noelio Oliveira Dantas, Jéssica Peixoto Rodrigues, Yi Liu, Morteza Sasani Ghamsari

Notice

First published in London, United Kingdom, 2018 by IntechOpen
eBook (PDF) Published by IntechOpen, 2019
IntechOpen is the global imprint of INTECHOPEN LIMITED, registered in England and Wales, registration number: 11086078, The Shard, 25th floor, 32 London Bridge Street
London, SE19SG – United Kingdom
Printed in Croatia

British Library Cataloguing-in-Publication Data
A catalogue record for this book is available from the British Library

Additional hard and PDF copies can be obtained from orders@intechopen.com

State of the Art in Nano-bioimaging
Edited by Morteza Sasani Ghamsari

p. cm.

Print ISBN 978-1-78923-294-3

Online ISBN 978-1-78923-295-0

eBook (PDF) ISBN 978-1-83881-453-3

Meet the editor

Dr. Morteza Sasani Ghamsari is a senior researcher in the Photonics and Quantum Technologies Research School of Iranian Nuclear Science and Technology Research Institute. He has respectively received his BSc and MSc degrees from Sharif University of Technology of Iran and his PhD degree from the National University of Malaysia (UKM). His research focused on the preparation and characterization of solid-state laser crystals, scintillators, and nonlinear optical materials. His recent interests lie also on nanophotonics including metamaterials, quantum dots, plasmonic nanomaterials, and photonic nanodevices. He is an editorial board member and a reviewer of different international journals and has collaborated with some local and international academics/researchers on graduation of postgraduate students and research projects. He edited 2 books and published 3 chapters in books and over 85 articles in scientific journals as well as in reviewed conference proceedings.

Contents

Preface

As a unique platform, this book provides a perspective on the current status of bioimaging technology, furthering the evolution of nano-bioimaging. The chapters in this book are provided by experts who reviewed the recent developments in the nano-bioimaging technology and its application.

The book starts with a general introduction, presenting basic information on the nano-bioimaging technology. The following chapters discuss the technological aspects of nano-bioimaging and its applications, as well as the recent progress in employment of nanomaterials. Also covered is the recent development in the application of bioimaging for multidisciplinary research and among various professions, including computed tomography, cancer detection, and clinical medicine.

The first chapter in the book is an Introductory Chapter. In the second chapter, diverse research on nanomaterial-based optical imaging for effective cancer therapy is introduced. In the third chapter, we look at the unique properties of carbon quantum dots, their synthesis, material as well as optical characterizations, origin of fluorescence nature, and applications of carbon quantum dots in bioimaging. In the fourth chapter, the recently developed electromagnetic tomography (EMT) is reviewed. As a promising diagnostic tool for lung cancer and biosensing techniques for early-stage lung cancer detection, the electromagnetic tomography technique has been proposed. In addition, developing label-free and cost-effective biosensors for target tumor marker detection has attracted attentions worldwide. The research status of low-dose technology from the following aspects low-dose scan implementation, reconstruction methods, and image processing methods is introduced in the fifth chapter. Furthermore, other technologies related to the development tendency of computed tomography (CT), such as automatic tube current modulation technology, rapid peak kilovoltage (kVp) switching technology, and dual source CT technology, are also summarized. Finally, the future research prospects are discussed and analyzed. In the final chapter, the advantages of magic-sized quantum dots (MSQDs) as luminescent markers and probes to bioimage applications are demonstrated. In addition, the visualization of magic-sized quantum dots (MSQDs) bioconjugated with biological probes in cells was performed.

Morteza Sasani Ghamsari
Photonics and Quantum Technologies Research School
NSTRI, Tehran, Iran

Chapter 1

Introductory Chapter: Nano-bioimaging—Past, Present, and Future

Morteza Sasani Ghamsari

Additional information is available at the end of the chapter

http://dx.doi.org/10.5772/intechopen.74959

1. Introduction

From the 1960s to the present, the image processing technology was dramatically improved, and an enormous growth rate in the use of image processing technology can be seen today in almost every field. It is a computer vision technology with the ability to replace the human vision by an artificial vision for observation of objects and processes. Historically, the potential of image processing for biological applications has been understood by researchers in later years of the 1980s and in the early 1990s, and many attempts have been made to focus on conducting research for the employment of this technique in biological imaging [1]. For instance, the milestones of optical imaging in autophagy research are shown in **Figure 1**. As it has been reported by Wang et al. [2], these events involve specific fluorescence probing methods that localize the selected autophagic components and optical imaging platforms. They confirmed that most of the new investigative methods and advanced imaging equipment were developed during the past decade, during which some super-resolution optical imaging technologies have emerged.

Biological imaging or bioimaging is a precision technique for the recording of information relevant to biological materials using a variety of imaging equipments and processings. Usually, it is defined as a visualization method in which a biological process can be recognized non-invasively or to record the information from the biological specimen. Bioimaging aims to interfere as little as possible with life processes. Moreover, it is often used to gain information on the 3D structure of the observed specimen from the outside, i.e., without physical interference. In addition, the subcellular structures and the entire cells over tissues up to the entire multicellular organisms can be observed using bioimaging. Also, in cell biology, the cellular process or the ion or metabolite levels can be evaluated by bioimaging. Over three decades various biological imaging techniques such as X-ray, thermal imaging, X-ray computed

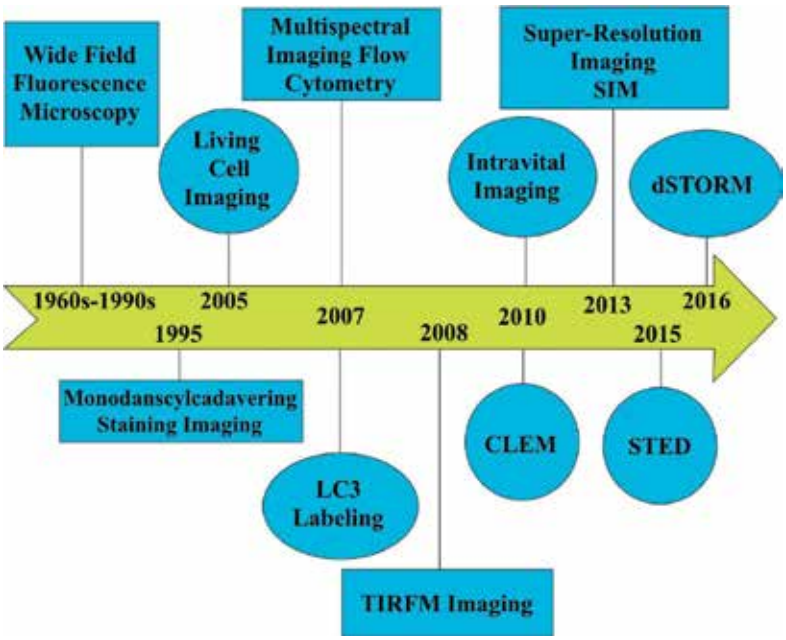

Figure 1. Milestones of optical imaging in autophagy research. All abbreviations are as follows: CLEM, correlated light and electron microscopy; dSTORM, direct stochastic optical reconstruction microscopy; LC3, light chain 3; LSCM, laser scanning confocal microscopy; SIM, structured illumination microscope; STED, stimulated emission depletion microscopy; TIRFM, total internal reflection fluorescence microscopy [2].

tomography (CT), hyperspectral imaging, optical, and magnetic resonance imaging (MRI) have been developed that are different in principles and equipment [3]. Due to their wide application potential in various fields, these techniques have continuously seen the rapid growths and the tremendous improvements. To carry out bioimaging, a setup of equipment is needed. Each kind of imaging requires different equipments, but the basic components in any imaging system are essentially the same. Usually, the following basic components such as a camera, illumination, frame grabber, and image processing hardware and software are used in a biological imaging system [1]. In bioimaging process, the image of the biological object is primary captured by a camera, and its external characteristics, such as color, shape, size, and surface texture, are evaluated using a sensor including a charge-coupled device (CCD) camera, X-ray, X-ray CT, ultrasound, and MRI. CCD camera is the most commonly used sensor for this purpose. After that, the conversion process named as digitization is used to convert the analog video signal from the camera into a digital signal. The conversion of pictorial images into digital form is performed by the frame grabber (or digitizer). Following that, digital image must be processed by the image processing hardware and software to analyze the captured images and obtain the necessary output. There are several steps including image acquisition, image preprocessing, enhancement, segmentation, representation, and description that need to be performed for image processing [1]. In each step, a process is performed. For example, the process of acquiring the raw binary data from the image of the area of interest is achieved by image acquisition, and the reduction of the unwanted features

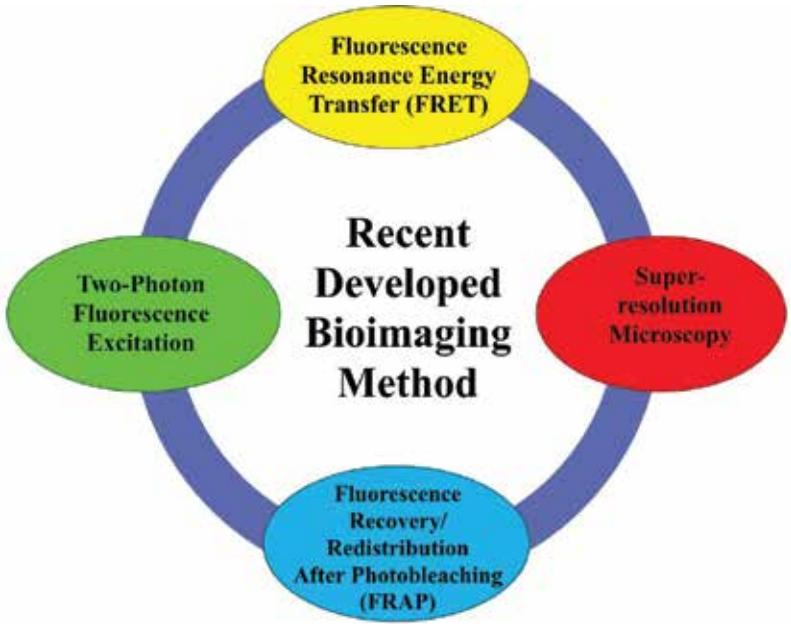

Figure 2. Recently developed techniques for bioimaging.

in the images is followed by the image processing. Over three decades, many developments have been achieved in equipments and image processing steps. As can be seen in **Figure 2**, recent progresses in bioimaging include super-resolution, two-photon fluorescence excitation microscopy, fluorescence recovery/redistribution after photobleaching (FRAP), and fluorescence resonance energy transfer (FRET).

2. Nano-bioimaging

As it is mentioned above, considerable advancements have been achieved in bioimaging. Nevertheless, the limitation of image resolution is a barrier that needs to circumvent for the next generation of bioimaging technology. Recently, the super-resolution microscopy was purposed for image resolution betterment [4]. It is found that the super-resolution microscopy can address some of the difficulties inherent in earlier microscopy techniques, provide new advances in biomedicine, and in those fields deal with the study of biological systems [4, 5]. However, it is suffering from the special equipment requirement which makes it as complex as it needs to be and hard to operate [6]. On the other hand, biologists believe that only a single type of technique cannot be used to obtain all information about a biological system [7]. Hauser et al. [8] found that the integration of two or more microscopy techniques performed on the same sample has been highly successful in overcoming the aforementioned limits of each method. They demonstrate how a correlative approach adds new dimensions of information and provides new opportunities in the fast-growing field of super-resolution microscopy. Additionally, other super-resolution microscopy methods such as structured

illumination microscopy (SIM) were developed for resolution enhancement. Despite their great success, all of these techniques are intrinsically involving with their limitations and challenges. For example, an expensive hardware and an expensive software are needed to overcome the spatial resolution improvement of SIM providing excellent super-resolution in 2D or 3D [9]. Ponsetto et al. explained that all of these methods have trade-offs between several factors such as resolution, speed, field of view, biocompatibility, sensitivity, and experimental complexity [10]. So et al. [11] compared the advancements of the widely used fluorescence microscopic techniques, stochastic optical reconstruction microscopy (STORM) or photoactivated localization microscopy (PALM), stimulated emission depletion (STED), and SIM. They explained that the label-free optical microscopic techniques whose functions are originated from nanoscale structures such as micro-curvilinear lens, super-oscillatory, and metamaterials can provide the conventional microscopy procedure with the ability for the new generation of nanoscopy. These approaches can break the barrier of diffraction limit, which is literally not a limit any more [11].

It is expected that the barrier of high-resolution image construction can be solved by nanotechnology. It seems that nanotechnology is able to advance medical imaging to the next level by increasing the resolution of current techniques [12]. This approach enhances the specificity of targeted imaging using the unique designed nanoconstructs. The increasing role of nanomaterials in biological and medical imaging research can reflect the impact of nanotechnology in bioimaging. As it has been mentioned, the contrast improvement of image is the most important reason for nanoparticle combination with imaging [13]. Usually, to utilize the enhancement of image contrast, contrast agents are needed. Traditionally, small-molecule contrast agents are used and biocompatible nanocrystals with the ability to provide a strong imaging signal. Also, plasmonic nanostructures can exhibit the field confinement effect which is locally amplified within subdiffraction-limited volume and is useful in many biomedical sensing and imaging applications [14]. Willets et al. reviewed the vital role of plasmonic nanoparticles in improvement of super-resolution imaging and described the growing partnership between super-resolution imaging and plasmonics, by describing the various ways in which the two topics mutually benefit one another to enhance our understanding of the nanoscale world [15]. They demonstrated that the plasmonic nanoparticles are explored as image contrast agents for super-localization and super-resolution imaging, offering benefits such as high photostability, large signal-to-noise ratio, and distance-dependent spectral features but presenting challenges for localizing individual nanoparticles within a diffraction-limited spot. In addition, they found that the subdiffraction-limited spatial resolution can be achieved by using the plasmon-tailored excitation fields [15]. Their study confirms that the localized surface plasmons and the surface plasmon polaritons can be used to create confined excitation volumes or image magnification to enhance spatial resolution. As powerful analytical tools, luminescent bioprobes are another example of the nanomaterial employment for optical imaging [16]. Shewring et al. described an Ir(III)-based small-molecule, multimodal probe for use in both light and electron microscopies [17]. Their finding confirmed the use of Ir(III) complexes as probes that provide excellent image contrast and quality for both luminescence and electron microscopy imagings. All of these correlative techniques are categorized in

http://dx.doi.org/10.5772/intechopen.74959

nano-bioimaging. Nanotechnology can also be used in other imaging techniques. For instance, Goel et al. reported that the hybridization of the dynamic synergism of positron emission tomography (PET) and nanotechnology can enhance the sensitivity and quantitative nature of PET which can help overcome certain key challenges in the field [18]. Fluorescence bioimaging in the second near-infrared spectral region (NIR-II, 1000–1700 nm) can be considered as attractive nanoparticles in nano-bioimaging. It can provide advantages of high spatial resolution and large penetration depth, due to low light scattering [18]. Their finding illustrates that NIR-II quantum dots (QDs) can be used in biomedical and clinical applications due to their excellent biocompatibility, photostability and brightness which require deep tissue imaging [19].

Lanthanide-doped upconversion nanoparticles (UCNPs) are the interesting nanomaterials with a great potential for nano-bioimaging applications [20, 21]. Their exceptional optical and physicochemical properties made them to be considered for design of the novel UCNP-based nanoplatform for luminescent and whole-body imaging [22]. Generalova et al. [22] demonstrated applications of UCNPs as a new nanoplatform for optical and multimodal cancer imaging in vitro and in vivo and extend discussions to delivery of UCNP-based therapeutic agents for photodynamic and photothermal cancer treatments. Similar to other semiconductor nanocrystals such as CdS, ZnO, TiO_2, and CdSe/ZnS core shells, lanthanide-doped upconversion nanoparticles can be used for magnetic resonance imaging (MRI), computed tomography (CT), and positron emission tomography (PET)/single photon emission computed tomography (SPECT) [23–25]. **Figure 3** shows the schematic applications of semiconductor nanocrystals in bioimaging. As it is mentioned by Chen et al. [26, 27], semiconductor polymer dots (SPDs) can also be utilized in biological imaging because of their outstanding photophysical properties, such as high brightness, extraordinary photostability, and favorable biocompatibility, in comparison with those of quantum dots (QDs), organic dyes, and reversibly switchable fluorescent proteins (RSFPs).

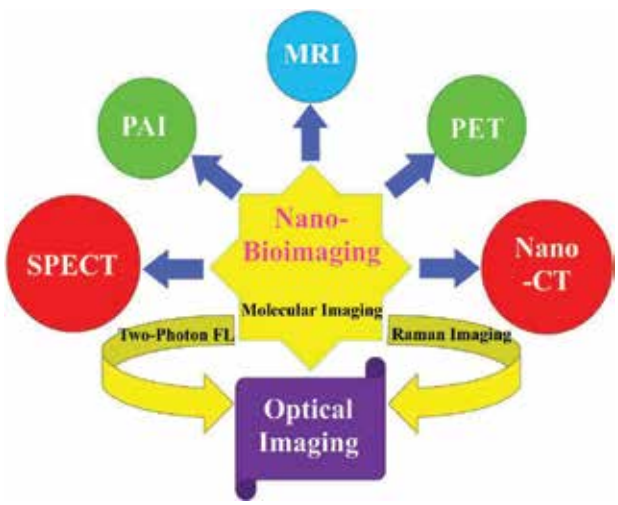

Figure 3. Schematic illustration of semiconductor nanocrystal applications in bioimaging.

3. Graphene-based materials for nano-bioimaging

Among all nanomaterials that are considered as potential candidates for nano-bioimaging applications, graphene has attracted great attentions. As it has been expressed by Lin et al. [28], the biomedical applications of graphene and its derivatives are extensively investigated for diagnostics, drug delivery, near-infrared (NIR) light-induced photothermal therapy, and bioimaging. Due to the versatile surface functionalization and ultrahigh surface area of graphene and its derivatives, they can be easily functionalized by small-molecule dyes, polymers, nanoparticles, drugs, or biomolecules to obtain graphene-based nanomaterials for different bioimaging applications [28]. Lin et al. [28], focused on applying graphene-based nanomaterials for different molecular imaging modalities, and their review confirmed that the graphene-based materials can be employed for optical imaging (FL, two-photon FL, and Raman imaging), PET/SPECT (positron emission tomography/single photon emission computed tomography), MRI (magnetic resonance imaging), PAI (photoacoustic imaging), CT (computed tomography), and multimodal imaging (**Figure 4**). Graphene quantum dots (GQDs) are one of the graphene-based materials that have a considerable potential for bioimaging applications. Due to the photoluminescence (PL) and high structural stability, low cytotoxicity, and good biocompatibility, fluorescent graphene quantum dots (GQDs) have

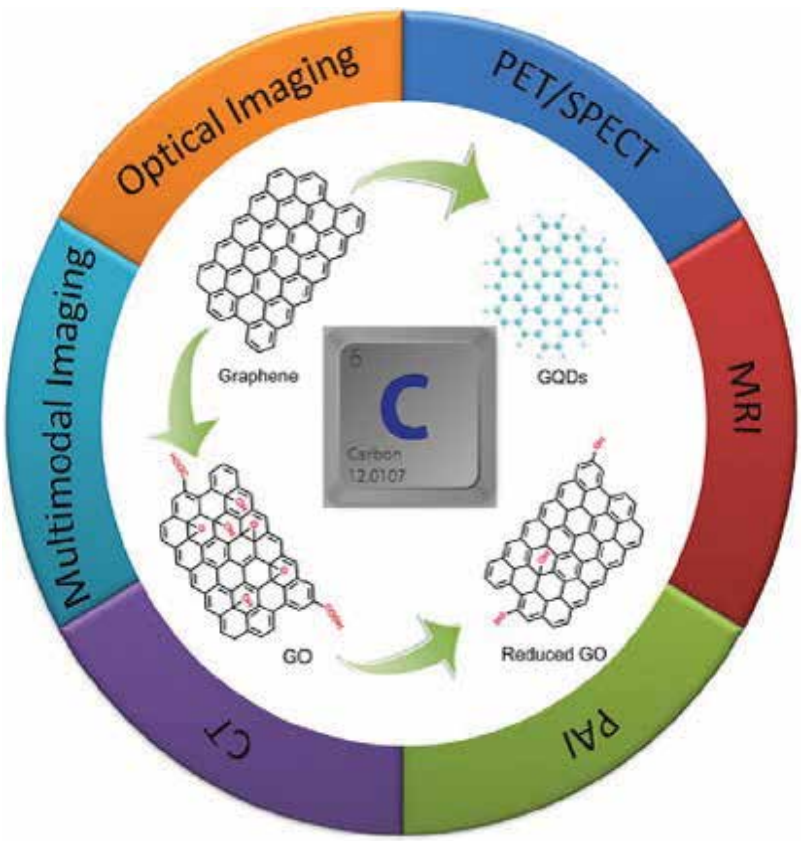

Figure 4. The biomedical applications of graphene. Adapted from Ref. [28].

recently attracted an increasing interest in cancer bioimaging [29, 30]. Chen et al. [31] evaluated the recent advances and future challenges of biomedical applications of graphene quantum dots. They expressed that the wide applications of graphene quantum dots in biological imaging can be attributed to the relatively high quantum yields with high molar extinction coefficients, broad absorption with narrow emission spectra and high photostability, the strong quantum confinement, and edge effects stir of GQDs. In addition, in comparison with a traditional imaging modality, the highly stable and bright fluorescence characters of GQD-derived nanomaterials lead to generate the optical signal with the small number of GQDs [31]. On the other hand, the ability of GQDs for near-infrared reflectance emission makes them as promising candidates for the imaging of deeper tissue samples. Based on the above reasons, applying GQDs as contrast agents for in vivo imaging has been the area of high expectations and recurring attention. The near-infrared emitting window shows great advantages for biomedical imaging because of the low tissue absorption and reduced light scattering in more than 650 nm wavelengths' region [31]. Functionalized graphene oxide (GO; 2D)-based nanocomposites are one of the graphene-based nanomaterials that have a great potential for biomedical applications. In recent years, because of their unique and highly enriched physical and chemical properties, such as excellent biocompatibility, ready cellular uptake, flexible chemical modifications, unique optical properties, and thermal and electrical conductivity, they have been used in biological fields, such as biomedicine, biosensors, drug delivery, and bioimaging [32]. Qiu et al. [33] developed the graphene oxide (GO)-wrapped gold nanorods (GO@GNRs) that can be used as a smart and robust nanoplatform for ultrafast NIR SERS bioimaging. Their finding demonstrated that the fabricated GO@GNRs could efficiently load various NIR probes, and the in vitro evaluation indicated that the nanoplatform could exhibit a higher NIR SERS activity in comparison with traditional gold nanostructures.

Author details

Morteza Sasani Ghamsari

Address all correspondence to: msghamsari@yahoo.com

Photonics and Quantum Technologies Research School, NSTRI, Tehran, Iran

References

[1] Vadivambal R, Jayas Digvir S, editors. Bio-Imaging Principles, Techniques and Applications. Boca Raton: CRC Press, Taylor & Francis Group; 2016

[2] Wang Y, Li Y, Wei F, Duan Y. Optical imaging paves the way for autophagy research. Trends in Biotechnology. 2017;**35**(12):1181-1193

[3] Bronzino JD, Peterson DR, editors. Biomedical Signals, Imaging, and Informatics. Boca Raton: CRC Press, Taylor & Francis Group; 2015

[4] Diaspro A, van Zandvoort MAMJ, editors. Super-resolution Imaging in Biomedicine. Boca Raton: CRC Press, Taylor & Francis Group; 2017

[5] Heintzmann R, Huser T. Super-resolution structured illumination microscopy. Chemical Reviews. 2017;**117**:13890-13908

[6] Peeters Y, Vandenberg W, Duwé S, Bouwens A, Lukeš T, Ruckebusch C, Lasser T, Dedecker P. Correcting for photodestruction in super-resolution optical fluctuation imaging. Scientific Reports. 2017;**7**(1):10470

[7] Hanssen E, editor. Cellular Imaging: Electron Tomography and Related Techniques. AG: Springer International Publishing; 2018

[8] Hauser M, Wojcik M, Kim D, Mahmoudi M, Li W, Xu K. Correlative super-resolution microscopy: New dimensions and new opportunities. Chemical Reviews. 2017;**117**:7428-7456

[9] Demmerle J, Innocent C, North AJ, Ball G, Müller M, Miron E, Matsuda A, Dobbie IM, Markaki Y, Schermelleh L. Strategic and practical guidelines for successful structured illumination microscopy. Nature Protocols. 2017;**12**:988-1010

[10] Ponsetto JL, Bezryadina A, Wei F, Onishi K, Shen H, Huang E, Ferrari L, Ma Q, Zou Y, Liu Z. Experimental demonstration of localized plasmonic structured illumination microscopy. ACS Nano. 2017;**11**:5344-5350

[11] So S, Kim M, Lee D, Nguyen DM, Rho J. Overcoming diffraction limit: From microscopy to nanoscopy. Applied Spectroscopy Reviews. 2017;**4**:1-23

[12] JWM B, MMJ M, editors. Design and Applications of Nanoparticles in Biomedical Imaging. Switzerland: Springer International Publishing; 2017

[13] Padmanabhan P, Kumar A, Kumar S, Kumar Chaudhary R, Gulyás B. Nanoparticles in practice for molecular-imaging applications: An overview. Acta Biomaterialia. 2016;**41**:1-16

[14] Kim K, Oh Y, Lee W, Kim D. Plasmonics-based spatially activated light microscopy for super-resolution imaging of molecular fluorescence. Optics Letters. 2010;**35**:3501-3503

[15] Willets KA, Wilson AJ, Sundaresan V, Joshi PB. Super-resolution imaging and plasmonics. Chemical Reviews. 2017;**117**(11):7538-7582

[16] Mei J, Huang Y, Tian H. Progress and trends in AIE-based bioprobes: A brief overview. ACS Applied Materials & Interfaces. 2018. DOI: 10.1021/acsami.7b14343

[17] Shewring JR, Cankut AJ, McKenzie LK, Crowston BJ, Botchway SW, Weinstein JA, Edwards E, Ward MD. Multimodal probes: Superresolution and transmission electron microscopy imaging of mitochondria, and oxygen mapping of cells, using small-molecule Ir(III) Luminescent complexes. Inorganic Chemistry. 2017;**56**(24):15259-15270

[18] Goel S, England CG, Chen F, Cai W. Positron emission tomography and nanotechnology: A dynamic duo for cancer theranostics. Advanced Drug Delivery Reviews. 2017;**113**:157-176

[19] Zebibula A, Alifu N, Xia L, Sun C, Yu X, Xue D, Liu L, Li G, Qian J. Ultrastable and biocompatible NIR-II quantum dots for functional bioimaging. Advanced Functional Materials. 2018;**1**:1703451

[20] Liu Y, Lu Y, Yang X, Zheng X, Wen S, Wang F, Vidal X, Zhao J, Liu D, Zhou Z, Ma C, Zhou J, Piper JA, Xi P, Jin D. Amplified stimulated emission in upconversion nanoparticles for super-resolution nanoscopy. Nature. 2017;**543**:229-233

[21] Reineck P, Gibson BC. Near-infrared fluorescent nanomaterials for bioimaging and sensing. Advanced Optical Materials. 2017;**5**:1600446

[22] Generalova AN, Chichkov BN, Khaydukov EV. Multicomponent nanocrystals with anti-Stokes luminescence as contrast agents for modern imaging techniques. Advances in Colloid and Interface Science. 2017;**245**:1-19

[23] Duan C, Liang L, Li L, Zhang R, Xu ZP. Recent progress in upconversion luminescence nanomaterials for biomedical applications. Journal of Materials Chemistry B. 2018;**6**:192-209

[24] Chandan HR, Schiffman JD, Balakrishna RG. Quantum dots as fluorescent probes: Synthesis, surface chemistry, energy transfer mechanisms, and applications. Sensors and Actuators B. 2018;**258**:1191-1214

[25] Martynenko IV, Litvin AP, Purcell-Milton F, Baranov AV, Fedorov AV, Gunko YK. Application of semiconductor quantum dots in bioimaging and biosensing. Journal of Materials Chemistry B. 2017;**5**:6701-6727

[26] Chen X, Li R, Liu Z, Sun K, Sun Z, Chen D, Xu G, Xi P, Wu C, Sun Y. Small photoblinking semiconductor polymer dots for fluorescence nanoscopy. Advanced Materials. 2017;**29**:1604850

[27] Chen X, Liu Z, Li R, Shan C, Zeng Z, Xue B, Yuan W, Mo C, Xi P, Wu C, Sun Y. Multicolor super-resolution fluorescence microscopy with blue and carmine small photoblinking polymer dots. ACS Nano. 2017;**11**:8084-8091

[28] Lin J, Chen X, Huang P. Graphene-based nanomaterials for bioimaging. Advanced Drug Delivery Reviews. 2016;**105**:242-254

[29] Li K, Zhao X, Wei G, Su Z. Recent advances in the cancer bioimaging with graphene quantum dots. Current Medicinal Chemistry. 2017;**24**:1-18

[30] Luo Z, Yang D, Yang C, Wu X, Hu Y, Zhang Y, Yuwen L, Yeow EKL, Weng L, Huang W, Wang L. Graphene quantum dots modified with adenine for efficient two-photon bioimaging and white light-activated antibacterial. Applied Surface Science. 2018;**434**:155-116

[31] Chen F, Gao W, Qiu X, Zhang H, Liu L, Liao P, Fu W, Luo Y. Graphene quantum dots in biomedical applications: Recent advances and future challenges. Frontiers in Laboratory Medicine. 2018. DOI: 0.1016/j.flm.2017.12.006

[32] Jang SC, Kang SM, Lee JY, Oh SY, Vilian AE, Lee I, Han YK, Park JH, Cho WS, Roh C, Huh YS. Nano-graphene oxide composite for in vivo imaging. International Journal of Nanomedicine. 2018;**13**:221-234

[33] Qiu X, You X, Chen X, Chen H, Dhinakar A, Liu S, Guo Z, Wu J, Liu Z. Development of graphene oxide-wrapped gold nanorods as robust nanoplatform for ultrafast near-infrared SERS bioimaging. International Journal of Nanomedicine. 2017;**12**:4349-4360

Chapter 2

Recent Advances in Bioimaging for Cancer Research

Jae-Woo Lim, Seong Uk Son and Eun-Kyung Lim

Additional information is available at the end of the chapter

http://dx.doi.org/10.5772/intechopen.72725

Abstract

Molecular imaging techniques as well as nanoparticle applicable to molecular imaging are being explored to improve the cancer detection accuracy, which help to manage efficiently at the early stage. Among the various imaging technologies, optical imaging is a highly sensitive detection technique that allows direct observation of specific molecular events, biological pathways, and disease processes in real time through imaging probes that emit light in a range of wavelengths. Recently, nanoparticles have provided significant progresses that can be simultaneously used for cancer diagnosis and therapy (cancer theranostics). Theranostics aims to provide "image-guided cancer therapy," by integrating therapeutic and imaging agents in a single platform. In addition, molecular imaging techniques facilitate "image-guided surgery" enabling maximization of tumor excision and minimization of side effects. The optical signals generated by fluorescence nanoparticles offer the possibility to distinguish tumor sites and normal tissues during surgery by real-time guidance, thereby increasing the long-term patient survival. These techniques will considerably contribute to reducing cancer recurrence and developing more effective cures. In this chapter, we will introduce diverse research on nanomaterials-based optical imaging for effective cancer therapy.

Keywords: molecular imaging, optical imaging, nanoprobe, cancer diagnosis, imaging-guided therapy, imaging-guided surgery

1. Introduction

Cancer is one of the leading causes of death. So many researchers have made great efforts to improve cancer management [1]. An early cancer diagnosis provides the most efficient and effective management of cancer treatment with the use of surgical methods or chemotherapeutic agents. Therefore, techniques for detecting cancer at early stages have been developed to improve the detection accuracy. Molecular imaging techniques have undergone explosive growth over the past several decades and are important tools for cancer diagnosis and prognosis

in the clinic; they include positron emission tomography (PET), computed tomography (CT), magnetic resonance (MR) imaging, and optical imaging [2–4]. Molecular imaging techniques can identify the cancer mass on the basis of its physical properties, which may have major benefits for personalized diagnosis and for the prediction and monitoring of the response to therapy. Many researchers have made efforts to develop diverse imaging probes or contrast agents, thereby enabling the visualization of cellular function and the characterization and measurement of molecular processes in living organisms at the cellular and molecular levels without perturbing them. Such tools can help obtain more accurate information about early-stage cancer using molecular imaging [4]. Among the molecular imaging tools, optical imaging, which includes fluorescence and bioluminescent imaging, can provide particularly highly sensitive detection by using the various wavelengths emitted by fluorescent nanoparticles. In the UV and visible regions, light does not deeply penetrate into tissues, because it is easily absorbed and scattered by endogenous biomolecules (e.g., water and hemoglobin), and tissues generate strong auto-fluorescence [4]. However, light in the near-infrared (NIR) region (~650–900 nm) is minimally absorbed in living tissues and can penetrate more deeply, to a depth of several centimeters, with high signal-to-noise ratios (SNRs) [2]. The development of specific, sensitive, and targeted imaging probes is required for the success of optical imaging techniques in cancer diagnosis. Recently, nanomaterial-based optical imaging probes have been used extensively to non-invasively monitor the target biomolecules or biological pathways for cancer diagnosis and therapy compared with single molecule-based imaging agents. Fluorescent proteins and organic dyes are conventionally used to label cells and subcellular targets due to their small size, good biocompatibility, and water dispersibility. However, fluorescent nanomaterials such as quantum dots (QDs), gold nanoparticles, up-conversion nanocrystals, and silicon nanoparticles have shown several distinct advantages compared to fluorescent proteins and organic dyes [5–9]. These advantages include high resistance to photobleaching (photostability) and high quantum yields (QY), thus enabling the acquisition of optimal information of biological interest with high sensitivity in both *in vitro* and *in vivo* models [9]. In addition, nanomaterials (or nanoparticles) have the advantage that they can be easily modified with different molecules and delivered to the tumor along blood vessels with

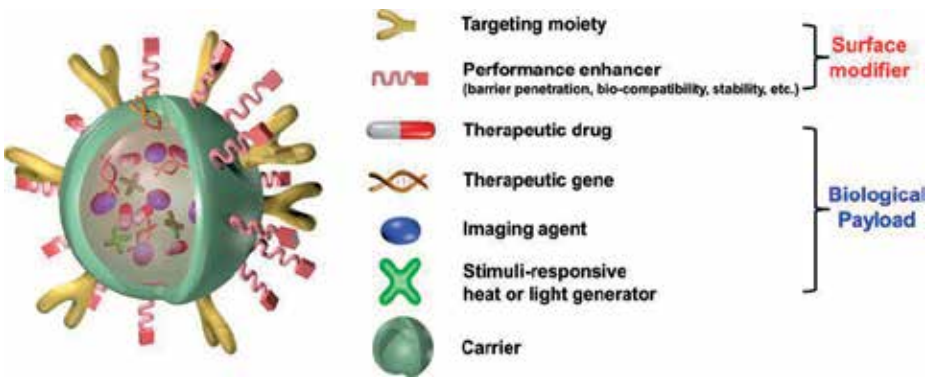

Figure 1. Schematic illustration of a multifunctional nanocomposite. Reproduced from Ref. [12] with permission of ACS Publications.

immune systems [10–13]. In this chapter, we explain the benefits of optical imaging and the importance of nanomaterial-based imaging agents for effective cancer therapy. We will focus on research on using nanomaterials as optical imaging agents and their diverse applications (**Figure 1**).

2. Passive and active targeting for cancer imaging

2.1. Passive targeting

Various nanoparticle systems are being explored for their potential use in bioimaging for cancer diagnosis or treatment because of their unique properties, including their large surface-to-volume ratio, high biocompatibility, facile surface modification, and overall structural robustness. In addition, they have unique optical, magnetic, and electron properties, which make them ideal candidates for signal generation and transduction in the development of sensing systems [5–8, 12, 14–20]. Moreover, some nano-sized materials exhibit unique physical properties, such as a proper size, surface charge, stability, shape, and hydrophilicity, which can aid their effective delivery to the desired site. The delivery of nano-sized agents is affected by the enhanced permeability and retention (EPR) effect, which is a unique property of solid tumors that is related to their anatomical and pathological differences from normal tissues. Unlike normal tissues, when tumor tissue produces neovascularization, it contains a discontinuous or absent basement membrane, making it "leaky." Therefore, the pore sizes of the blood vessels in most peripheral human tumors are hundreds of nanometers in diameter. This EPR effect leads to the passive accumulation of large molecules and small particles in tumor tissues due to the cut-off size of the leaky vasculature and retention with long circulation times, which is called passive targeting [21–26]. For successful bioimaging via passive targeting, both a size ranging from 100 to 200 nm in diameter and a prolonged circulation half-life in the blood with biocompatibility are required. Hydrophilic materials such as poly(ethylene glycol) (PEG) have been extensively investigated as effective ways to provide hydrophilic "stealth" properties, resulting in both the inhibition of plasma protein (opsonin) absorption and decreased recognition by the mononuclear phagocytic system (MPS) in the reticuloendothelial system (RES), such as the liver and spleen, thus producing longer circulation times (**Figure 2**) [27–29].

In addition, positively charged (cationic) nanoparticles can easily enhance endocytosis or phagocytosis for cell labeling via electrostatic interactions with the negatively charged cellular membrane. Among bio-imaging techniques, well-tailored superparamagnetic nanocrystals are of great interest for cancer detection via magnetic resonance (MR) imaging due to their high sensitivity and specificity due to the nanoeffect. Lim et al. [30–32] reported the successful fabrication of various types of water-soluble PEGylated magnetic complexes for magnetism-related biomedical applications and demonstrated their potential as highly efficient MRI imaging agents. Fluorescence and optical imaging techniques are important tools for *in vivo* and cellular imaging, and they can provide vital information for cancer diagnosis and therapy in its early stages. In particular, for the fluorescence wavelength, near-infrared (NIR) light is

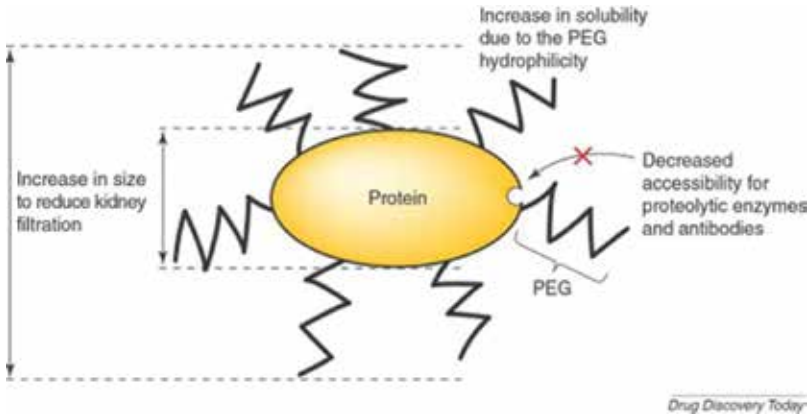

Figure 2. Main advantages of the PEGylated proteins. PEG is a shielding the protein surface from degradation agents by steric hindrance. Moreover, the increased size of the conjugate decreases the kidney clearance of the PEGylated protein. Reproduced from Ref. [27] with permission of Elsevier.

preferred for tissue and *in vivo* imaging compared to visible light because of its minimal damage to the tissue, which allows deep tissue penetration, and low auto-fluorescence interference due to the reduced scattering of long wavelength photons [9].

2.2. Active targeting

Active targeting, is also called as ligand-mediated targeting, involves utilizing targeting moieties that are anchored on the surface of nanoparticles and form strong interactions with a particular cell surface marker (e.g., EGFR, HER2/neu, transferrin, CD44) of the target cancer (**Figure 3**) [33, 34].

Targeting moieties, such as antibodies, peptides (Arg-Glyc-Asp (RGD)), nucleic acids (aptamers), and polysaccharides (hyaluronan, dextran), lead to enhanced selective delivery and uptake in the target cells, tissues, organs, or subcellular domains and minimize uptake by the RES system [34–53]. Active tumor targeting is more efficient and specific than passive targeting, and can facilitate early cancer detection. In particular, active tumor-targeted imaging can quantify the target expression through molecular imaging, so it is an indispensable tool in diagnosis and disease management. For example, for the selective detection of tumors expressing a high level of epidermal growth factor receptors (EGFR), anti-EGFR antibody-modified nanoparticles are widely used as imaging agents for MR, CT, and optical imaging. CD44 is a cell surface glycoprotein that is overexpressed in breast cancer and gastric cancer stem cells and is associated with cancer growth, migration, invasion, and angiogenesis. Hyaluronan (HA), which is an immune–neutral polysaccharide, forms a specific interaction with CD44. Lim et al. [50, 51] developed a hyaluronan-modified magnetic nanoprobe for detecting CD44-overexpressing breast cancer via MR imaging, which showed superior targeting efficiency with MR sensitivity in *in vitro* and *in vivo* studies. Angiogenesis appears to be one of the most crucial steps in tumor translation to the metastatic form, in which it is

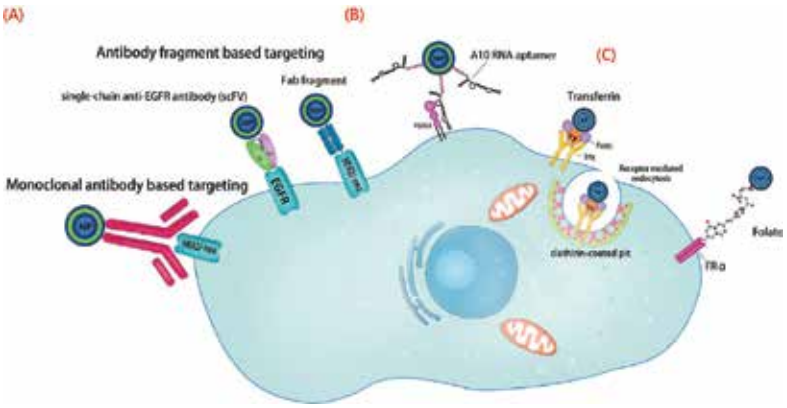

Figure 3. A schematic illustration showing methods used for active targeting of nanoparticles. (A) Antibody-based targeting, (B) Aptamer-based targeting, and (C) Ligand-based targeting of nanoparticels. Reproduced from Ref. [34] with permission of Springer.

capable of spreading to other parts of the body by degrading the basement membrane and forming a new vascular structure. During angiogenesis, a variety of proangiogenic factors is secreted by tumor cells, including vascular endothelial growth factor (VEGF), platelet-derived growth factor (PDGF), basic fibroblast growth factor (bFGF), interleukin-8 (IL-8), and integrin $\alpha_v\beta_3$. Targeted-molecular imaging of vascular or angiogenesis can provide accurate anatomic details for effective cancer management. Aptamers (Apt) are short nucleic acid molecules that can bind to target antigens with high affinity and specificity. To understand neovascularization and angiogenesis in cancer, $Apt_{\alpha v\beta 3}$-conjugated magnetic nanoparticles ($Apt_{\alpha v\beta 3}$-MNPs) have been developed to enable the precise detection of integrin-expressing cancer cells using MRI imaging. This work demonstrated that $Apt_{\alpha v\beta 3}$-MNPs have the potential to be used for accurate tumor diagnosis [52]. In addition, vascular endothelial growth factor (VEGF121)/rGel modified MRI imaging agents were developed to obtain sensitive angiogenesis imaging of orthotopic bladder tumors that showed the development of a clear neoangiogenic vascular distribution [53]. The tumor microenvironment plays a critical role in tumor initiation, progression, metastasis, and resistance to therapy [54–61]. The microenvironment differs from that of normal tissues because of the dynamic network within normal tissues, including blood and lymphatic vessels, extracellular matrix proteins, and both enzyme and immune components. These unique characteristics lead to a matrix remodeling (e.g., up-regulation of matrix proteins and activation of specific proteases), a deficiency of oxygen and other nutrients, a decreased pH (low pH), hypoxia and increased amounts of reactive oxygen species (ROS) [57]. The changes in the physiological characteristics of tumor microenvironments are consistent, regardless of the type of cancer, so it is possible to use these as a universal indicator for cancer detection. Vesicular pH plays a pivotal role in cell metabolism processes, such as proliferation and apoptosis. Choi et al. [58] developed a colorimetric redox-polyaniline nanoindicator to simply detect and quantify a broader biogenic pH range with superior sensitivity by employing one-dimensional turn-on of the FRET signal (**Figure 4**). They fabricated polyaniline-based

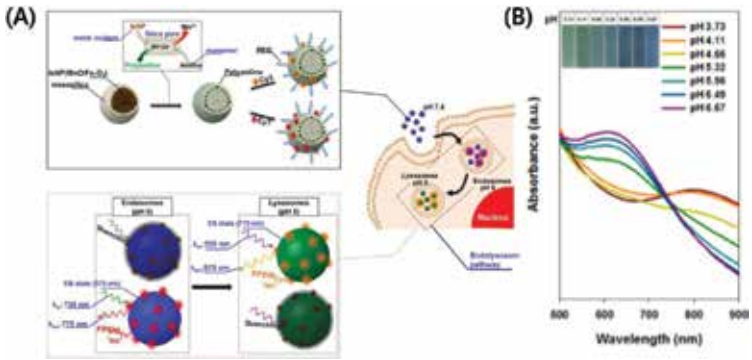

Figure 4. (A) Schematic illustration of organic nanoindicator based on polyaniline nanoparticle for the detection of endolysosomal compartments. Synthesis steps of nanoindicator based on polyaniline in mesosilica template when using heterometal nanoparticle (IsNP) as oxidant. Emission of FPSNICy7 appears at endosomes. While migrating from endosomes to lysosomes, transition state of polyaniline transferred to emeraldine salt state due to the increment of proton concentration. The emission of FPSNICy3 gradually appears at lysosomes. (B) Redox switching property and sensitivity of PSNI from pH 3.95 to 7.23. Reproduced from Ref. [58] with permission of Springer.

nanoprobes that exhibited convertible transition states according to the proton concentration as an *in situ* indicator of the vesicular transport pH [58].

The tumor pH is usually more acidic than that of normal tissues due to increased aerobic glycolysis, which is called the Warburg effect (tumor have a pH of 6.2–6.9, and normal tissues have a pH of 7.4) [62, 63]. This can promote tumor metastasis by generating an invasive environment for tearing down the extracellular matrix and for tissue remodeling. Many studies have reported signal "off–on" imaging agents activated by pH, such as fluorescence probes and MRI contrast agents that target the acidic pH conditions of tumors for tumor imaging [12, 13, 59]. Kim et al. [59] have developed a pH-responsive T1 (which is the recovery of magnetization along the longitudinal axis) contrast agent for MR imaging. Core–shell MnO@ Mn_3O_4 urchin-shaped nanoparticles are synthesized via an anisotropic etching process. The manganese ions released from the MnO phase in the low-pH sites within tumor cells lead to an enhanced T1 contrast image for the entire tumor mass. In addition, specific stromal cell-derived proteases, such as matrix metalloproteases (MMP), matrix cysteine cathepsins, and serine proteases, are overexpressed in primary tumors. These proteases induce the epithelial-to-mesenchymal transition (EMT) and promote invasion and metastasis by degrading the extracellular membrane. Molecular imaging of the activity of proteases has the potential to determine tumor malignancy, guide the development of diagnostic tools, and evaluate the efficacy of treatment (**Figure 5(A)**) [60]. MMPs are the most prominent family of proteases associated with tumorigenesis. Their expression and activity are highly enhanced in many types of human cancer and are strongly implicated in advanced cancer states. Tumor microenvironment-targeted molecular imaging has the potential to provide clinically significant progress. Emerging evidence suggests that microRNAs can also function as a diagnostic biomarker for human cancers because they can act as tumor suppressor genes or oncogenes. Imaging the intracellular distribution of specific miRNAs should provide insight into the mechanisms of metastasis and invasion. Kim et al. [61] reported smart nanoprobes,

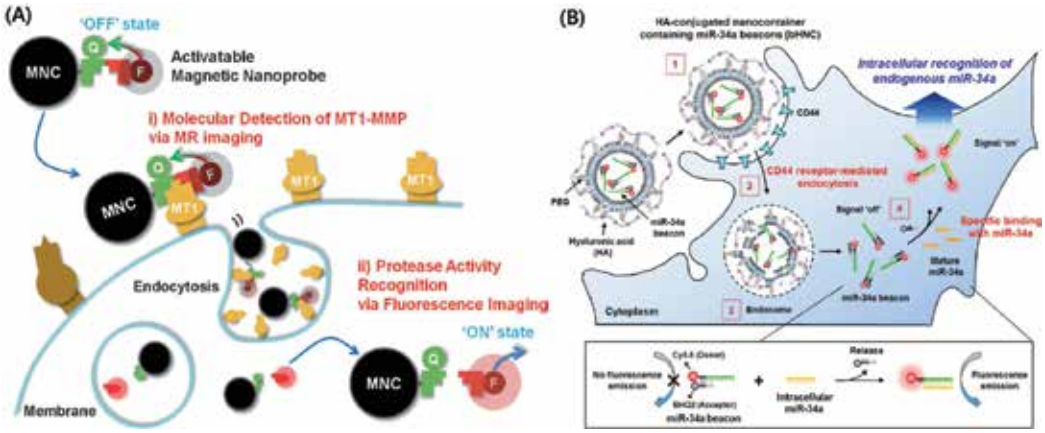

Figure 5. (A) Schematic illustration of the dual imaging process of anchored proteinase-targetable optomagentic nanoprobes with activatable fluorogenic peptides (MNC-ActFP). Reproduced from Ref. [60] with permission of Wiley-VCH. (B) Schematic illustration of miR-34a beacon delivery system for targeted intracellular recognition of miR-34a based on Hyaluronic acid (HA)-coated nanocontainers that encapsulate the miR-34a beacons (bHNCs). Reproduced from Ref. [61] with permission of ACS Publications.

i.e., hyaluronic acid (HA)-based nanocontainers containing miRNA-34a beacons (bHNCs), for the intracellular recognition of miRNA-34a levels in metastatic breast cancer cells. They confirmed the microRNA-34a expression levels through *in vitro* and *in vivo* optical imaging using bHNCs (**Figure 5(B)**) [61].

3. Multimodal imaging for cancer imaging

Current imaging techniques play an important role in enabling the early detection of several diseases, including cancer, due to their ability to locate tumors and assess the tumor activity. The characteristics of various imaging modalities are briefly summarized (**Table 1**) [7, 64]. However, these techniques are insufficient to provide reliable and accurate information at the disease site, due to their low sensitivity or limits in their spatial resolution (**Table 1**).

Computed tomography (CT) is useful for tumor staging but offers poor soft tissue contrast, with resulting poor sensitivity and specificity in screening. Magnetic resonance imaging (MRI) offers excellent contrast without ionizing radiation but has temporal and financial needs that are likely inconsistent with high-throughput screening. Positron emission tomography (PET), which has very high sensitivity, can investigate various molecular and biochemical properties but is more suitable for monitoring the response to therapy than for detecting early lesions due to its limited spatial resolution. Therefore, multimodal imaging, i.e., the integration of two or more imaging techniques in a single examination, should offer the synergistic advantages of each to provide accurate information for tumor diagnosis such as high spatial resolution, soft tissue contrast, and biological information on the molecular level with high sensitivity [46, 65–73]. Recently, various types of hybrid nanoparticles have

been used for multimodal imaging by combining the strengths of individual components into single nano-structured systems. Multimodal imaging probes enable both magnetic and optical imaging to provide great benefits for *in vivo* disease diagnosis and the *in situ* monitoring of living cells. In addition, it is reported that MR/CT multimodal nanoprobes can provide complementary information for tumor-associated blood vessels and the tumor microenvironment [71]. Uniformly sized tantalum oxide nanoparticles were synthesized using a microemulsion method and were modified using various silane derivatives, such as polyethylene glycol (PEG) and fluorescent dye molecules, through simple *in situ* sol-gel reaction. These nanoparticles exhibited remarkable performances in *in vivo* simultaneous fluorescence imaging as well as X-ray CT angiography and bimodal image-guided lymph node mapping [72].

Lim et al. [73] developed fluorescent magnetic nanoprobes to acquire biological information at different object levels, i.e., *in vivo* detection and *ex vivo* validation, for characterizing tumor angiogenesis, in which magnetic nanocrystals are encapsulated by the fluorescent amphiphilic polymer (**Figure 6**). Additionally, targeted multimodal imaging systems by modifying targeting moieties to increase the selective accumulation at the disease site has shown promising results. In this case, several factors should be considered, including the appropriate choice of a targeting moiety and its conjugation method. Yang et al. [49] developed

Modality	Energy source	Depth	Temporal resolution	Advantage	Disadvantage
Optical imaging	Visible light or near-infrared	<1 cm	Seconds to minutes	Noninvasiveness, no harmful effect by nonionizing radiation	Relatively low spatial resolution
MR imaging	Radiofrequency magnetic field	No limit	Minutes to hours	Noninvasiveness, high spatial resolution	Relative low sensitivity, long scan and post-processing time, mass quantity of probe may be needed
PET imaging	High-energy γ rays	No limit	10 s to minutes	Noninvasiveness, high sensitivity	Exposure to ionizing radiation, relatively low spatial resolution
Ultrasound imaging	High-frequency sound	mm to cm	Second to minutes	Noninvasiveness, real time, low cost, no harmful effects by nonionizing radiation	Limited spatial resolution, unsuitable for examination of digestive organs and bone
CT imaging	X-ray	No limit	Minutes	Noninvasiveness, high contrast resolution	Relatively high dose of ionizing radiation, limited soft tissue resolution, exposure to ionizing radiation

Reproduced from Ref. [12] with permission of ACS Publications.

Table 1. Characteristics of imaging modalities.

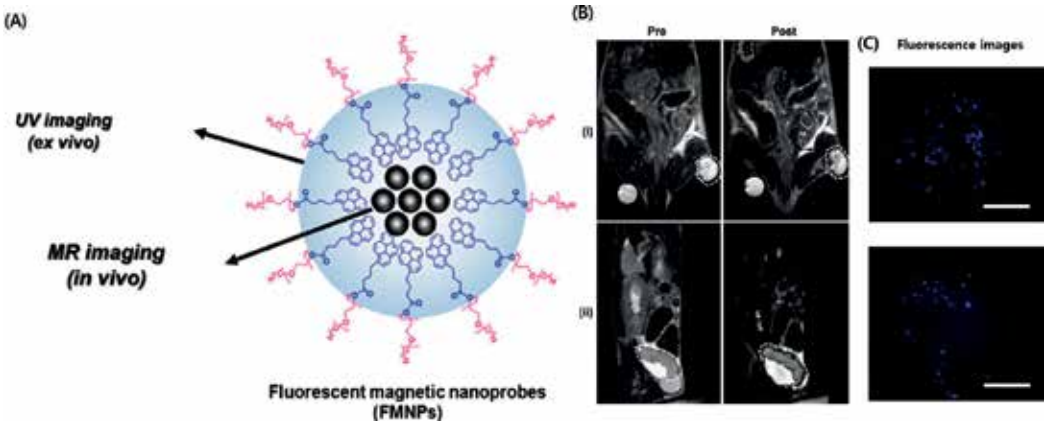

Figure 6. (A) Illustration of simultaneously self-assembled fluorescent magnetic nanoprobes (FMNPs) as multimodal biomedical imaging probes. (B) MR images of tumor-bearing mice after injection of the FMNPs (i: xenograft tumor model and ii: orthotopic bladder tumor model) and (C) fluorescence images of their excised tumor slides, respectively. Reproduced from Ref. [73] with permission of Elsevier.

Cetuximab-conjugated fluorescent magnetic nanohybrids (CET-FMNHs) that served as effective agents for both magnetic resonance (MR) and fluorescence optical imaging of human epithelial cancer.

4. Optical-imaging-based cancer therapy

4.1. Optical imaging in drug delivery (Theranostics)

Recently, nanoparticles have provided significant progress in cancer theranostics due to their unique physicochemical properties, in which both diagnosis and therapeutic functions can be achieved simultaneously. Theranostics aims to provide image-guided cancer therapy by integrating imaging and therapy, which are particularly interesting fields in Nanomedicine [12]. Theranostic nanoparticles comprise at least three components: (i) the biological payload, (ii) the carrier, and (iii) surface modifiers (**Figure 1**) [74–93]. Biological payloads include imaging agents and therapeutic agents. Therefore, they can allow the simultaneous delivery of therapeutic agents to the tumor site and real-time tracking of their biodistribution *in vivo*. Optical imaging has advantages in theranostics because it allows the non-invasive monitoring of the progression of diseases and therapy [84]. For example, Misra et al. [85] synthesized blue-light-emitting ZnO quantum dots combined with biodegradable chitosan (N-acetylglucosamine) for tumor-targeted drug delivery (a ZnO-QD-chitosan-folate carrier), which was loaded with an anti-cancer drug (DOX). The DOX-loaded ZnO-QD-chitosan-folate carrier exhibited highly stable QDs because of its hydrophilicity and the cationic charge of chitosan as well as a rapid drug release profile with a controlled release.

Ryu et al. [86–89] developed chitosan-based nanoparticles (CNPs) that were labeled with Cy 5.5 for optical imaging and encapsulated with paclitaxel (PTX) as an anticancer drug

(PTX-Cy5.5-CNP) (**Figure 7**). They confirmed that the PTX-Cy5.5-CNP was effectively delivered to the tumor sites by optical imaging and that it showed enhanced therapeutic efficacy in tumor tissues while minimizing its toxicity to normal tissues. Smart theranostic nanosystems that respond to environmental changes (e.g., pH) have been designed for controlled drug release, low drug loss and low side effects [90–92]. Wu et al. prepared nanogels via the *in situ* immobilization of CdSe quantum dots (QDs) in the interior of pH and temperature-responsive hydroxypropylcellulose-poly(acrylic acid) (HPC-PAA) semi-interpenetrating (semi-IPN) polymer networks (HPC-PAA-CdSe hybrid nanogels). These nanogels demonstrated potential as excellent drug carriers, providing a high drug loading capacity for TMZ as a model anticancer drug and offering the possibility of pH-regulated drug delivery [93]. Jang et al. [94] used nanovesicles containing poly(L-lysine-graft-imidazole) (PLI)/miR complexes (NVs/miR) to systemically deliver miR-34a for CD44 expression-based cancer therapy (**Figure 8**).

In this system, the PLI acts to deliver miRNA to the site of action via the buffering effect of the imidazole residues under endosomal pH. This systemic delivery of miR-34a using our NVs shows the most favorable delivery efficiency, a significant suppression of CD44 expression, and increased apoptosis in the *in vivo* models [94]. In optical imaging, fluorophores, such as fluorescent dyes, bioluminescent proteins and fluorescent proteins, are widely used to monitor molecular events. However, they are easily susceptible to photobleaching. Fluorescent nanoparticles (e.g., quantum dots, upconversion nanoparticles) were developed that complement the weakness of fluorophores; however, they also exhibited potential toxicity [95]. Among various nanoparticles, gold nanoparticles are the most widely used in the biomedical field because of their advantageous properties such as biocompatibility and facile modification [96–102]. According to their size, shape, and structure, they also have controllable surface plasmon resonance (SPR). Among gold nanoparticles, rod-shaped gold nanoparticles

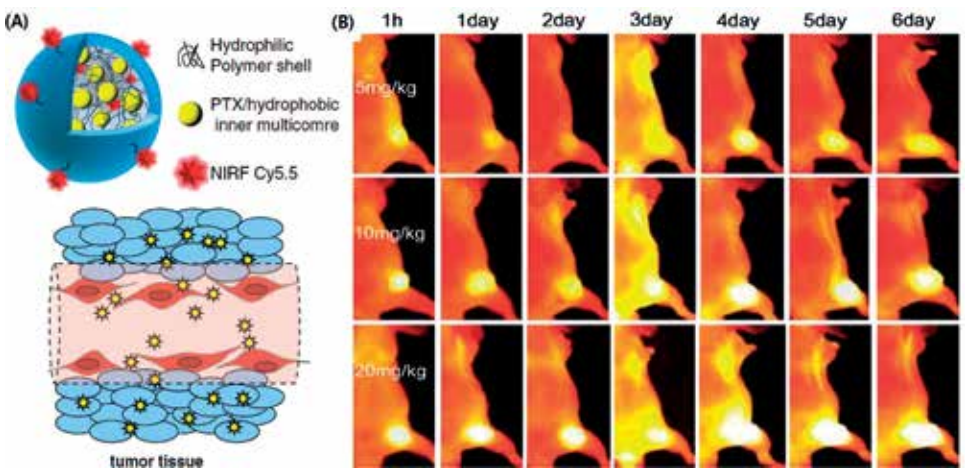

Figure 7. Theragnostic chitosan-based nanoparticles (CNPs) for cancer imaging and chemotherapy. (A) Conceptual description of theragnostic nanoparticles labeled with Cy5.5 for imaging and encapsulated with PTX for cancer therapy (PTX–Cy5.5–CNP). (B) *In vivo* images of the tumor-bearing mice treated with PTX–Cy5.5–CNP of different drug concentrations (5, 10, and 20 mg/kg) every third day. Reproduced from Ref. [88] with permission of Elsevier.

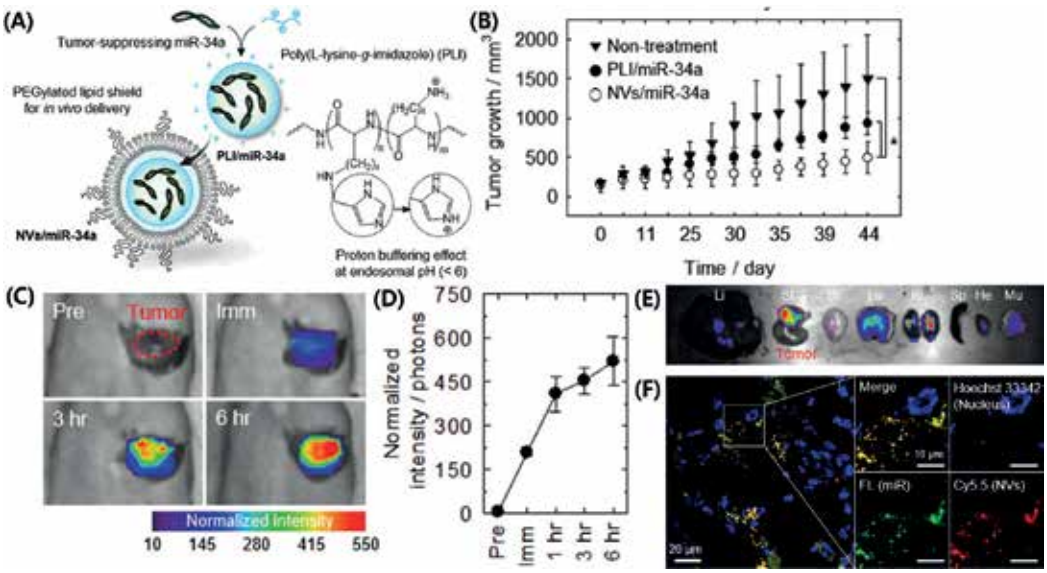

Figure 8. (A) Schematic illustration and characterization of nanovesicles containing PLI/miR complexes (NVs/miR) that proton buffering promoted by protonation of a pH-responsive cationic polymer, poly(L-lysine-graft-imidazole (PLI), at endosomal pH, (B) *in vivo* anti-tumor effects induced by NVs/miR-34a, (C) I optical images of Cy5.5-labeled NVs containing PLI/fluorescein-labeled miR (Cy5.5-NVs/FL-miR) in an MKN-74 gastric subcutaneous xenograft model after intravenous injection of Cy5.5-NVs/FL-miR at various time intervals (pre-injection, 0, 3, and 6 h) and (D) its photon counts from the tumor regions after injection of Cy5.5-NVs/FL-miR. (E) *Ex vivo* optical images of excised organs (liver, stomach, brain, lung, kidney, spleen, heart, and muscle) at 6 h after injection of Cy5.5-NVs/FL-miR. The intensity maps on the fluorescence images display normalized photon counts and (D) confocal microscopy images of tumor sections from mice treated with Cy5.5-NVs/FL-miR. Green, red, and blue represent FL from miR, Cy5.5 from NVs, and Hoechst 33342 from nucleus, respectively. Reproduced from Ref. [94] with permission of Elsevier.

(gold nanorods) can be used as direct NIR absorption imaging probes because their main absorption band is located in the NIR region due to the longitudinal surface plasmon.

Choi et al. noted that cRGD-conjugated gold nanorods showed excellent tumor targeting ability via NIR absorption imaging with no cytotoxicity. Additionally, the nanorods showed sufficient cellular uptake in a glioblastoma *in vivo* model, thus demonstrating their potential as $\alpha_v\beta_3$ integrin-targeted imaging probes [103, 104]. In particular, gold nanoparticles are useful for image-guided thermal therapy (also called hyperthermia or photothermal therapy) because they can absorb laser irradiation and convert the energy into a heat source via electron excitation and relaxation. Hyperthermia can induce apoptotic cell death in tumor tissues via heat generation, which provides a less invasive and localized therapy for cancer. As a result, it has been used to improve therapeutic efficacy and survival rates in combination with radiotherapy or chemotherapy for tumors. Choi et al. [105, 106] also prepared Cetuximab (CET)-conjugated gold nanorods and evaluated their hyperthermal properties under NIR irradiation (**Figure 9**). Gold nanorods have been frequently used to trigger hyperthermia in combination with an NIR laser, which is more effective for tissue penetration than are UV and visible light. After NIR laser irradiation, CET-PGNRs showed strong therapeutic efficacy in tumor-bearing mice, thus demonstrating the potential of CET-PGNRs for simultaneous

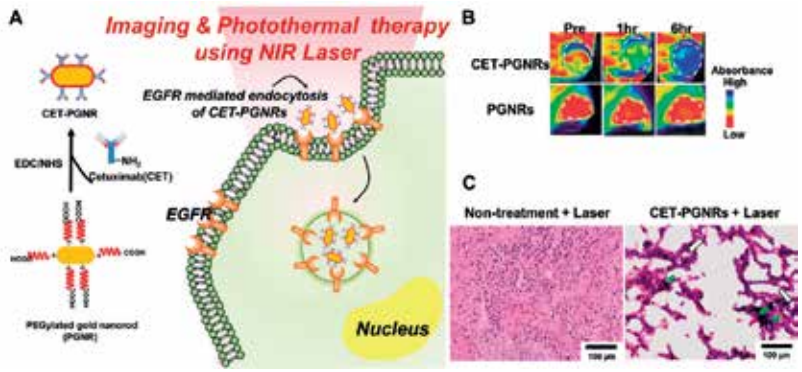

Figure 9. (A) Schematic illustration of CET-PGNRs as NIR absorption imaging and photothermal therapeutic agents for epithelial cancer. (B) Noninvasive NIR absorption *in vivo* images of tumor tissues for intravenous injected CET-PGNRs or PGNRs (control); white-dotted circles indicate the tumor regions. (C) Silver staining eosin. Tumor region was characterized by extensive pyknosis (green arrows) and cell vacuolization (white arrows) only in mice treated with CET-PGNRs after NIR laser irradiation. Reproduced from Ref. [12] with permission of ACS Publications.

absorption imaging and photothermal ablation of epithelial cancer cells with excellent targeting ability. Additionally, Choi et al. demonstrated highly sensitive terahertz (THz) molecular imaging using same probe (CET-PGNR) in both *in vitro* and *in vivo* models, indicating that its high thermal sensitivity can help extend photonic-based photothermal molecular imaging and be used for monitoring drug delivery processes and for early cancer diagnosis [105, 106]. Nam et al. developed "smart" gold nanoparticles that enable aggregation in mild acidic intracellular environments due to their hydrolysis-susceptible citraconic amide surface, which induces a shift in the absorption to longer wavelength, in the far-red and near-infrared (NIR) regions. This smart feature is useful for photothermal cancer therapy [107].

4.2. Optical imaging guided surgery

The primary goal of cancer surgery is to maximize the tumor excision and minimize the collateral damage. Molecular imaging techniques are required to achieve these goals, leading to "image-guided surgery" [108–117]. Especially, optical imaging is the most suitable for image-guided surgery (or targeted surgery) because fluorescence signals can provide real-time guidance to differentiate positive tumor margins and local malignant masses from normal tissues during surgery, thereby increasing the long-term patient survival. Near-infrared (NIR) imaging has particular potential to remove all neoplastic tissue at the surgical site because it is possible to obtain a low background signal and perform non-invasive real-time monitoring. Image-guided surgery is suitable for tumors that are difficult to differentiate from adjacent normal tissues (such as breast cancers), tumors that are next to complex structures with crucial physiological functions (such as brain tumors), or tumors that have high local recurrence or positive margin rates. Suitable probes for image-guide surgery must specifically detect and target cancerous tissues by showing maximum signal from the target and minimum signal from the background.

A natural fluorophore called protoporphyrin (PpIX) has been clinically used for image-guided surgical resection of brain tumors (glioblastomas), demonstrating that its fluorescence signals

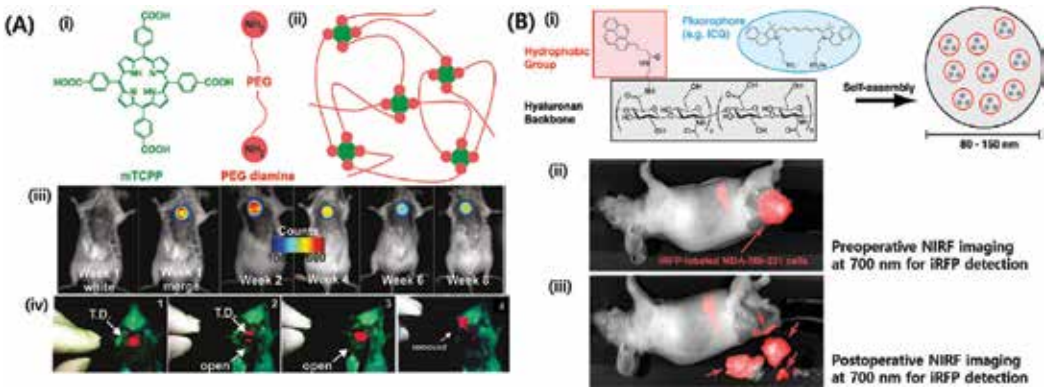

Figure 10. (A) Porphyrin-cross-linked hydrogels and noninvasive monitoring and image-guided surgical resection by using them. (i) Structures of mTCPP (green) and PEG diamine (red). (ii) Schematic of the hydrogel. (e), from left to right, (iii) fluorescence images of a mouse with the hydrogel implanted subcutaneously and monitored noninvasively. (iv) Screen captures from a fluorescence camera used to guide fluorescently the surgical removal of the hydrogel in real time. Fluorescence was readily apparent transdermally (T.D.) or through the open incision, as indicated. (B) Hydrophobic moieties conjugated to HLA drive self-assembly into nanoparticles that can entrap ICG. Indocyanine green-loaded nanoparticles for image-guided tumor surgery (i) hydrophobic moieties conjugated to HLA drive self-assembly into nanoparticles that can entrap ICG. (ii) Preoperative imaging and (iii) postoperative imaging of iRFP shows the location of MDA-MB-231 breast tumor xenograft. Red arrows indicated extracted tumors, where iRFP signal showed due to the presence of NanoICG. Reproduced from Refs. [116, 117] with permission of ACS Publications.

are highly specific to tumor cells. Lovell et al. [116] have developed hydrogels using cross-linked porphyrin co-monomers as strong optical tracers (**Figure 10(A)**). In *in vivo* studies, these could be used for the non-invasive fluorescence monitoring of subcutaneously implanted hydrogels over 2 months, without adverse effects or behavior. In addition, it was possible to non-invasively visualize where the gel was located and whether hydrogel degradation or photobleaching occurred. After surgical resection, while no residual fluorescence was detected in the mouse, hydrogel fluorescence was definitely recognized in the removed gel [116]. Hill et al. [117] demonstrated hyaluronic acid (HLA)-derived nanoparticles containing an indocyanine green (ICG) as near-infrared dye (NanoICG) for well delivery to tumors (**Figure 10(B)**). NanoICG exhibited quenched fluorescence and could be activated by disassembly in a mixed solvent (DMSO:H_2O = 50:50). Strong fluorescence enhancement of the NanoICG was observed in a breast tumor xenograft model. The NanoICG were more completely delivered to tumors compared to free ICG, with strong contrast enhancement in the tumor with a lower background signal in the surrounding tissue, thus demonstrating the potential of the NanoICG as a probe.

5. Conclusion

Optical imaging is a powerful tool that can provide the real-time and direct observation of specific molecular events, biological pathways, and disease processes. As described in this chapter, design strategies for imaging probes are important for accurate imaging to enable effective cancer management both *in vitro* and *in vivo*. Nanomaterial-based imaging probes can obtain

simultaneous imaging of multiple targets with high sensitivity, multimodal imaging, and imaging-guided therapy (theranostics) in combination with therapeutic agents. In particular, due to the advantages of optical imaging, the surgeon can simultaneously perform surgery while identifying where the cancer is located (imaging-guided surgery). These techniques will greatly contribute in reducing cancer recurrence and developing more effective cures.

Acknowledgements

This study was supported by the Ministry of Science and ICT (MSIT), Global Frontier Project through the Center for BioNano Health-Guard (H-GUARD_2014M3A6B2060507) and by the KRIBB Research Initiative Program of the Republic of Korea.

Author details

Jae-Woo Lim[1,2], Seong Uk Son[1] and Eun-Kyung Lim[1,2]*

*Address all correspondence to: eklim1112@kribb.re.kr

1 Hazards Monitoring BioNano Research Center, Korea Research Institute of Bioscience and Biotechnology, Daejeon, Republic of Korea

2 Department of Nanobiotechnology, Korea Research Institute of Bioscience and Biotechnology, School of Biotechnology, Daejeon, Republic of Korea

References

[1] Paulmurugan R. Introduction to cancer biology. In: Chen X, editor. Molecular Imaging Probes for Cancer Research. Singapore: World Scientific; 2012. pp. 3-27

[2] Massoud TF, Gambhi SS. Molecular imaging in living subjects: Seeing fundamental biological processes in a new light. Genes Development. 2003;**17**:545-580

[3] Kircher MF, Hricak H, Larson SM. Molecular imaging for personalized cancer care. Molecular Oncology. 2012;**6**(2):182-195

[4] Weissleder R, Mahmood U. Molecular imaging. Radiology. 2001;**219**:316-333

[5] Song Y, Zhu S, Yang B. Bioimaging based on fluorescent carbon dots. RSC Advances. 2014;**4**:27184-27200

[6] Nune SK, Gunda P, Thallapally PK, Lin Y-Y, Laird Forrest M, Berkland CJ. Nanoparticles for biomedical imaging. Expert Opinion on Drug Delivery. 2009;**6**:1175-1194

[7] Lin J, Chen X, Huang P. Graphene-based nanomaterials for bioimaging. Advanced Drug Delivery Reviews. 2016;**105**:242-254

[8] Zhang H, Grüner G, Zhao Y. Recent advancements of graphene in biomedicine. Journal of Materials Chemistry B. 2013;**1**:2542-2567

[9] Lim E-K, Keem JO, Yun H-S, Jung J, Chung BH. Smart nanoprobes for the detection of alkaline phosphatase activity during osteoblast differentiation. Chemical Communications. 2015;**51**:3270-3272

[10] Lim E-K, Chung BH, Chung SJ. Recent advances in pH-sensitive polymeric nanoparticles for smart drug delivery in cancer therapy. Current Drug Targets. 2016;**17**(16):1-18

[11] Kim J-H, Park K, Nam HY, Lee S, Kim K, Kwon IC. Polymers for bioimaging. Progress in Polymer Science. 2007;**32**:1031-1053

[12] Lim E-K, Kim T, Paik S, Haam S, Huh Y-M, Lee K. Nanomaterials for theranostics: Recent advances and future challenges. Chemical Reviews. 2015;**115**:327-394

[13] Lim E-K, Chung BH. Preparation of pyrenyl-based multifunctional nanocomposites for biomedical applications. Nature Protocols. 2016;**11**(2):236-251

[14] Singh SK. Red and near infrared persistent luminescence nano-probes for bioimaging and targeting applications. RSC Advances. 2014;**4**:58674-58698

[15] Biju V. Chemical modifications and bioconjugate reactions of nanomaterials for sensing, imaging, drug delivery and therapy:.Chemical Society Reviews. 2014;**43**:744-764

[16] Rong H, Zhang X-B, Kong R-M, Zhao X-H, Jiang J, Tan W. Nucleic acid-functionalized nanomaterials for bioimaging applications. Journal of Materials Chemistry. 2011;**21**:16323-16334

[17] Crich SG, Terreno E, Aime S. Nano-sized and other improved reporters for magnetic resonance imaging of angiogenesis. Advanced Drug Delivery Reviews. 2017;**119**:61-72. DOI: https://doi.org/10.1016/j.addr.2017.08.004

[18] Tallury P, Malhotra A, Byrne LM, Santra S. Nanobioimaging and sensing of infectious disease. Advanced Drug Delivery Reviews. 2010;**62**:424-437

[19] Li K, Liu B. Polymer encapsulated conjugated polymer nanoparticles for fluorescence bioimaging. Journal of Materials Chemistry. 2012;**22**:1257-1264

[20] Gong Y-J, Zhang X-B, Mao G-J, Li S, Meng H-M, Tan W, Feng S, Zhang G. A unique approach toward near-infrared fluorescence probes for bioimaging with remarkably enhanced contrast. Chemical Science. 2016;**7**:2275-2285

[21] Maruyama K. Intracellular targeting delivery of liposomal drugs to solid tumors based on EPR effects. Advanced Drug Delivery Reviews. 2011;**63**:161-169

[22] Fang J, Nakamura H, Maeda H. The EPR effect: Unique features of tumor blood vessels for drug delivery, factors involved, and limitations and augmentation of the effect. Advanced Drug Delivery Reviews. 2011;**63**:136-151

[23] Maeda H, Bharate GY, Daruwalla J. Polymeric drugs for efficient tumor-targeted drug delivery based on EPR-effect. European Journal of Pharmaceutics and Biopharmaceutics. 2009;**71**(3):409-419

[24] Torchilin V. Tumor delivery of macromolecular drugs based on the EPR effect. Advanced Drug Delivery Reviews. 2011;**63**(3):131-135

[25] Kobayashi H, Watanabe R, Choyke PL. Improving conventional enhanced permeability and retention (EPR) effects; what is the appropriate target? Theranostics. 2014;**4**:81-89

[26] Hatakeyama H, Akita H, Harashima H. A multifunctional envelope type nano device (MEND) for gene delivery to tumours based on the EPR effect: A strategy for overcoming the PEG dilemma. Advanced Drug Delivery Reviews. 2011;**63**:152-160

[27] Veronese FM, Pasut G. PEGylation, successful approach to drug delivery. Drug Discovery Today. 2005;**10**:1451-1458

[28] Takeuchi H, Kojima H, Yamamoto H, Kawashima Y. Polymer coating of liposomes with a modified polyvinyl alcohol and their systemic circulation and RES uptake in rats. Journal of Controlled Release. 2000;**68**:195-205

[29] Lim E-K, Lee K, Huh Y-M, Haam S. Remotely triggered drug release from gold nanoparticle-based systems. In: Alvarez-Lorenzo C, Concheiro A, editors. Smart Materials for Drug Delivery: Volume 2. Cambridge, UK: RSC Publishing; 2013. pp. 1-31

[30] Lim E-K, Yang J, Suh J-S, Huh Y-M, Haam S. Synthesis of aminated polysorbate 80 for polyplex-mediated gene transfection. Biotechnology Progress. 2010;**26**:1528-1533

[31] Lim E-K, Yang J, Park M-y, Park J, Suh J-S, Yoon H-G, Huh Y-M, Haam S. Synthesis of water soluble PEGylated magnetic complexes using mPEG-fatty acid for biomedical applications. Colloids and Surfaces B: Biointerfaces. 2008;**64**:111-117

[32] Lim E-K, Yang J, Suh J-S, Huh Y-M, Haam S. Self-labeled magneto nanoprobes using tri-aminated polysorbate 80 for detection of human mesenchymal stem cells. Journal of Materials Chemistry. 2009;**19**:8958-8963

[33] Cassette E, Helle M, Bezdetnaya L, Marchal F, Dubertret B, Pons T. Design of new quantum dot materials for deep tissue infrared imaging. Advanced Drug Delivery Reviews. 2013;**65**:719-731

[34] Bazak R, Houri M, El Achy S, Kamel S, Refaat T. Cancer active targeting by nanoparticles: A comprehensive review. Journal of Cancer Research and Clinical Oncology. 2015;**141**:769-784

[35] Bertrand N, Wub J, Xu X, Kamaly N, Farokhzad OC. Cancer nanotechnology: The impact of passive and active targeting in the era of modern cancer biology. Advanced Drug Delivery Reviews. 2014;**66**:2-25

[36] Brannon-Peppas L, Blanchette JO. Nanoparticle and targeted systems for cancer therapy. Advanced Drug Delivery Reveiws. 2004;**56**:1649-1659

[37] Sapra P, Allen TM. Ligand-targeted liposomal anticancer drugs. Progress in Lipid Research. 2003;**42**:439-462

[38] Byrne JD, Betancourt T, Brannon-Peppas L. Active targeting schemes for nanoparticle systems in cancer therapeutics. Advanced Drug Delivery Reviews. 2008;**60**:1615-1626

[39] Lukyanov AN, Elbayoumi TA, Chakilam AR, Torchilin VP. Tumor-targeted liposomes: Doxorubicin-loaded long-circulating liposomes modified with anti-cancer antibody. Journal of Controlled Release. 2004;**100**:135-144

[40] Benezra M, Penate-Medina O, Zanzonico PB, Schaer D, Ow H, Burns A, DeStanchina E, Longo V, Herz E, Iyer S, Wolchok J, Larson SM, Wiesner U, Bradbury MS. Multimodal silica nanoparticles are effective cancer-targeted probes in a model of human melanoma. The Journal of Clinical Investigation. 2011;**121**:2768-2780

[41] Sun X, Li Y, Liu T, Li Z, Zhang X, Chen X. Peptide-based imaging agents for cancer detection. Advanced Drug Delivery Reviews. 2017;**110-111**:38-51

[42] Atukorale PU, Covarrubias G, Bauer L, Karathanasis E. Vascular targeting of nanoparticles for molecular imaging of diseased endothelium. Advanced Drug Delivery Reviews. 2017;**113**:141-156

[43] Farokhzad OC, Karp JM, Langer R. Nanoparticle–aptamer bioconjugates for cancer targeting. Expert Opinion Drug Delivery. 2006;**3**:311-324

[44] Hwang DW, Ko HY, Lee JH, Kang H, Ryu SH, Song IC, Lee DS, Kim S. A nucleolin-targeted multimodal nanoparticle imaging probe for tracking cancer cells using an aptamer. The Journal of Nuclear Medicine. 2010;**51**:98-105

[45] Reuveni T, Motiei M, Romman Z, Popovtzer A, Popovtzer R. Targeted gold nanoparticles enable molecular CT imaging of cancer: An in vivo study. International Journal of Nanomedicine. 2011;**6**:2859-2864

[46] Lewis Phillips GD, Li G, Dugger DL, Crocker LM, Parsons KL, Mai E, Blättler WA, Lambert JM, Chari RVJ, Lutz RJ, Wong WLT, Jacobson FS, Koeppen H, Schwall RH, Kenkare-Mitra SR, Spencer SD, Sliwkowsk MX. Targeting HER2-positive breast cancer with trastuzumab-DM1, an antibody-cytotoxic drug conjugate. Cancer Research. 2008;**68**:9280-9290

[47] Zhou T, Wu B, Xing D. Bio-modified Fe_3O_4 core/au shell nanoparticles for targeting and multimodal imaging of cancer cells. Journal of Materials Chemistry. 2012;**22**:470-477

[48] Lim E-K, Jang E, Kim B, Choi J, Lee K, Suh J-S, Huh Y-M, Haam S. Dextran-coated magnetic nanoclusters as highly sensitive contrast agents for magnetic resonance imaging of inflammatory macorphages. Journal of Materials Chemistry. 2011;**21**:12473-12478

[49] Yang J, Lim E-K, Lee HJ, Park J, Lee SC, Lee K, Yoon H-G, Suh J-S, Huh Y-M, Haam S. Fluorescent magnetic nanohybrids as multimodal imaging agnets for human epithelial cancer detection. Biomaterials. 2008;**29**:2548-2555

[50] Lim E-K, Kim H-O, Jang E, Park J, Lee K, Suh J-S, Huh Y-M, Haam S. Hyaluronan-modified magnetic nanoclusters for detection of CD44-overexpressing breast cancer by MR imaging. Biomaterials. 2011;**32**:7941-7950

[51] Lim E-K, Lee J, Kang B, Choi J, Park HS, Suh J-S, Huh Y-M, Haam E. Efficient CD44-targeted magnetic resonance imaging (MRI) of breast cancer cells using hyaluronic acid (HA)-modified $MnFe_2O_4$ nanocrystals. Nanoscale Reseach Letters. 2013;**8**:149-157

[52] Lim E-K, Kim B, Choi Y, Ro Y, Cho E-J, Lee JH, Ryu S-H, Suh J-S, Haam S, Huh Y-M. Aptamer-conjugated magnetic nanoparticles enable efficient targeted detection of integrin $\alpha v\beta 3$ via magnetic resonance imaging. Journal of Biomedical Research A. 2014;**102**:49-59

[53] Cho E-J, Yang J, Mohamedali KA, Lim E-K, Kim E-J, Farhangfar CJ, Suh J-S, Haam S, Rosenblum MG, Huh Y-M. Sensitive angiogenesis imaging of orthotopic bladder tumors in mice using a selective magnetic resonance imaging contrast agent containing VEGF121/rGel. Investigative Radiology. 2011;**46**:441-449

[54] Penet M-F, Krishnamachary B, Chen Z, Jin J, Bhujwalla ZM. Molecular imaging of the tumor microenvironment. Advances in Cancer Research. 2014;**124**:235-256

[55] Xiong H, Kos P, Yan Y, Zhou K, Miller JB, Elkassih S, Siegwart DJ. Activatable water-soluble probes enhance tumor imaging by responding to dysregulated pH and exhibiting high tumor-to-liver fluorescence emission contrast. Bioconjugate Chemistry. 2016;**27**:1737-1744

[56] Luling W, Li X, Huang C, Jia N. Dual-modal colorimetric/fluorescence molecular probe for ratiometric sensing of pH and its application. Analytical Chemistry. 2016;**88**:8332-8338

[57] Choi J, Hong Y, Lee E, Kim M-H, Yoon DS, Suh J, Huh Y, Haam S, Yang J. Redox-sensitive colorimetric polyaniline nanoprobes synthesized by a solvent-shift process. Nano Research. 2013;**6**:356-364

[58] Choi EB, Choi J, Bae SR, Kim H-O, Jang E, Kang B, Kim M-H, Kim B, Suh J-S, Lee K, Huh Y-M, Haam S. Colourimetric redox-polyaniline nanoindicator for in situ vesicular trafficking of intracellular transport. Nano Research. 2015;**8**:1169-1179

[59] Kim T, Cho E-J, Chae Y, Kim M, Aram O, Jin J, Lee E-S, Baik H, Haam S, Suh J-S, Huh Y-M, Lee K. Urchin-shaped manganese oxide nanoparticles as pH-responsive activatable T1 contrast agents for magnetic resonance imaging. Angewandte Chemie International Edition. 2011;**50**:10589-10593

[60] Park J, Yang J, Lim E-K, Kim E, Choi J, Ryu JK, Kim NH, Suh J-S, In Yook J, Huh Y-M, Haam S. Anchored proteinase-targetable optomagnetic nanoprobes for molecular imaging of invasive cancer cells. Angewandte Chemie International Edition. 2012;**51**:945-948

[61] Kim E, Yang J, Park J, Kim S, Kim NH, In Yook J, Suh J-S, Haam S, Huh Y-M. Consecutive targetable smart nanoprobe for molecular recognition of cytoplasmic microRNA in metastatic breast cancer. ACS Nano. 2012;**6**:8525-8535

[62] Newell K, Franchi A, Pouysségur J, Tannock L. Studies with glycolysis-deficient cells suggest that production of lactic acid is not the only cause of tumor acidity. Proceedings of the National Academy of Sciences. 1993;**90**:1127-1131

[63] Gatenby RA, Gawlinski ET, Gmitro AF, Kaylor B, Gillies RJ. Acid-mediated tumor invasion: A multidisciplinary study. Cancer Research. 2006;**66**:5216-5223

[64] YongLee S, Jeon SI, Jung S, Chung IJ, Ahn C-H. Targeted multimodal imaging modalities. Advanced Drug Delivery Reviews. 2014;**76**:60-78

[65] Martí-Bonmatí L, Sopena R, Bartumeus P, Sopena P. Multimodality imaging techniques. Contrast Media & Molecular Imaging. 2010;**5**:180-189

[66] Lu X, Zhang Z, Xia Q, Hou M, Yan C, Chen Z, Xu Y, Liu R. Glucose functionalized carbon quantum dot containing organic radical for optical/MR dual-modality bioimaging. Materials Science and Engineering: C. 2018;**82**:190-196

[67] Wang M, Mao C, Wang H, Ling X, Wu Z, Li Z, Ming X. Molecular imaging of P-glycoprotein in chemoresistant tumors using a dual-modality PET/fluorescence probe. Molecular Phamaceutics. 2017;**14**:3391-3398

[68] Hekman MCH, Boerman OC, Bos DL, Massuger LFAG, Weil S, Grasso L, Rybinski KA, Oosterwijk E, Mulders PFA, Rijpkema M. Improved intraoperative detection of ovarian cancer by folate receptor alpha targeted dual-modality imaging. Molecular Pharmaceutics. 2017;**14**:3457-3463

[69] Jokers JV, Cole AJ, Van de Sompel D, Gambhir SS. Gold nanorods for ovarian cancer detection with photoacoustic imaging and resection guidance via Raman imaging in living mice. ACS Nano. 2012;**6**:10366-10377

[70] Keunen O, Taxt T, Grüner R, Lund-Johansend M, Tonn J-C, Pavling T, Bjerkvig R, Nicloua SP, Thorsen F. Multimodal imaging of gliomas in the context of evolving cellular and molecular therapies. Advanced Drug Delivery Reviews. 2014;**76**:98-115

[71] Oh MH, Lee N, Kim H, Park SP, Piao Y, Lee J, Jun SW, Moon WK, Choi SH, Hyeon T. Large-scale synthesis of bioinert tantalum oxide nanoparticles for X-ray computed tomography imaging and bimodal image-guided sentinel lymph node mapping. Journal of American Chemical Society. 2011;**133**:5508-5515

[72] Wang Q, Lv L, Ling Z, Wang Y, Liu Y, Li L, Liu G, Shen L, Yan J, Wang Y. Long-circulating iodinated albumin–gadolinium nanoparticles as enhanced magnetic resonance and computed tomography imaging probes for osteosarcoma visualization. Analytical Chemistry. 2015;**87**:4299-4304

[73] Lim E-K, Yang J, Dinney CPN, Suh J-S, Huh Y-M, Haama S. Self-assembled fluorescent magnetic nanoprobes for multimode-biomedical imaging. Biomaterials. 2010;**31**:9310-9319

[74] Wang J, Mi P, Lin G, Wáng YXJ, Liu G, Chen X. Imaging-guided delivery of RNAi for anticancer treatment. Advanced Drug Delivery Reviews. 2016;**104**:44-60

[75] Zhao R, Hollis CP, Zhang H, Sun L, Gemeinhart RA, Li T. Hybrid nanocrystals: Achieving concurrent therapeutic and bioimaging functionalities toward solid tumors. Molecular Pharmaceutics. 2011;**8**:1985-1991

[76] Bennett KM, Jo J-i, Cabral H, Bakalova R, Aoki I. MR imaging techniques for nanopathophysiology and theranostics. Advanced Drug Delivery Reviews. 2014;**74**:75-94

[77] Xu H, Cheng L, Wang C, Ma X, Li Y, Liu Z. Polymer encapsulated upconversion nanoparticle/iron oxide nanocomposites for multimodal imaging and magnetic targeted drug delivery. Biomaterials. 2011;**32**:9364-9373

[78] Petersen AL, Hansen AE, Gabizon A, Andresen TL. Liposome imaging agents in personalized medicine. Advanced Drug Delivery Reviews. 2012;**64**:1417-1435

[79] Phillipsa WT, Bao A, Brenner AJ, Goins BA. Image-guided interventional therapy for cancer with radiotherapeutic nanoparticles. Advanced Drug Delivery Reviews. 2014;**76**: 39-59

[80] Kiessling F, Fokong S, Bzyl J, Lederle W, Palmowski M, Lammers T. Recent advances in molecular, multimodal and theranostic ultrasound imaging. Advanced Drug Delivery Reviews. 2014;**15**:15-27

[81] Cheng Y, Morshed RA, Auffinger B, Tobias AL, Lesniak MS. Multifunctional nanoparticles for brain tumor imaging and therapy. Advanced Drug Delivery Reviews. 2014;**66**: 42-57

[82] Lee H, Kim H-O, Son H-Y, Lee S-B, Jang E, Kang B, Haam S, Lim E-K, Huh Y-M. Magnetic nanovector enabling miRNA-34a delivery for CD44 suppression with concurrent MR imaging. Journal of Nanoscience and Nanotechnology. 2016;**16**:12939-12946

[83] Kim E, Lee H, An Y, Jang E, Lim E-K, Kang B, Suh J-S, Huh Y-M, Haam S. Imidazolized magnetic nanovectors with endosome disrupting moieties for the intracellular delivery and imaging of siRNA. Journal of Materials Chemistry B. 2014;**2**:8566-8575

[84] Jiang S, Gnanasammandhan MK, Zhang Y. Optical imaging-guided cancer therapy with fluorescent nanoparticles. Journal of the Royal Society. 2010;**7**:3-18

[85] Yuan Q, Hein S, Misra RDK. New generation of chitosan-encapsulated ZnO quantum dots loaded with drug: Synthesis, characterization and in vitro drug delivery response. Acta Biomaterialia. 2010;**6**:2732-2739

[86] Ryu JH, Koo H, Sun I-C, Yuk SH, Choi K, Kim K, Kwon IC. Tumor-targeting multifunctional nanoparticles for theragnosis: New paradigm for cancer therapy. Advanced Drug Delivery Reviews. 2012;**64**:1447-1458

[87] Min KH, Park K, Kim Y-S, Bae SM, Lee S, Jo HG, Park R-W, Kim I-S, Jeong SY, Kim K, Kwon IC. Hydrophobically modified glycol chitosan nanoparticles-encapsulated camptothecin enhance the drug stability and tumor targeting in cancer therapy. Journal of Controlled Release. 2008;**127**:208-218

[88] Cho H-J, Yoon HY, Koo H, Ko S-H, Shim J-S, Lee J-H, Kim K, Kwon IC, Kim D-D. Self-assembled nanoparticles based on hyaluronic acid-ceramide (HA-CE) and Pluronic® for tumor-targeted delivery of docetaxel. Biomaterials. 2011;**32**:7181-7190

[89] Ryu JH, Kim SA, Koo H, Yhee JY, Lee A, Na JH, Youn I, Choi K, Kwon IC, Kim B-S, Kim K. Cathepsin B-sensitive nanoprobe for in vivo tumor diagnosis. Journal of Materials Chemistry. 2011;**21**:17631-17634

[90] Lim E-K, Huh Y-M, Yang J, Lee K, Suh J-S, Haam S. pH-triggered drug-releasing magnetic nanoparticles for cancer therapy guided by molecular imaging by MRI. Advanced Materials. 2011;**23**:2436-2442

[91] Phan VN, Lim E-K, Kim T, Kim M, Choi Y, Kim B, Lee M, Oh A, Jin J, Chae Y, Baik H, Suh J-S, Haam S, Huh Y-M, Lee K. A highly crystalline manganese-doped iron oxide nanocontainer with predesigned void volume and shape for theranostic applications. Advanced Materials. 2013;**25**:3202-3208

[92] Lim E-K, Sajomsang W, Choi Y, Jang E, Lee H, Kang B, Kim E, Haam S, Suh J-S, Chung SJ, Huh Y-M. Chitosan-based intelligent theragnosis nanocomposites enable pH-sensitive drug release with MR-guided imaging for cancer therapy. Nanoscale Research Letters. 2013;**8**:467-479

[93] Wu W, Aiello M, Zhou T, Berliner A, Banerjee P, Zhou S. In-situ immobilization of quantum dots in polysaccharide-based nanogels for integration of optical pH-sensing, tumor cell imaging, and drug delivery. Biomaterials. 2010;**31**:3023-3031

[94] Kim E, Son H-Y, Lim E-K, Le H, Choi Y, Par K, Han S, Suh J-S, Hu Y-M, Haam S. Nanovesicle-mediated systemic delivery of microRNA-34a for CD44 overexpressing gastric cancer stem cell therapy. Biomaterials. 2016;**105**:12-24

[95] Yue X, Zhang Q, Dai Z. Near-infrared light-activatable polymeric nanoformulations for combined therapy and imaging of cancer. Advanced Drug Delivery Reviews. 2017; **115**:155-170

[96] Yang K, Hu L, Ma X, Ye S, Liang C, Shi X, Li C, Li Y, Li Z. Multimodal imaging guided photothermal therapy using functionalized graphene nanosheets anchored with magnetic nanoparticles. Advanced Materials. 2012;**24**:1868-1872

[97] Jin Y, Li Y, Ma X, Zha Z, Shi L, Tian J, Dai Z. Encapsulating tantalum oxide into polypyrrole nanoparticles for X-ray CT/photoacoustic bimodal imaging-guided photothermal ablation of cancer. Biomaterials. 2014;**35**:5795-5804

[98] Chen D, Zhao C, Ye J, Li Q, Liu X, Meina S, Jiang H, Amatore C, Selke M, Wang X. In situ biosynthesis of fluorescent platinum nanoclusters: Toward self-bioimaging-guided cancer theranostics. Applied Materials & Interfaces. 2015;**7**:18163-18169

[99] Kumawat MK, Thakur M, Gurung RB, Srivastava R. Graphene quantum dots from *Mangifera indica*: Application in near-infrared bioimaging and intracellular nanothermometry. ACS Sustainable Chemistry & Engineering. 2017;**5**:1382-1391

[100] Li Y, Liu Z, Hou Y, Yang G, Fei X, Zhao H, Guo Y, Chengkang S, Wang Z, Zhong H, Zhuang Z, Guo Z. Multifunctional nanoplatform based on black phosphorus quantum dots for bioimaging and photodynamic/photothermal synergistic cancer therapy. Applied Materials & Interfaces. 2017;**9**:2508-25106

[101] Ju Y, Zhang H, Yu J, Tong S, Tian N, Wang Z, Wang X, Su X, Chu X, Lin J, Ding Y, Li G, Sheng F, Hou Y. Monodisperse au-Fe_2C janus nanoparticles: An attractive multifunctional material for triple-modal imaging-guided tumor photothermal therapy. ACS Nano. 2017;**11**:9239-9248

[102] Jing L, Liang X, Deng Z, Feng S, Li X, Huang M, Li C, Dai Z. Prussian blue coated gold nanoparticles for simultaneous photoacoustic/CT bimodal imaging and photothermal ablation of cancer. Biomaterials. 2014;**35**:5814-5821

[103] Choi J, Yang J, Park J, Kim E, Suh J-S, Huh Y-M, Haam S. Specific near-IR absorption imaging of glioblastomas using integrin-targeting gold nanorods. Advanced Functional Materials. 2011;**21**:1082-1088

[104] Choi J, Yang J, Bang D, Park J, Suh J-S, Huh Y-M, Haam S. Targetable gold nanorods for epithelial cancer therapy guided by near-IR absorption imaging. Small. 2012;**8**:746-753

[105] Oh SJ, Choi J, Maeng I, Park JY, Lee K, Huh Y-M, Suh J-S, Haam S, Son J-H. Molecular imaging with terahertz waves. Optics Express. 2011;**19**:4009-4016

[106] Oh SJ, Kang J, Maeng I, Suh J-S, Huh Y-M, Haam S, Son J-H. Nanoparticle-enabled terahertz imaging for cancer diagnosis. Optics Express. 2009;**17**:3469-3475

[107] Nam J, Won N, Jin H, Chung H, Kim S. pH-induced aggregation of gold nanoparticles for photothermal cancer therapy. Journal of the American Chemical Society. 2009;**131**:13639-13645

[108] Hussain T, Nguyen QT. Molecular imaging for cancer diagnosis and surgery. Advanced Drug Delivery Reviews. 2014;**66**:90-100

[109] Bu L, Shenb B, Cheng Z. Fluorescent imaging of cancerous tissues for targeted surgery. Advanced Drug Delivery Reviews. 2014;**76**:21-38

[110] Ofori LO, Withana NP, Prestwood TR, Verdoes M, Brady JJ, Winslow MM, Sorger J, Bogyo M. Design of protease activated optical contrast agents that exploit a latent lysosomotropic effect for use in fluorescence-guided surgery. ACS Chemical Biology. 2015;**10**:1977-1988

[111] Kairdolf BA, Bouras A, Kaluzova M, Sharma AK, Wang MD, Hadjipanayis CG, Nie S. Intraoperative spectroscopy with ultrahigh sensitivity for image-guided surgery of malignant brain tumors. Analytical Chemistry. 2016;**88**:858-867

[112] Kelderhouse LE, Chelvam V, Wayua C, Mahalingam S, Poh S, Kularatne SA, Low PS. Development of tumor-targeted near infrared probes for fluorescence guided surgery. Bioconjugate Chemistry. 2013;**24**:1075-1080

[113] Njiojob CN, Owens EA, Narayana L, Hyun H, Choi HS, Henary M. Tailored near-infrared contrast agents for image guided surgery. Journal of Medicinal Chemistry. 2015;**58**:2845-2854

[114] Owens EA, Hyun H, Dost TL, Lee JH, Park GL, Pham DH, Park MH, Choi HS, Henary M. Near-infrared illumination of native tissues for image-guided surgery. Journal of Medicinal Chemistry. 2016;**59**:5311-5323

[115] Keereweer S, Kerrebijn JDF, van Driel PBAA, Xie B, Kaijzel EL, Snoeks TJA, Que I, Hutteman M, van der Vorst JR, Mieog JSD, Vahrmeijer AL, van de Velde CJH, Baatenburg

de Jong RJ, Löwik CWGM. Optical image-guided surgery—Where do we stand? Molecular Imaging and Biology. 2011;**13**:199-207

[116] Lovell JF, Roxin A, Ng KK, Qi Q, McMullen JD, DaCosta RS, Zheng G. Porphyrin-cross-linked hydrogel for fluorescence-guided monitoring and surgical resection. Biomacromolecules. 2011;**12**:3115-3118

[117] Hill TK, Abdulahad A, Kelkar SS, Marini FC, Long TE, Provenzale JM, Mohs AM. Indocyanine green-loaded nanoparticles for image-guided tumor surgery. Bioconjugate Chemistry. 2015;**26**:294-303

Chapter 3

Carbon Quantum Dots for Bioimaging

Mariadoss Asha Jhonsi

Additional information is available at the end of the chapter

http://dx.doi.org/10.5772/intechopen.72723

Abstract

Carbon is nature's most abundant and useful element. Carbon nanomaterials with small size and unique optical properties have attracted tremendous interest for their promising biomedical applications. Carbon nanoparticles that exhibit fluorescence property are called as carbon quantum dots and they have emerged as a new class of carbon-based nanomaterials. In this chapter, we look at the unique properties of carbon quantum dots, their synthesis, material as well as optical characterizations, origin of fluorescence nature and applications of carbon quantum dots in bioimaging.

Keywords: carbon quantum dots, bioimaging, nontoxic fluorogens, fluorescence, optical imaging and green synthesis

1. Introduction

Fluorescent nanodots have drawn much attention in the twenty-first century for a wide range of applications specifically in biomedical field such as bioimaging, biosensing, drug delivery and photodynamic therapy. In the midst of various biomedical fields, bioimaging is one of the most powerful tools for live cell imaging studies via fluorescence microscopy. It endows with the direct visualization of processes occurring in biological species. Copious reports are available for the usage of organic and inorganic nanomaterials as fluorophores toward bioimaging applications.

In bioimaging studies, it is necessary to use a fluorescent probe to view the image of the cells/specimen species. Numerous organic fluorophores are commercially available which exhibits high-emission quantum yield (ϕ). The better one is Rhodamine 6G, which shows the ϕ value of 80%. But there are few laggings in the usage of organic fluorophores in bioimaging: they are prone to photobleaching and are easy to drip out from the cytoplasm to media, have

less photostability (i.e., the fluorophore will undergo degradation while irradiating with light during the imaging process), narrow excitation and emission wavelength (no possibility of tuning the optical properties) and cytotoxicity (during the bioimaging process, organic fluorophore may change the metabolism of live cells), etc.

Compared to organic fluorophores, metal-based chalcogenide inorganic semiconductor nanocrystals such as quantum dots (QDs) like CdX (X = Se, Te) capped with various long-chain alkyl thiols were extensively used as fluorescent probe during the last decade. The advantages of semiconductor QDs over organic fluorophores are due to their unique property such as quantum confinement effect (i.e., change in particle of QDs leads to changes in optical properties, for example, increase in particle size will shift the absorption in the longer wavelength due to the reduction in bandgap energy), one can vary the optical properties (absorption, emission wavelengths and emission quantum yield) simply by tuning the particle size during the synthesis process or postsynthetic treatments. Moreover, quantum dots show high photostability compared to organic fluorophores since they have the core-shell structure capped with ligands. At the same time, their drawback is in view of biocompatibility, since most of the QDs exist with the presence of toxic heavy metals like Cd, Pb and Hg in their composition. Even though they were enfolded with the surface coverage, within the cell during the imaging analysis, there is a chance of release of those toxic metals into the medium that are harmful to the live cells.

So, in order to conquer the abovementioned problems of unfortunate biodegradability and toxicity, novel fluorescent materials with better optical and biological properties should be developed for bioimaging of live cells. In this context, carbon quantum dots (CQDs), one of the present century invented member of nanocarbon family (**Figure 1**), have emerged as potential candidates for application in such essential field. Compared to the conventional organic fluorophores and recent inorganic semiconductor QDs, the newly emerged carbon

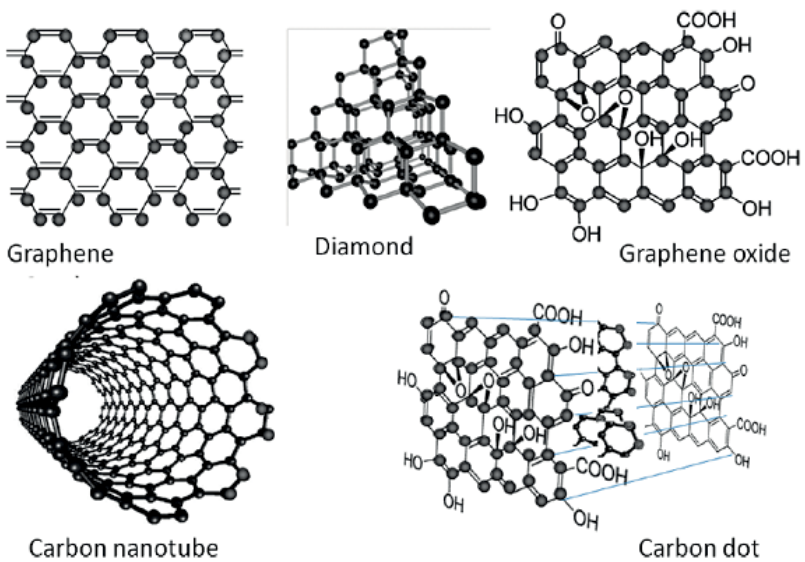

Figure 1. Structures of nanocarbon family members (reproduced with permission from [2]).

quantum dots are superior in terms of resistance to photobleaching, chemical inertness, facile surface functionalization, etc. Interestingly, carbon quantum dots are exhibiting low cytotoxicity, high aqueous solubility and are rich in emission quantum yield that entrusts them for the utilization in the field of biomedical research especially in *in vivo* and *in vitro* bioimaging.

The discovery of fluorescent carbon nanoparticles was accidental, during the separation and purification of single-walled carbon nanotubes via electrophoresis by Xu in the year of 2004 [1]. After 2 years, Sun and his research group named the small carbon nanoparticles as carbon quantum dots derived from graphite powder using laser ablation technique. In these 12 years, carbon quantum dots have attracted most of the chemists as well as biologists owing to their distinct properties such as abundance in nature, inexpensiveness, facile synthesis, high surface area, flexible functionalization, nontoxicity, photostability, high emission quantum yield, high water soluble nature, etc. This chapter focuses on the synthesis, functionalization, electronic structure, origin of fluorescence property and process involved in the application of carbon quantum dots in bioimaging.

2. Synthesis of carbon quantum dots

During the last 10 years, there were numerous methods reported for the synthesis of carbon quantum dots, which can be broadly classified into two types such as top-down and bottom-up approaches. In both the types, one needs to tackle the problems such as aggregation during the carbonization process, homogeneity as well as particle size control and surface properties. In order to overcome these obstacles, there are solutions given like adopting perfect synthetic routes and postsynthetic treatments. Carbon quantum dots can be synthesized from various precursors such as chemical, green and waste materials. In this section, few effective synthetic methods in view of simple, large-scale production and economical were discussed.

2.1. Top-down synthetic routes

2.1.1. Electrochemical

This technique is based on the electrochemical carbonization of low-molecular weight organic compounds by applying direct current. Electrochemical workstation instrument can be used for this method. In this process, low-molecular weight organic compounds like alcohols undergo electrochemical carbonization reaction under basic conditions. Three-electrode system contains two Pt sheets as the working and counter electrodes, as well as a calomel electrode mounted on a freely adjustable Luggin capillary acted as the reference electrode; these three electrodes were fixed with a rubber plug, and the distance between the two Pt sheets to be about 3 cm. The precursor solution is prepared by mixing alcohol with water in the ratio 14:1 in a basic medium by adding sodium hydroxide under stirring. The duration of reaction is about 4 h at a suitable potential until the transparent solution turns dark brown in color. The current density can be varied from 15 to 100 mA cm^2 depending on the precursor molecules selected. Once the reaction is completed, equal volume of ethanol is added in the reaction mixture to salt out the NaOH, and the mixture is left overnight. Further evaporation

of solvent, the solid product can be derived that needs separation and purification for the removal of unreacted small molecules by dialysis against water using membrane to obtain the carbon quantum dots. **Figure 2** shows the overview of preparation.

Advantages of this method are as follows: amorphous carbon quantum dots can be obtained by this technique that imparts high fluorescence quantum yield (maximum of 16%). Quantum confinement effect can be achieved by this technique such as size-dependent photoluminescent properties simply by tuning the applied current density. Purification of the product obtained is facile, and easy surface passivation is possible. At the same time, there are few limitations such as this method is economically costlier for large-scale production; surface defects cannot be avoided and production yield will be lower.

2.1.2. Laser irradiation

In this process, a carbon target in the presence of water vapor with an inert gas as a carrier under high temperature and pressure is irradiated with laser beam. In a typical procedure, carbon precursor is dispersed in some solvent by ultrasonication, and the suspension is dropped into a glass cell for laser irradiation. Generally, Nd:YAG pulsed laser with a second harmonic wavelength of ~530 nm is used to irradiate the suspension. After laser irradiation for different times, the reaction mixture undergoes centrifugation, purification and surface passivation processes to obtain fluorescent carbon quantum dots. **Figure 3** shows the process involved in laser irradiation technique. Advantages of the laser irradiation technique are that it is a fast synthetic route and environmentally friendly approach for the synthesis of carbon quantum dots, but this method is economically not favorable, skilled personal is necessary to conduct the synthesis and postsynthetic process such as surface passivation is necessary to impart fluorescent nature.

2.2. Bottom-up synthetic routes

2.2.1. Microwave pyrolysis

This method involves the microwave irradiation of organic compounds in presence of reaction medium. This is a rapid and low-cost method to prepare carbon quantum dots, and in general, sugar moieties were used as a carbon source and polymeric oligomers as reaction media

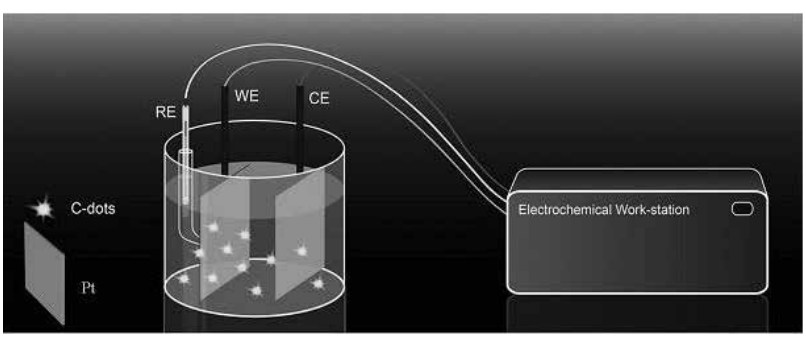

Figure 2. Electrochemical synthesis of C-dots. Under basic conditions (reproduced with permission from [3]).

http://dx.doi.org/10.5772/intechopen.72723

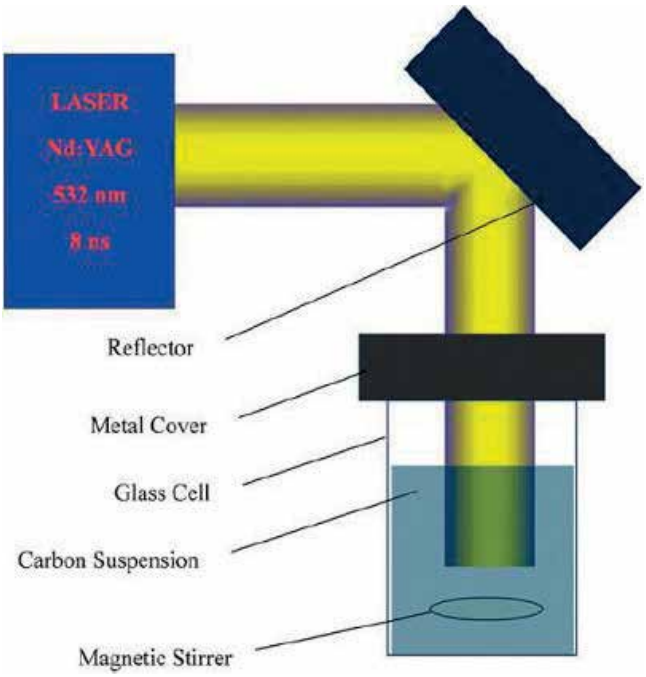

Figure 3. Schematic illustration of experimental setup for the synthesis of carbon quantum dots by laser irradiation technique (reproduced with permission from [4]).

and amine molecules play a role of nitrogen dopants and surface-passivating agents in order to improve the emission quantum yields. Initially, different amounts of reaction medium and carbon precursor are mixed with distilled water. Further, the resultant transparent solution is heated in a microwave oven of 500 W for 2–10 min. Within a minute, color changes from colorless to pale yellow, and further, it increases to dark brown indicating the formation of carbon quantum dots. After cooled to room temperature, the product undergoes separation and purification processes to obtain fluorescent carbon quantum dots (**Figure 4**). Advantages of microwave pyrolysis route are as follows: simple, rapid and efficient method for the synthesis of carbon quantum dots [5]. At the same time, there are few limitations: being costly and the presence of harmful microwave radiation, which is to be handled with precautions.

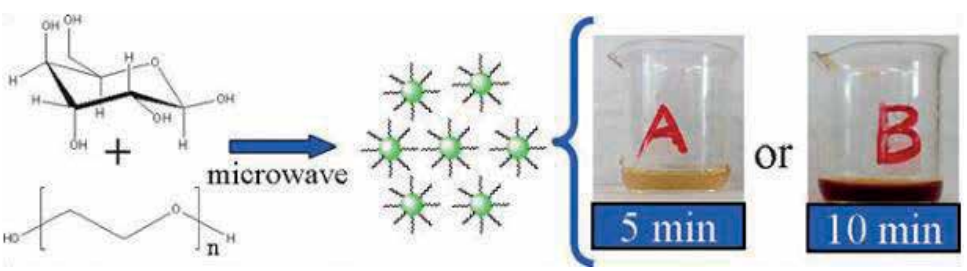

Figure 4. Microwave pyrolysis approach for the synthesis of carbon quantum dots (reproduced with permission from [5]).

2.2.2. Oxidative acid treatment

This treatment includes the refluxion of waste soot in acidic medium followed by centrifugation, neutralization and purification via dialysis against water. Typically, a few gram of waste soot collected by combustion of either natural gas or any other fuel material is mixed with 5 M nitric acid and refluxed for 12 h. After cooled down to room temperature, fluorescent carbon particles were collected by centrifugation. Alternatively, the mixture was first neutralized by Na_2CO_3, and then extensively dialyzed against double distilled water through dialysis membrane (MWCO 1000). **Figure 5** shows the images of carbon soot and carbon quantum dots derived after the oxidative acid treatment process. Advantages of this acid treatment are effective to introduce functional groups such as carbonyl, carboxyl, amines and epoxy, etc., toward greater water-soluble nature of carbon quantum dots, postsynthetic aggregation can be avoided, and without surface passivation, the prepared carbon quantum dots can be used for imaging applications. A disadvantage of this treatment process is defects may reduce the storage stability of prepared carbon quantum dots.

2.2.3. Hydrothermal/solvothermal synthesis

This is the most popular and facile method for the synthesis of fluorescent carbon quantum dots in which various sources such as chemical as well as green precursor can be used for the synthesis of carbon quantum dots. This technique involves a solution of organic precursor in the presence of either water or some organic solvent sealed in an autoclave (reactor setup which is made up of stainless steel outer and Teflon-coated inner lining to withstand high temperature and pressure, **Figure 6**) and reacted at high temperature (less than the critical temperature of the solvent taken). After complete carbonization, it is autoclaved to allow cooling down to room temperature naturally, and the products can be extracted with an organic

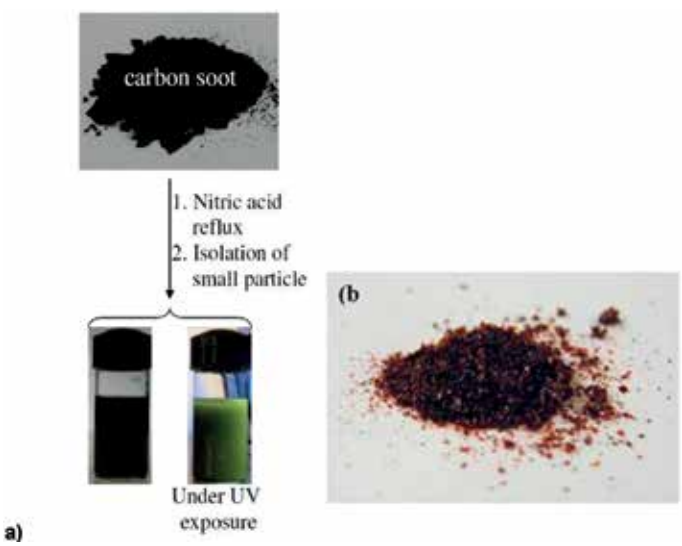

Figure 5. Oxidative acid treatment for the synthesis of green fluorescent carbon quantum dots and image of the functionalized carbon quantum dots. (reproduced with permission from [6]).

Figure 6. Synthesis of blue emissive carbon quantum dots from gelatin via hydrothermal carbonization process (reproduced with permission from [7]).

solvent. By adopting this technique, one can synthesis both hydrophilic and hydrophobic fluorescent carbon quantum dots simply by selecting the appropriate precursors.

Compared with other routes, the hydrothermal carbonization process has some of the advantages such as low toxicological impact of materials and processes, the use of renewable resources, facile instrumentation techniques and high atom economy. This method is cost-effective, ecofriendly and nontoxic. Using this technique, large-scale production is possible and reaction conditions such as time and temperature are adjustable. Postsynthetic surface passivation is not necessary. The only limitation of this method is poor control over particle sizes [7].

2.3. Sources of precursors

Carbon quantum dots can be synthesized from wide variety of precursors like both chemical and green resources. **Table** 1 shows the range of precursor materials reported for the synthesis of carbon quantum dots especially for bioimaging application with the value of emission quantum yield.

Precursor	Synthetic method	Quantum yield (ϕ)	Reference [8]
Glucose	Hydrothermal treatment at 200°C	1.1–2.4	55
Candle soot	HNO_3 oxidation	3	57
Ascorbic acid	Hydrothermal treatment at 140°C	5.7	53
Sugarcane juice	Hydrothermal treatment at 120°C	5.76	62
Watermelon peels	Carbonization at 220°C	7.1	58
Hair fiber	H_2SO_4	11.1	68
Phenol/formaldehyde resin, silica particle	Carbonization at 900°C, NaOH etching	14.7	3
Orange juice	Hydrothermal treatment at 120°C	26	60
Gelatin	Hydrothermal treatment at 200°C	31.6	67
Chitosan	Hydrothermal treatment at 180°C	43	64

Table 1. Carbon quantum dots synthesized by green route for imaging applications [8].

2.4. Surface functionalization and passivation

Modification of the surface of carbon quantum dots is necessary for selective application like bioimaging which can be achieved by either surface passivation or functionalization (**Figure 7**). The former one reduces the detrimental effect of surface contamination to their optical properties and to impart high fluorescent intensity. This can be done by formation of a thin insulating layer of coating materials such as oligomers (poly ethylene glycol (PEG)), thionyl chloride, thiols and spiropyrans, etc., on the surface of carbon quantum dots. The process of acid treatment and surface passivation enhances the quantum yield of carbon quantum dots to the maximum of 55–60% which can be attained by the soft shell of passivation agents that surround the hard fluorescent core of the carbon quantum dots. Thus, one can achieve the improved fluorescence emissions.

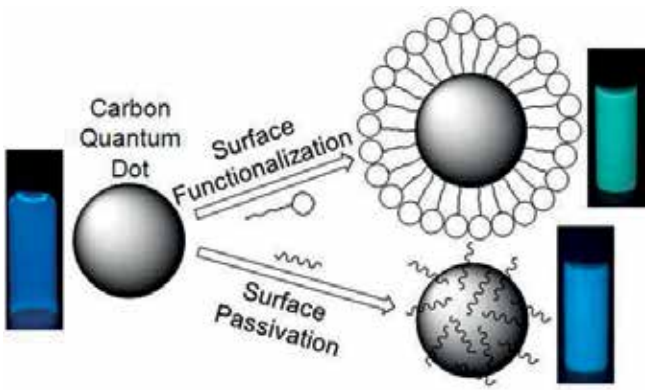

Figure 7. Graphical representation of surface passivation and functionalization of carbon quantum dots (reproduced with permission from [9]).

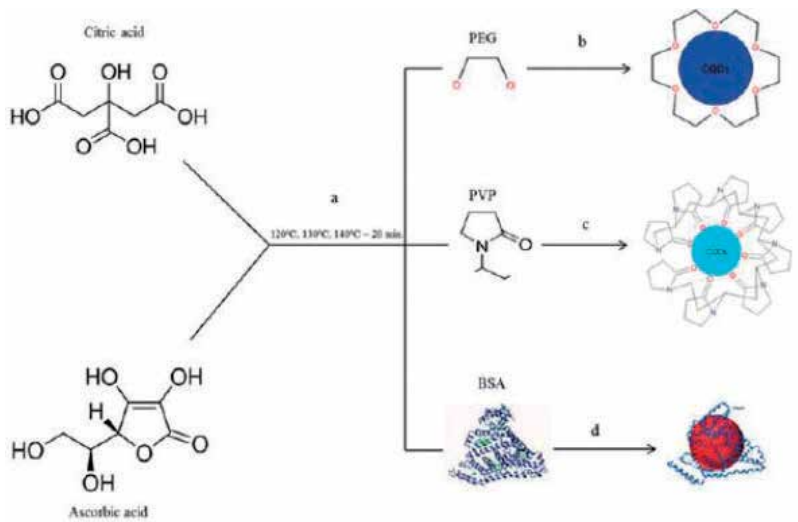

Figure 8. Carbon quantum dots synthesized from citric acid and ascorbic acid functionalized with (a) polyethylene glycol, (b) polyvinylpyrrolidone and (c) bovine serum albumin (reproduced with permission from [10]).

The later process such as surface functionalization (**Figure 8**) is important due to the introduction of functional groups like, carbonyl, carboxyl and amines which can impose various surface defects on carbon quantum dots. These defects can act as surface energy traps and lead to variations in fluorescence emission behavior of carbon quantum dots. Surface functionalization can be attained by surface chemistry or interactions like coordination, π-π interactions and covalent bonding, etc. Since the carbon quantum dots are oxygenous in nature, they are feasible to covalent bonding with functionalizing agents. Compared to bare carbon quantum dots, the functionalized one are excellent in photoreversibility, high stability, good biocompatibility and low toxicity.

Sometimes, few compounds may use as both passivating and functionalizing agent in which there is no need of additional modification steps during the postsynthetic treatments [11]. High emission quantum yield is essential for carbon quantum dots in order to overcome their counterparts such as organic dye molecules and inorganic semiconductor quantum dots. Other than surface passivation and functionalization, one can use the doping of carbon quantum dots with heteroatoms and nitrogen which can enhance the quantum yield up to 83%.

3. Characterization techniques

This section introduces some commonly used sophisticated techniques for the characterization of carbon quantum dots.

3.1. Microscopes

These are highly useful to analyze the surface morphology, particle size, structure and even more composition of carbon quantum dots (**Figure 9**). Few powerful microscopes such as high-resolution scanning electron microscope (HR-SEM), transmission electron microscope (TEM) and atomic force microscope (AFM) are able to resolve the structure of carbon quantum dots up to atomic resolution. The TEM specimen can be prepared by depositing a few drops of a diluted carbon dot solution onto a carbon-coated copper grid, followed by complete evaporation of the water solvent. Diameter of carbon quantum dots can be calculated by using Image J software resulting in the area of particles present: $A = \pi r^2$, $r = \sqrt{(A/\pi)}$ and $D = 2 \times r$. In this, A is the area of particles occupied, r is the radius of particles and D is the diameter of the particles [12]. The AFM specimen on a mica surface is usually prepared as similar to TEM analysis and both tapping and noncontact modes can be used for the AFM image measurement. SEM measurement is usually done for powder sample.

3.2. Diffraction techniques

Diffraction techniques are mostly used for structural determination (amorphous/crystalline) and average particle size analysis (crystallite size). Powder X-ray diffraction (XRD) and small-angle X-ray scattering (SAXS) are the commonly used techniques.

3.3. Spectroscopic techniques

Wide range of spectroscopic techniques can be used for the analysis of optical properties of carbon quantum dots. These techniques are useful for chemical state analysis (bonding or

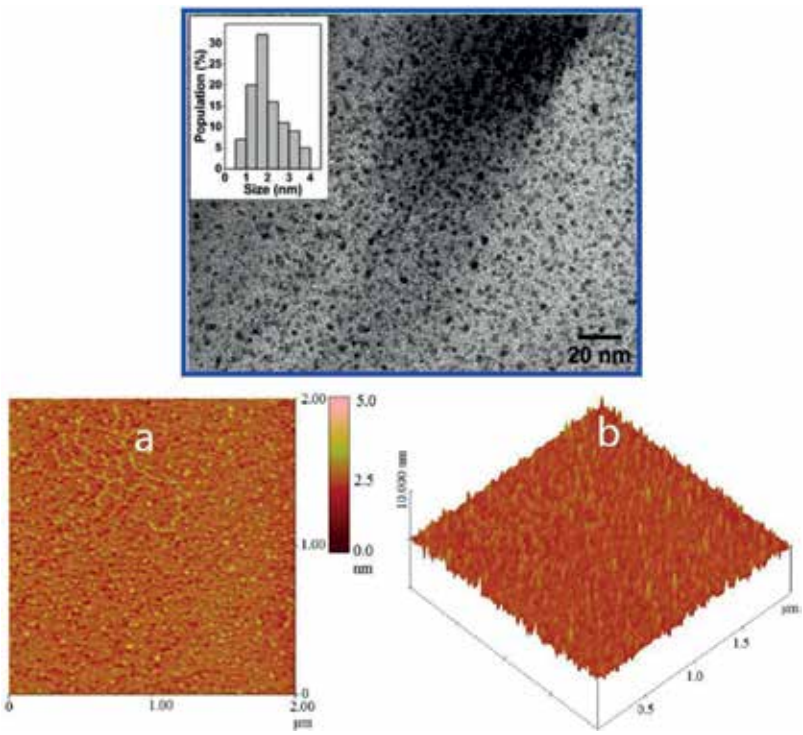

Figure 9. High-resolution TEM and AFM images of carbon quantum dots (reproduced with permission from [13]).

charge transfer among the atoms) and electronic structure (bandgap energy, level of impurity, band formation and possibilities of electronic transitions, etc.). This includes UV-visible-near IR absorption (both transmission and reflection mode), Fourier transform infrared (FT-IR), atomic absorption spectroscopy (AAS), nuclear magnetic resonance (NMR, both ^{1}H and ^{13}C NMR), Raman spectroscopy, X-ray photoelectron spectroscopy (XPS), Auger electron spectroscopy (AES) and electron spectroscopy (both spin and resonance, ESR and EPR) (**Figure 10**).

Carbon quantum dots typically show two optical absorption band (**Figure 11**) in the UV region with extended tail in the visible range. The two absorption shoulders are attributed to the π-π^* transitions in C=C bonds and n-π^* transition of C=O and other oxygenous carbon-containing functional groups.

3.4. Other techniques

Other than the abovementioned techniques, few techniques such as elemental analysis, zeta potential analyzer, dynamic light scattering analysis, fluorescence spectroscopy and time-correlated single photon counting (TCSPC) techniques are useful for the study of percentage of elemental composition, surface charge/dispersivity nature, hydrodynamic particle size (average particle size in solution medium), emission nature (wavelength of emission as well as emission quantum yield) and excited-state lifetime of carbon quantum dots, respectively.

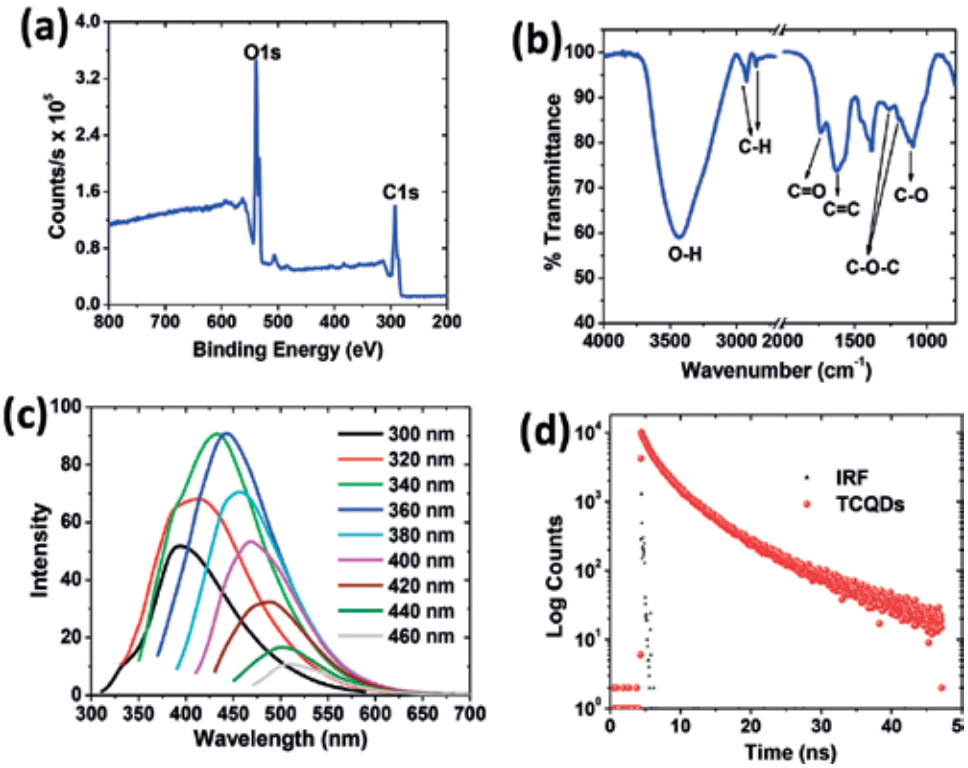

Figure 10. (a) XPS survey spectrum, (b) FTIR spectrum, (c) excitation-dependent emission spectra and (d) fluorescence decay of carbon dots prepared from tamarind (reproduced with permission from [14]).

3.5. Structure of carbon quantum dots

Fluorescent nanodots can be classified into four types (**Figure 12**) such as semiconductor quantum dots (SQDs), graphene quantum dots (GQDs), carbon quantum dots (CQDs) and carbon nanodots (CNDs).

SQDs are nanometer scale semiconductor crystals composed of group II metal ions as building blocks, and are defined as particles with physical dimensions smaller than the exciton Bohr radius (~7 nm). The excitons in these particles are confined in the spatial dimensions with quantized energy states. The best examples for SQDs are chalcogenide-based CdX QDs (X = S, Se, Te).

CNDs are amorphous quasispherical nanodots that lack in quantum confinement, and when the nanodots present as π-conjugated single sheet, i.e., a disk of graphene sheet in the size range of 2–10 nm, they are called GQDs.

CQDs are typically quasispherical nanoparticles comprising amorphous to nanocrystalline cores with predominantly graphitic or turbostratic carbon (sp2 carbon) or graphene and graphene oxide sheets fused by diamond-like sp3 hybridized carbon insertions. CQDs exhibit

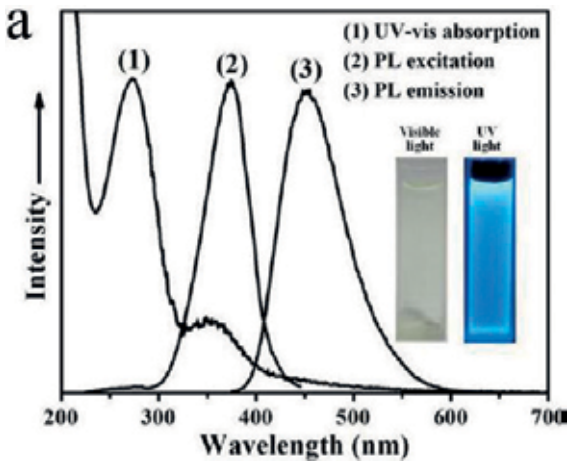

Figure 11. Absorption, excitation and emission bands of carbon quantum dots (reproduced with permission from [15]).

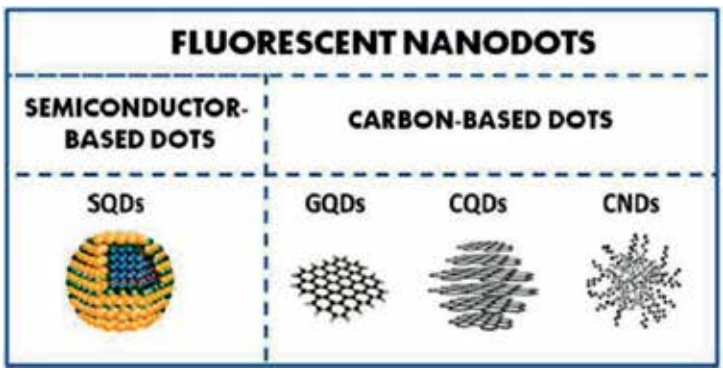

Figure 12. Classification of fluorescent nanodots: semiconductor quantum dots (SQDs), graphene quantum dots (GQDs), carbon quantum dots (CQDs) and carbon nanodots (CNDs) (reproduced with permission from [16]).

quantum confinement effect (size-dependent optical properties). Depending on the synthetic route, the oxygen content in the oxidized CQDs ranges from 5 to 50% (weight). Figure shows the difference among the various fluorescent nanodots with their plausible structure.

3.6. Fluorescent properties of carbon quantum dots

The exact origins of the fluorescence emission nature of carbon quantum dots remain debatable, and lot of research is ongoing to draw a clear picture of the fluorescence mechanism. For the two types of emissions observed for carbon quantum dots such as excitation dependent/excitation independent, two classes of mechanism have been proposed (**Figure 13**). The first class is bandgap transitions caused by π-domains, and the second class is associated with surface defects on carbon quantum dots [17].

The bandgap electronic transitions display strong absorption in the ultraviolet region, but weak emission and the surface defect-derived origin exhibits weak absorption in the near-UV

http://dx.doi.org/10.5772/intechopen.72723

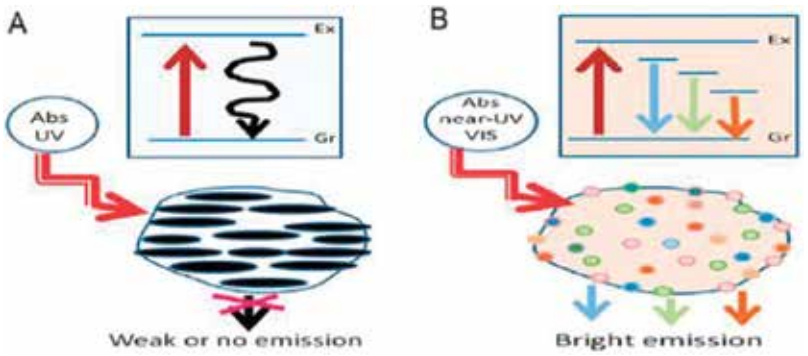

Figure 13. (a) Bandgap transitions caused by π-π domains and (b) transition caused by surface defects on carbon quantum dots (reproduced with permission from [18]).

and strong emission in the visible region [18]. In addition, due to surface passivation/functionalization, the defect becomes more stable to facilitate more effective radiative recombination of surface-confined electron and hole leads to more bright emissions.

The quantum yield (ϕ) of carbon dots can be calculated by using quinine sulfate as a reference compound in which ϕ value is reported as 0.53 [20]. For the measurement of ϕ, the optical density of tamarind carbon dots (TCDs) in water (η = 1.33) was fixed to less than 0.1 at the wavelength of 360 nm. Quinine sulfate is dissolved in 0.1 M H_2SO_4 (η = 1.33). For both the sample and reference, emission spectra were recorded at the same excitation at 360 nm. Fluorescence quantum yield (ϕ_F) for TCDs was calculated by using Eq. (1)

$$\phi_F = (A_R/A_S)(I_S/I_R)(\eta_S/\eta_R)^2 \phi_R \quad (1)$$

where the subscript 'S' refers to the samples, the subscript 'R' refers to quinine sulfate, A is the absorbance at the excitation wavelength, I is the integrated emission area and η is the solvent refraction index.

3.6.1. Enhanced fluorescent properties of carbon quantum dots by doping

Carbon quantum dots with enhanced emission quantum yield are necessary for better imaging of cells. Other than surface passivation, doping and codoping of heteroatoms such as nitrogen and sulfur imparts high quantum efficiency. Recently, it is reported that about 80–83% of quantum yield can be achieved by doping of carbon quantum dots with nitrogen and Mg ion. Doping with metal ions also improves the optical properties in addition with creation of novel functionalities. But one has to concern about the chance of increase in toxicity by doping with metal ion. Compared to metal ion doping, heteroatoms show better advantages due to their atomic size comparable with carbon quantum dots.

Owing to the close resemblance between nitrogen and carbon, the former one is preferentially used as a dopant for carbon quantum dots. Here, nitrogen can donate its electrons to carbon quantum dots, which change the electronic configuration leading to improvement in quantum yield. Nitrogen can be incorporated with carbon quantum dots either during the synthesis

via adding nitrogen-containing precursors or postsynthetic functionalization by agents built with nitrogen atom such as amine derivatives. Sulfur, phosphorous and boron atoms have also been as dopants in view of enhancing the fluorescence quantum yield of carbon quantum dots. Codoping of multiple heteroatoms in carbon quantum dots has gained more attention because of the synergistic effect between codoped heteroatoms and carbon quantum dots creating unique electronic structure [19].

4. Application of carbon quantum dots: bioimaging

Live cell bioimaging is becoming an increasingly popular tool for elucidation of biological mechanisms and is instrumental in unraveling the dynamics and functions of many cellular processes. Bioimaging is a method for direct visualization of biological processes in real time which often used to gain information on the 3D structure of the observed specimen from the outside, i.e., without physical interference. Bioimaging spans the observation of subcellular structures using light, fluorescence, electrons, ultrasound, X-ray, magnetic resonance and positrons as sources for imaging. It can be used to follow cellular processes, quantify ion or metabolite levels and measure interactions of molecules live. Appropriate tracers, e.g., specific fluorochromes, and advanced microscopic instruments, e.g., confocal laser scanning microscopes (CLSM, **Figure 14**), are a prerequisite for most applications.

4.1. Basic requirements for successful imaging

Imaging of biological processes in cells is highly dependent on the conditions provided. In view of avoiding the cellular stress, the environmental conditions should be nearly close to natural cellular ambience. Depending on the type of cell, the medium has to be changed. Generally, Dulbecco's modification of MEM (DMEM) and Roswell Park Memorial Institute (RPMI) are used as medium in which serum is added to provide all the essential nutrients for cell growth. Most of the mammalian cells grow between the pH 7.2–7.4. In bicarbonate-based medium, buffering is made by CO_2 whose withdrawal leads to cell growth. Considering

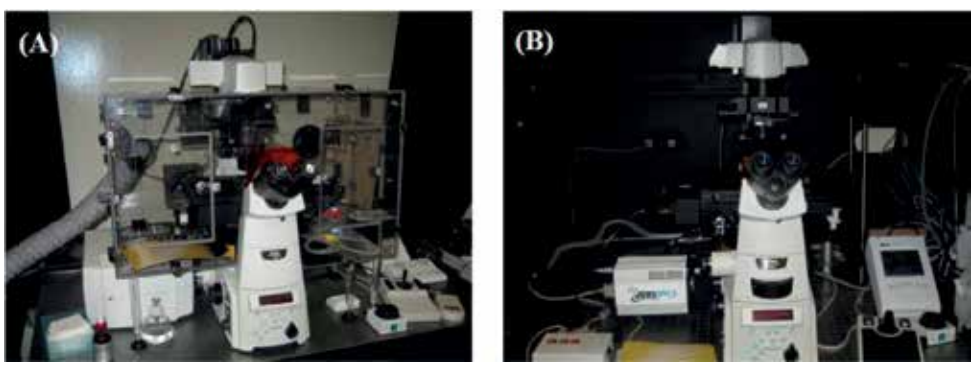

Figure 14. Bioimaging equipment with confocal facility (reproduced with permission from [21]).

cellular toxicity, compared to RPMI, DMEM is more prone to pH changes. So in view of minimizing the pH changes, (4-(2-hydroxyethyl)-1-piperazineethanesulfonic acid (HEPES), a zwitterionic organic chemical, buffering agent is generally used in imaging studies.

It is also necessary to maintain a physiological temperature to avoid the cellular detachment or changes in morphology during prolonged exposure of cells. Generally, 37°C is maintained by temperature regulatory system to avoid the rapid evaporation of the medium during prolonged imaging process. Phototoxicity and photobleaching are the two common challenges of live cell imaging. For instance, changes in membrane structure, cell death, vacuolation and blebbing are the possible effect of high-energy light radiation such as laser or ultraviolet light as a light source. This is because when the light radiation interacts with the cells, the rise in temperature due to excitation of light active molecules may stimulate the formation of free radicals (which may attack cellular membrane, lipids, etc.) and laser light may trigger heat stress (oxidative stress). So in order to reduce the oxidative stress and extreme changes in the temperature of medium, it is necessary to use minimum energy/low-intense light radiation source (**Figure 15**).

Loss of fluorescent signals during overtime of live cell imaging is called photobleaching. Photosensitivity of fluorescent dyes, the expression level of fluorescent proteins and size of imaging objects are the factors influencing the photobleaching process. Live cell imaging of small fluorescent vesicles is more susceptible to photobleaching compared to the image acquisition of larger fluorescent organelles like nucleus.

4.2. Role of carbon quantum dots in successful bioimaging

As discussed in the above section, the factors affecting the live cell bioimaging are cell viability, efficiency as well as resolution of confocal microscope and nature of the fluorescent component used. The last one such as a fluorescent contrast agent, which should possess biocompatibility and low biocytotoxicity, is necessary for straightforward fluorescence imaging of live cells and tissues. Depending on the encapsulation/functionalization, carbon quantum dots are either localized in the cell membrane or cytoplasm. Distribution of carbon quantum dots throughout the cytoplasm is also important for the high resolution of the image.

It is necessary to check the cytotoxic nature of carbon quantum dots before using it as a fluorescent contrast agent in bioimaging. For that, 3-(4,5-dimethyl-2-thiazolyl)-2,5-diphenyl-2H-tetrazolium bromide (MTT) assay is generally followed in which the type of interest cells

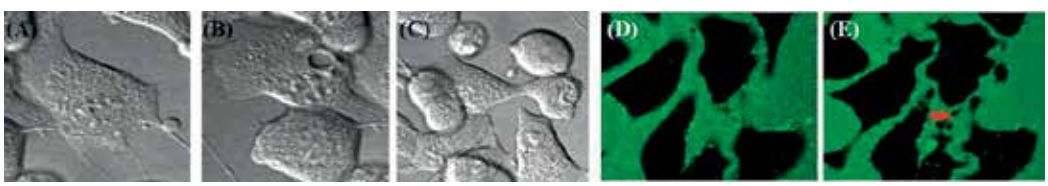

Figure 15. Morphological changes in BHK cells due to phototoxicity such as (A) spindle-shaped membranes, (B) vacuolation and (C) rounding of cells. As shown in (D), the BHK cells displayed normal cell shape before imaging but prolonged exposure to activation laser caused membrane blebbing (indicated by arrow) and cell death (E) (reproduced with permission from [21]).

was harvested and the cell concentration was adjusted to 1 × 104 cells/ml; cells were placed in a 96-well flat-bottom culture plates (180 μl/well) and incubated with various concentrations (0.78, 3.185, 12.5, 25.0, 50.0, 100.0 and 200.0 μl/ml) of carbon quantum dots (in 20 μl). All cultures were incubated for 72 h at 37°C and 5% CO_2 in a humidified incubator. Viable cell concentration was checked by MTT (3-(4,5-Dimethyl-2-thiazolyl)-2,5-diphenyl-2H-tetrazolium bromide) assay.

Similarly, for the study of intracellular uptake, the cell line (maintained in Dulbecco's modified Eagle's medium or DMEM supplemented with 10% fetal bovine serum or FBS) was trypsinized and seeded in tissue culture plates at 3 × 104 cells/well. After overnight incubation inside humidified 5% CO_2 incubator for cell attachment, the cells were treated with the carbon quantum dots at a final concentration of 200 μg/ml in 300 μl of media and incubated for 12 h. Prior to the imaging experiment, the cells were washed three times with fresh media.

This internalization of carbon quantum dots by the cells is a temperature-dependent process that happens at the ambient temperature (37°C). In general, carbon quantum dots likely translocate into the cell by endocytosis (i.e., process in which a substance gains entry into a cell without passing through the cell membrane resulting in the formation of an intracellular vesicle by virtue of the invagination of the plasma membrane and membrane fusion). The uptake of carbon quantum dots can be enhanced by coupling of carbon quantum with few membrane translocating peptides, so that it can facilitate the translocation process by overcoming the cell membrane barrier.

The excitation-dependent emission behavior of carbon quantum dots allows one to control and choose the excitation and emission wavelength. Carbon quantum dots with or without surface

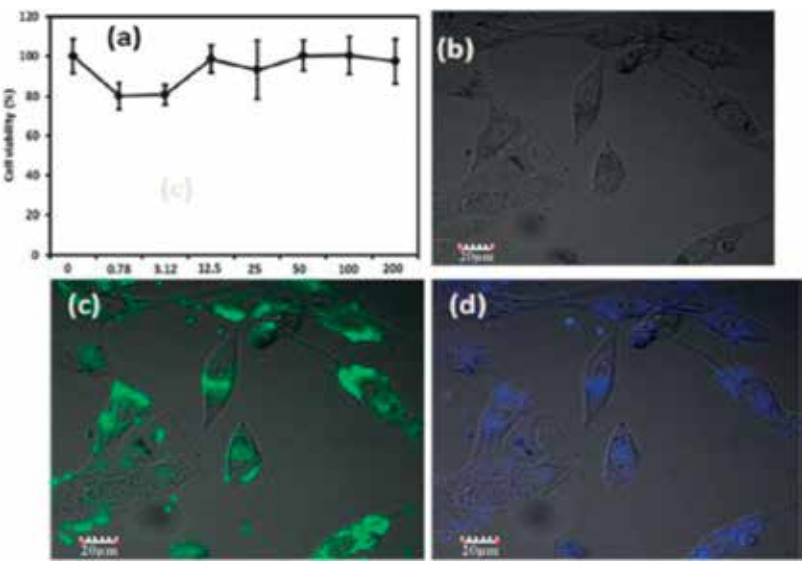

Figure 16. (a) Cell viability by MTT assay, (b) MG-63 cells under bright field, by excitation at (c) 488 nm and (d) 405 nm (reproduced with permission from [21]).

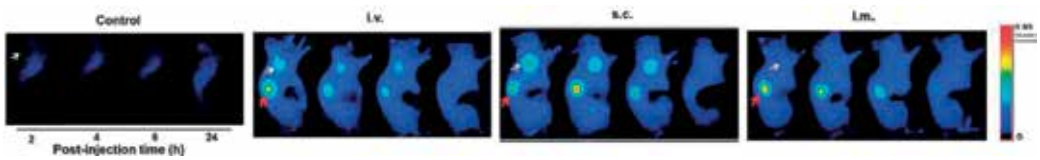

Figure 17. Fluorescence images of tumor-bearing mice (reproduced with permission from [21]).

passivation can be used as a labeling agent if it exhibits high emission quantum yield. The exact mechanism of carbon quantum dots uptake by cells remains to be elucidated, at the same time it is suggested that internalization with significant infiltration in to the cell nucleus. Carbon quantum dots can be used as fluorescent markers to probe various cellular organelles including lysosome/endosome, golgi body, mitochondria and endoplasmic reticulum (**Figure 16**). For *in vivo*, intravenous injection is used and the organs were harvested and sliced for imaging. Heart, liver, spleen, kidneys, lungs, brain and small intestine can be viewed (**Figure 17**). CQDs can be efficiently and rapidly excreted from the body after injection in different routes. Their blood clearance was quick—only 1 h postintravenous injection. The retention time is somewhat longer after subcutaneous and intramuscular injection. Finally, the imaging process is done under confocal microscope with laser excitation of 405 and 488 nm, and fluorescence was collected in blue and green region.

5. Concluding remarks

Since the discovery of carbon quantum dots in a decade back, they were used as fluorescent contrast agents for imaging of live cells. The defects present in carbon quantum dots play an important role in the fluorescence nature. They can be synthesized by various simple methods using variety of precursors. Unfortunately, the high emission quantum yield of carbon quantum dots still remains rare and is essential to use them in bioimaging application. Moreover, the well-defined composition and structure of carbon quantum dots are not explored well. The origin of fluorescence from carbon quantum dots is also still in debate which follows different mechanisms. Imaging of nucleus of cell using carbon quantum dots is not yet reported, and the sensitivity or selectivity of bioimaging needs to be improved. So, in future, it is necessary to prepare carbon quantum dots which will overcome the abovementioned unexplored properties, and deep research to be done for the use of bioconjugated carbon quantum dots as theranostics agents for targeted drug delivery and therapeutic applications.

Author details

Mariadoss Asha Jhonsi

Address all correspondence to: asha@bsauniv.ac.in

B. S. Abdur Rahman Crescent University, Chennai, India

References

[1] Xu XY, Ray R, Gu YL, Ploehn HJ, Gearheart L, Raker K, Scrivens WA. Electrophoretic analysis and purification of fluorescent single-walled carbon nanotube fragments. Journal of the American Chemical Society. 2014;**126**:12736-12737

[2] Demchenko AP, Dekaliuk MO. Novel fluorescent carbonic nanomaterials for sensing and imaging. Methods and Applications in Fluorescence. 2013;**1**:042001:17

[3] Deng J, Qiujun L, Mi N, Li H, Liu M, Mancai X, Tan L, Xie Q, Zhang Y, Yao S. Electrochemical synthesis of carbon nanodots directly from alcohols. Chemistry—A European Journal. 2014;**20**:4993-4999

[4] Li X, Wang H, Shimizu Y, Pyatenko A, Kawaguchi K, Koshizaki N. Preparation of carbon quantum dots with tunable photoluminescence by rapid laser passivation in ordinary organic solvents. Chemical Communications. 2011;**47**:932-934

[5] Zhu H, Wang X, Li Y, Wang Z, Yang F, Yang X. Microwave synthesis of fluorescent carbon nanoparticles with electrochemiluminescence properties. Chemical Communications. 2009:5118-5120

[6] Ray SC, Saha A, Jana NR, Sarkar R. Fluorescent carbon nanoparticle: Synthesis, characterization and bio-imaging application. Journal of Physical Chemistry C. 2009;**113**(43): 18546-18551

[7] Liang Q, Ma W, Shi Y, Li Z, Yang X. Easy synthesis of highly fluorescent carbon quantum dots from gelatin and their luminescent properties and applications. Carbon. 2013; **60**:421-428

[8] Lim SY, Shen W, Gao Z. Carbon quantum dots and their applications. Chemical Society Reviews. 2015;**44**:362

[9] Park Y, Yoo J, Lim B, Kwon W, Rheea S-W. Improving functionality of carbon nanodots: Doping and surface functionalization. Journal of Materials Chemistry A. 2016;**4**: 11582-11603

[10] Milosavljevic V, Moulick A, Kopel P, Adam V, Kizek R. Microwave Preparation of Carbon Quantum Dots with Different Surface Modification. Available from: web2.mendelu.cz/af_239_nanotech/J_Met_Nano/0314

[11] Dong YQ, Wang RX, Li H, Shao JW, Chi YW, Lin XM, Chen GN. Polyamine-functionalized carbon quantum dots for chemical sensing. Carbon. 2012;**50**:2810-2815

[12] https://www.youtube.com/watch?v=JQAZ--c9YfI

[13] Hua X, Yang X, Li G, Zhao C, Liao X. Green synthesis of fluorescent carbon dots for selective detection of tartrazine in food samples. Journal of Agricultural and Food Chemistry. 2015;**63**(30):6707-6714

[14] Jhonsi MA, Thulasi S. A novel fluorescent carbon dots derived from tamarind. Chemical Physics Letters. 2016;**661**:179-184

[15] Yue X, Chun-Jing T, Hong H, Chao-Qun S, Ya-Kun Z, Qun-Feng Y, Ai-Jun W. Green synthesis of fluorescent carbon quantum dots for detection of Hg^{2+}. Chinese Journal of Analytical Chemistry. 2014;**42**(9):1252-1258

[16] Cayuela A, Soriano ML, Carrillo-Carrión C, Valcárcel M. Semiconductor and carbon-based fluorescent nanodots: The need for consistency. Chemical Communications. 2016; **52**:1311

[17] Cao L, Meziani MJ, Sahu S, Sun Y-P. Photoluminescence properties of graphene versus other carbon nanomaterials. Accounts of Chemical Research. 2013;**46**:171-180

[18] Demchenko P, Dekaliuk MO. Novel fluorescent carbonic nanomaterials for sensing and imaging. Methods and Applications in Fluorescence. 2013;**1**:042001

[19] Xu Q, Kuang T, Liu Y, Cai L, Peng X, Sreeprasad TS, Zhao P, Yu Z, Li N. Heteroatom-doped carbon dots: Synthesis, characterization, properties, photoluminescence mechanism and biological applications. Journal of Materials Chemistry B. 2016;**4**:7204-7219

[20] Adams MJ, Highfield JG, Kirkbright GF. Determination of absolute fluorescence quantum efficiency of quinine bisulfate in aqueous medium by optoacoustic spectrometry. Analytical Chemistry. 1977;**49**:1850-1852

[21] Terence TTT, Clement K, Mary MLNg. Microscopy: Science, Technology, Applications and Education. In: Méndez-Vilas A. Díaz J. editors

Chapter 4

Bioimaging and Bio-Sensing Techniques for Lung Cancer Detection

Lulu Wang and Jinzhang Xu

Additional information is available at the end of the chapter

http://dx.doi.org/10.5772/intechopen.72724

Abstract

Early cancer detection and suitable treatment improve the 5-year survival rates of lung cancer significantly. Many cancer diagnostic approaches have been investigated, including mammography, magnetic resonance imaging, ultrasound, computerized tomography, positron emission tomography and biopsy. However, these techniques have some drawbacks such as expensive and time-consuming. Electromagnetic tomography (EMT) has been proposed as a promising diagnostic tool for lung cancer detection. In addition, developing label-free and cost-effective biosensors for target tumor markers detection have attracted attentions worldwide. This chapter reviews the recently developed EMT and bio-sensing techniques for early-stage lung cancer detection.

Keywords: biomedical imaging, biomarker, biosensor, lung cancer, nanoparticles, electromagnetic imaging

1. Introduction

Cancer is a major public health problem worldwide and lung cancer is the leading cause of cancer related deaths [1], which has much lower survival rate than other cancers such as breast cancer [2]. Early diagnosis of cancer is critical, which is expected to contribute significantly to improve the 5-year survival rates [3].

Many medical imaging methods have been intensively investigated for cancer detection, such as computed tomography (CT), magnetic resonance imaging (MRI), positron emission tomography (PET), and ultrasound. They have some drawbacks, such as, expensive and insufficient sensitivity to detect early-stage cancers. CT is the current gold standard medical imaging tool for diagnosis of lung disease, which able to study some features of biological objects such as lesion size, morphological lesion characterization, and follow-up of lesion growth. However, it

Type	Advantage	Disadvantage	Time
Chest X-ray	Reliable	Ionizing radiation, low sensitivity and specificity, sensitivity drops with tissue density increases	Few seconds
CT	Reliable	Expensive, false negative scans, low sensitivity, radiation risks	5 min
MRI	Reliable	Some types of cancers cannot be detected such as ductal and lobular carcinoma, expensive	40–60 min
PET	Reliable	Expensive, need for radioactive substance and sophisticated instrument, not suitable for subjects with other complications	90–240 min

Table 1. Conventional lung screening methods [9].

produces unsafe radiations which may increase cancer risk [4]. To solve this problem, LDCT with lower radiation has been applied for imaging of lung [5]. However, LDCT is associated with high false positive rate (up to 96.4%) [6], this may increase morbidity from unnecessary surgical treatment and also serious psychological burden to the subjects. 18F-Fluorodeoxyglucose PET/CT has been applied in oncological imaging without achieve reliable results [7, 8]. **Table 1** demonstrates the conventional medical imaging methods for lung diseases detection [9].

Recently, electromagnetic tomography (EMT) has been proposed as a promising tool for diagnosis of early-stage diseases such as lung and brain due to its low-cost and high-sensitivity [10].

Biopsy is another common method to distinguish cancerous and benign tissues, but it is expensive and requires trained physicians [11]. Cytokeratin 21-1 (CYFRA21-1) is a sensitive and specific marker for non-small cell lung cancer (NSCLC), especially in squamous cell carcinoma [12]. Biosensors are analytical devices to identify a target sequence by hybridization with complementary probes immobilized on a solid substrate. Biosensors have attracted increased attention due to they have many advantages such as low-cost, easy-to-use and easy to fabricate. Over the past few years, various nanoparticles have been applied to develop biosensors to increase the sensitivity. Other factors affect stability, reproducibility, and sensitivity, including electrode design and probe immobilization. However, biosensor-based approaches are time-consuming and less sensitive for the low marker concentrations at early stages [13]. Therefore, developing a high-sensitivity label-free method for rapid diagnosis of lung diseases is urgently needed.

This paper describes the recent achievements on bio-imaging and bio-sensing approaches for identifying lung cancer. Recent trends in EMT and bio-sensing methods are also reviewed. Several EMT sensor systems, including benefits, limitations, and future research directions are addressed. The rest of this paper is organized as follows: Section 2 describes biomarkers for lung cancer detection; Section 3 reviews biosensor techniques for target lung markers detection; Section 4 presents EMT approaches and measurement systems for imaging of biological tissues; Section 5 presents current trends and future perspectives.

2. Biomarkers for lung cancer detection

Genetic and proteomics-based biomarkers are the two major types of biomarkers, which can be identified in patients through tumor cells, urine, sputum, blood, or other body fluids [14]. **Table 2**

Type	Biomarker
Proteomic biomarkers	Annexin II, APOA1, carcinoembryonic antigen (CEA), carbohydrate antigen 125 (CA125), carbohydrate antigen 19-9 (CA19-9), cytokeratin fragment 21-1 (CYFRA21-1), CD59 glycoprotein, transthyretin (TTR), GM2 activator protein (GM2AP), haptoglobin-R 2, Ig-free light chain, neuron-specific enolase (NSE), nitrated ceruloplasmin, plasma kallikrein B1, ProGRP, retinol binding protein (RBP), squamous cell carcinoma (SCC), vascular endothelial growth factor (VEGF), TPA, tumor M2-pyruvate kinase, ENO1, Neuroendocrine markers, HER2, TAG-72.3, hnRNP-A2/B1, PCNA, CD34, c-erbB2, FHIT, CTNNB1, MUC1, Cyclin D1
Gene biomarkers	p53, p16, K-ras, microRNAs, miR-21, miR-210, miR-182, miR-31, miR-200b, miR-205, miR-183, miR-126-3p, miR-30a, miR-30d, miR-486-5p, miR-451a, miR-126-5p, miR-143, miR-145, miR-206, miR-133b, hsa-mir-155, hsa-let-7a-2, TERT, TERF2, POT1, MiR-449c

Table 2. Lung cancer markers.

demonstrates the current available biomarkers for lung cancer detection [15–35]. DNA biomarkers provide useful information on the process of tumor growth but they are insufficient sensitivity to detect early-stage tumors due to low concentrations of cancer markers [36]. Protein biomarkers are the major indicator of lung cancer, which can be classified as predictive and prognostic markers [37]. Predictive protein markers provide information of the particular therapeutic intervention, while prognostic protein markers offer the overall information of the subjects.

2.1. Proteomic biomarkers

Carcinoembryonic antigen (CEA) is the most common proteomic biomarker to distinguish malignant and benign tissues. Normally, serum level of CEA is about 2.5–5 ng/mL in healthy subjects [36]. Neuron-specific enolase (NSE) is a useful marker to investigate neuronal differentiation and to visualize the entire nervous and neuroendocrine systems. It exhibits calcium-dependent manner to perform its functions and needs magnesium as a cofactor for catalysis and stabilization of the dimer. Serum levels of NSE are related to some diseases such as Alzheimer, Huntington's chorea, neuroblastoma, and small cell lung cancer (SCLC). Compared to CEA, NSE is more sensitive and specific serum marker for SCLC [37]. Serum levels of NSE is higher than 9 ng/mL in patients with lung cancer. The subjects are considered with SCLS if the levels of NSE are higher than 35 ng/mL. The combination of NSE with other markers such as CYFRA 21-1 and CEA offered more effective and reliable detection in univariate and multivariate analysis of lung cancers.

Annexin II and enolase 1 (ENO1) are another common lung cancer biomarkers [38]. Chromogranin A (CgA) is an acidic glycoprotein, which belongs to the granin family of neuroendocrine secretory proteins. The threshold level of CgA is 50 ng/mL in patients with lung cancer. The serum levels of CgA were much higher in SCLC patients than that in the control groups, and there was an association between survival time and serum levels of CgA [39]. SCLC patients observed the best responses, but the percentage of this histological type composes of only 20% of all patients with lung cancer.

Cytokeratin-19 is the smallest human cytokeratin, which has been recommended as a high sensitive and specific marker for lung cancer, particularly in NSCLS. All adenocarcinomas tested have been positive for CYFRA 21-1, which was about 80% of patients with lung cancers [40]. The specificity and sensitivity of CYFRA 21-1 was found higher than the other protein markers such

as CEA and squamous cell carcinoma (SCC) to evaluate NSCLS. The combination of CYFRA 21-1 and other proteomic markers could increase the positive results of lung cancers [41].

However, it is difficult to detect lung cancer with the present markers because they are nonspecific indicators. To improve the accurate, many researchers have investigated the protein biomarker panel that consists of CEA, retinol binding protein (RBP), R1-antitrypsin (AAT), and squamous cell carcinoma (SCC) antigen for accurate disease detection [42]. The sensitivity was also improved by the biomarker panel consists of CEA and some specific biomarkers such as ENO1, SCC, NSE, CYFRA21-1 [43].

2.2. Gene biomarkers

The p53 protein is not normally detected in healthy lung tissue. Approximately 50% of NSCLC patients have been reported with p53 mutation, and the spectrum changed between 34% and 82%. p53 expression was observed in about 58% of lung cancer patients [44]. In addition, the poor correlation relationship between bcl-2 and p53 over-expression was observed in lung cancer patients [45].

p16 methylation was detected in lung cancer patients, in particularly, in chromate lung cancers and smokers. p16 methylation was found in approximately 21~51% of NSCLC patients, while p16 loss of heterozygosity was observed in about 54~100% of NSCLC patients [46, 47].

Ras genes are responsible for the cancer-causing activities of the Harvey (H-ras) and Kirsten (K-ras) sarcoma viruses. Ras mutations were discovered in lung cancer patients (20~25%) and patients with specific cancers (up to 90%). Approximately 60% of Ras mutations were confined to codon 12 of K-ras [48]. K-Ras mutation was also discovered in lung cancer patients (up to 78%) and in patients with NSCLS, pleural effusion, sputum, serum, and bronchoalveolar lavage fluid [49]. Some telomere-related genes such as telomerase reverse transcriptase (TERT), telomerase-associated factor 2 (TERF2) and protection of telomeres 1 (POT1) are affected on lung diseases [50, 51]. The telomeres are the territories of repetitive DNA that exist at the end of the chromosomes and are responsible for the protection of the chromosome ends.

Tumor growth is associated with silence and overexpression miRNAs, thus overexpress miRNAs has potential to become a useful clinical diagnostic tool for early lung diseases detection [52]. Seven upregulated (miR-21, miR-210, miR-182, miR-31, miR-200b, miR-205 and miR-183) and eight downregulated (miR-126-3p, miR-30a, miR-30d, miR-486-5p, miR-451a, miR-126-5p, miR-143 and miR-145) miRNAs have been investigated for lung marker detection [53]. Additionally, serum miR-206 and miR-133b have been considered as potential markers for lung carcinogenesis [51]. High hsa-mir-155 and low hsa-let-7a-2 can detect lung cancer correctly [54]. MiR-449c with the target marker c-Myc has been applied for NSCLS, which could suppress cancer cells growth in vivo [55].

3. Biosensors for lung cancer biomarker detection

Table 3 shows some recent developed biosensors for detecting lung tumor markers [56–72]. Fluorescence, interferometric, surface plasmon resonance biosensors (SPR), optrode-based

Biomarker	Capture agent	Sample	Transducer	Limit of detection	Linear range	Refs.
VEGF	VEGFreceptor-1	Serum	Electrochemical	-	10–70 pg/mL	[56]
	Aptamer	-	Electrochemical	15 nM	-	[57]
VEGF165	Aptamer	Serum	Fluorescent	-	1.25 pM–1.25 μM	[58]
LAG3 protein	Antibody	Plasma	SPRi-MALDITOP MS	-	-	[59]
TP53 gene	DNA		SPR and QCM	-	0.3–2 μM	[60]
COX-2	Polyclona antibody	Simulated blood sample	SPR	1.35×10^{-4} ng/mL	$3.64x10^{-4}$ – $3.64x10^{2}$ ng/mL	[61]
			Fluorescence	1.02×10^{-4} ng/mL	$7.46x10^{-4}$ – 7.46x10 ng/mL	
CEA	Antibody	Serum	SPR	-	-	[62]
p53 antibody	p53 antigen	Serum	Microcantilever biosensor	-	20 ng/mL– 20 μg/mL	[63]
p53	ssDNA	-	Electrochemiluminescence	-	-	[64]
p53 (wild & total)	ds-DNA & antibody	-	SPR	10.6 and 1.06 pM	-	[65]
EGFR	Aptamer	Serum	Optical	-	-	[66]
CA 19-9	Antibody	-	SPR	66.7 U/mL	-	[67]
ALCAM	Antibody	10% Serum	SPRi	6 ng/mL	-	[68]
ALCAM & hCG	antibody	10%Serum	SPRi	45–100 ng/mL		[69]
TAGLN2	Antibody	10%Serum	SPRi	3 ng/mL		[70]
DNA mutations	ssDNA	Serum	SPR	50 nM		[71]
K-ras point mutation	PNA	-	SPR	-		[72]

Table 3. The recently developed biosensors for target lung tumor markers detection.

fiber, evanescent wave fiber, and resonant mirror biosensors are the main types of optical biosensors. SPR-based sensors are more attractive for lung cancer markers detection, which can be classified as label-free and real-time affinity reaction detection systems. A high-precision optical system was developed to detect CYFRA21-1 based on magnetic enzyme-linked immunoassay [73]. Experimental results demonstrated that the proposed optical system has potential to become a powerful tool for rapid diagnostic of lung cancer marker with several advantages such as compactness, sensitive, and fast. A plasmonic optical fiber immunosensor was also developed by Ribaut et al. to detect cytokeratin [74]. Their research findings offered an important milestone towards the clinical detection of biomarkers in tissues.

Quartz is a popular crystal to develop analytic devices such as quartz crystal microbalance (QCM) sensor. QCM-based sensors can detect point mutation in lung cancer patients [75], which measure frequency changes in quartz crystal resonators based on adsorbate recognition,

and the mass changes caused by selective binding can be detected by the corresponding changes in crystals. The advantages of piezoelectric sensors include easy-to-use, cost-effective, and sensitive.

Electrochemical biosensors measure the changes of dielectric properties, dimension, shape and charge distribution while antibody–antigen complex occurred on the electrode surface [76]. Electrochemical biosensors offer high sensitivity and specificity for lung tumor markers detection. Electrochemical-based transducers generally consists of semiconductors and screen-printed electrodes for constructing the biosensors, which able to detect molecules such as proteins, antibody, DNA, antigen and heavy metal ions. The recent advances in electrochemical nano-biosensors offer promising for diagnosis of molecules with significant benefits in inexpensive, simplicity, reliability and fast-response, high sensitivity and specificity.

4. Electromagnetic inductance tomography for lung cancer detection

Electromagnetic tomography (EMT) has attracted many attentions worldwide since it offers a promising alternative to existing medical imaging methods, such as CT or MRI. The approach uses non-ionizing radiation in the low GHz region of the EM spectrum. EMT approach is a safe and cost-effective diagnostic tool and provides structural and functional imaging in one device. Various EMT approaches have been applied for biomedical imaging with particular focus on imaging lung, brain, heart, liver tissue and biological tissues [77–90]. **Table 4** presents some recently developed EMT systems.

Watson et al. [91] developed an EMT with phase-stable amplifier for biomedical application. The phase-stable amplifiers and the gradiometers configurations need not be mutually exclusive, and it was reported that the highest measurement precision could be achieved by utilizing both approaches. The EMT image quality would be improved by increasing the number of transmitters and receivers, however, such method also increases the cost, complexity and operation time of the EMT system. A rotational EMT system containing a transceiver RF coil was developed for biomedical application. Compared to the conventional systems, the proposed rotational system offered a better field penetration depth towards the center of image.

Semenov et al. [92] investigated the ability of EMT technology to detect brain stroke within a human head phantom (see **Figure 1**). The FDTD method was applied to solve the 3D

	Frequency	Sampling rate	Driving level	Phase noise (m^o)	Phase drift (m^o)	Linearity
Bath Medical system	10 MHz	100MS/s	30 mA	4	25	$R^2 = 0.9996$
Cardiff Mk2 system [82, 83]	10 MHz	120MS/s	100mArms	9	119	$R^2 = 0.9998$
Craz Mk2 system [84]	50 kHz~ 1.5 MHz	60M/s	Max. 200 mA	N/A	N/A	N/A
Glamorgan system [85]	10 MHz	N/A	N/A	N/A	27	N/A
Phillips system [81]	10 MHz	192kS/s	50mArms	12.5	102	$R^2 = 0.9878$

Table 4. Some recently developed EMT systems.

http://dx.doi.org/10.5772/intechopen.72724

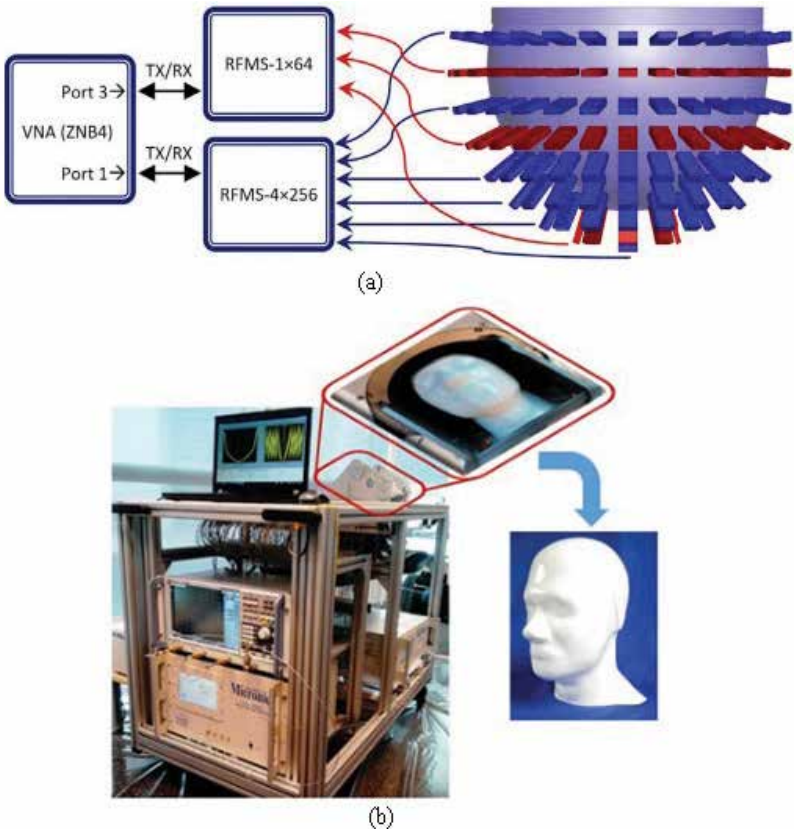

Figure 1. (**a**) The EMT system developed by Semenov et al. [92]; (**b**) a photograph of the EMT experimental setup using a head phantom for the imaging experiment.

electromagnetic problem, and the gradient-based approach was used to solve the inverse problem. The reconstructed images of head phantom are displayed in **Figure 2**. Their research findings demonstrated that EMT approach has the potential to become a useful tool for brain stroke detection in the future.

More recently, Wang et al. [93] proposed a single frequency EMT based approach for small lung tumor detection in human thorax models. As shown in **Figure 3**, the system made of 16 coils and each of them worked as both transmitter and receiver. The thorax model was located in the middle of the tank and was energized with a magnetic field generated by coils located outside of the tank wall. During data collection, the transmitting coils transmitted EM signals into the thorax, and the receiving coils measured the scattered magnetic fields from the thorax. A reconstructed image of the thorax model was obtained using the measured data.

Referring to **Figure 3**, if a point Q is located within the thorax model, the complex visibility data for any two coils can be obtained as [94]:

$$\overrightarrow{V_{i,j}} = < \vec{H}_{scat}\left(\vec{r}_i\right) \cdot \vec{H}^{*}_{scat}\left(\vec{r}_j\right) > \tag{1}$$

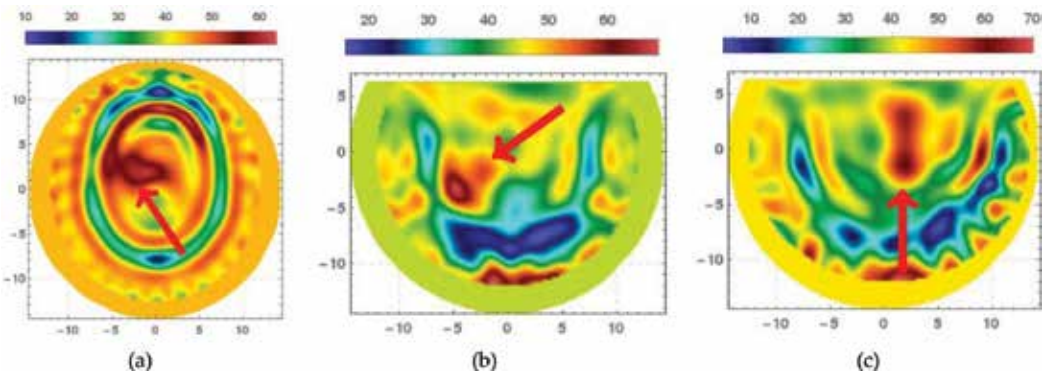

Figure 2. 3D reconstruction of the human head phantom featuring a h-stroke model. Three slices of the real part of the 3D ε-distribution, (**a**) axial slice; (**b**) coronal slice; (**c**) sagittal slice [92].

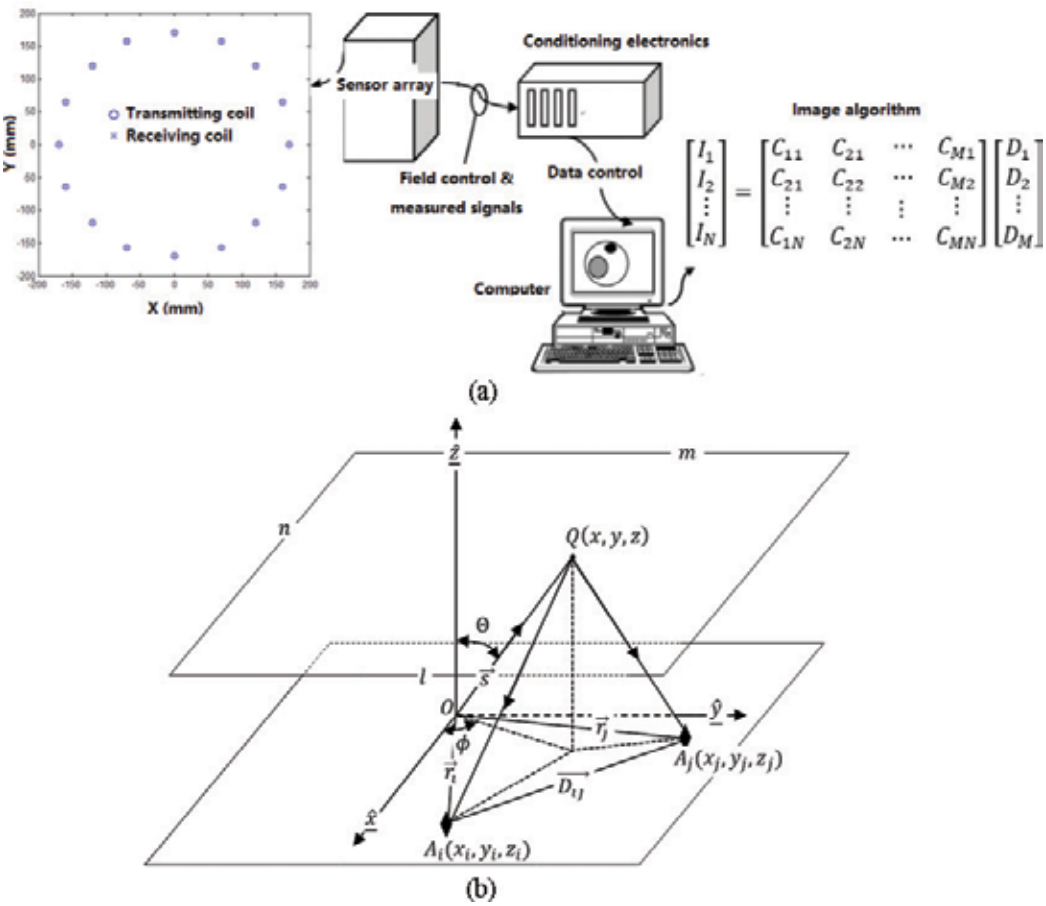

Figure 3. (**a**) The proposed EMT system by Wang et al. [93]; (**b**) a setup for any pair of coils.

Where $\vec{r}_i$ and $\vec{r}_j$ denote the coil locations, <> means the time average, **Table 3** lists all symbols and abbreviations. The total complex visibility data of N coils is $\vec{V} = \sum_i^N \overrightarrow{V_{i,j}}$, $N \geq 3$, $i \neq j$.

Define the intensity of thorax as:

$$I\left(\vec{s}\right) = \left(\frac{j\omega\mu_0}{4\pi}\right)^2 \left|\sigma(s) + j\omega\varepsilon_0\varepsilon_r'\right|^2 \overrightarrow{H_T}\left(\vec{s}\right) \cdot \overrightarrow{H_T^*}\left(\vec{s}'\right) \tag{2}$$

If all coils located at the same height, then a 2D image can be reconstructed:

$$\tilde{I}(l,m) = \iint V(u,v) e^{j2\pi\left(u_{ij}l + v_{ij}m\right)} du dv \tag{3}$$

Where $l = sin\theta cos\phi$ and $m = sin\theta sin\phi$, $u_{ij} = \left(\vec{x_j} - \vec{x_i}\right)/\lambda_0$ and $v_{ij} = \left(\vec{y_j} - \vec{y_i}\right)/\lambda_0$, λ_0 indicates the wavelength of free space (see **Figure 3**).

To study the feasibility of EMT for lung tumor detection, Wang et al. developed a numerical system using MATLAB software. The system made of 16 circular coils. The electric current density generated from transmitter was 1A/m^2. The finite element approach was applied to compute the voltage and the measured region was divided into triangular meshes. The working frequency was 2 MHz. The excitation current density $\vec{J_s}$ was simulated by:

$$\vec{J_s} = \nabla \times \left(\mu_0^{-1}\nabla \times \vec{A}\right) + j\omega\sigma\,\vec{A} \tag{4}$$

Eq. (4) can be rewritten from Maxwell's formulas by calculating the total electric field $\vec{E} = j\omega\,\vec{A} - \nabla\Omega$.

The scattered field measured by any receiver can be modeled as [95]:

$$\vec{H}_{scat}\left(\vec{r_0}\right) = \frac{-j}{4\pi\omega\mu_0}\int_V \left[\left(\vec{J_s}\cdot\nabla\right)\times\nabla + k_0^2\vec{J_M} + j\omega\mu_0\vec{J_S}\,\nabla\right] G\left(\vec{r},\vec{r_0}\right) dV \tag{5}$$

Where $\vec{J_s} = j\omega\varepsilon_0(\varepsilon_r - 1)\,\vec{E}$, $\overrightarrow{J_M} = j\omega\mu_0\left(\mu_r - 1\right)\overrightarrow{H_T}$, $\overrightarrow{H_T} = \vec{H}_{inc} + \vec{H}_{scat}$.

The following formula can be applied to compute the magnetic field:

$$\vec{H}_{scat}\left(\vec{r_0}\right) = \frac{k_0^2}{4\pi}\int_V \left[\left(a\,\vec{H} + b\left(\vec{H}\cdot\hat{r}\right)\hat{r}\right] G\left(\hat{r},\vec{r_0}\right) dV \tag{6}$$

Where $a = \mu_r\varepsilon_r - \frac{j\left(\mu_r - 1\right)}{k_0 R}\left(1 - \frac{j}{k_0 R}\right)$, $b = \left(\mu_r - 1\right)\left(-1 + \frac{3j}{k_0 R} + \frac{3}{(k_0 R)^2}\right)$, a and b are proportional to $1/R^2$(i.e. $k_0 R \ll 1$). Hence $k_0^2 a \cong -\left(\mu_r - 1\right)/R^2$ and $k_0^2 b \cong 3\left(\mu_r - 1\right)/R^2$.

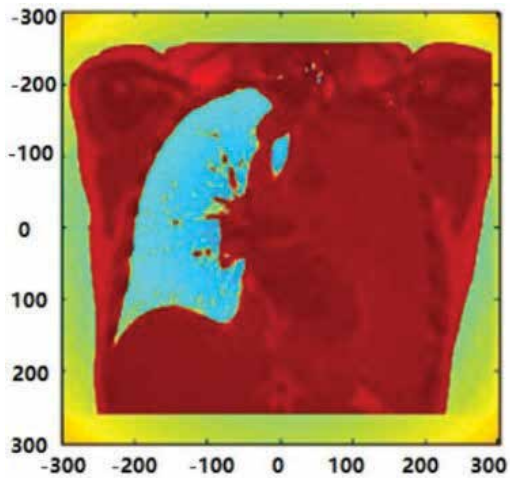

Figure 4. Simulation result of lung phantom obtained by Wang et al. [93].

Born Approximation was applied to solve the forward problem, thus Eq. (6) changes to [90]:

$$\vec{H}_{scat}\left(\vec{r_0}\right) = \frac{1}{4\pi}\int_V \frac{\mu_r - 1}{R^2}\left[-\vec{H} + 3\left(\vec{H}\cdot\hat{\underline{r}}\right)\hat{\underline{r}}\right] G\left(\vec{r}, \vec{r_0}\right) dV \tag{7}$$

Simulation result (see **Figure 4**) showed that various arbitrary shaped lung tumors with random sizes and locations could be identified in the thorax images. The proposed EMT approach offered crucial priority information that can be exploited to improve the capabilities of diagnostics methods. The advantages of the proposed method include simplified imaging processing due to the image quantity is proportional to the dielectric properties contrast.

5. Current trends and future perspectives

The current available lung screening approaches are effective but have some limitations as detailed above. EMT-based approaches have the potential to become an additional or alternative method to CT for lung disease detection. However, these techniques have some drawbacks, such as heavy computational imaging algorithm, difficult hardware systems for clinical applications, and limited spatial resolution. To solve these challenges, many researchers focused on developing a high dynamic hardware implementation system. Additionally, many investigators used more coils to improve the image quality. However, such method increases the mutual coupling signals between coils, which may reduce the detection accuracy. Moreover, the cost and complexities of the hardware implementation system also increased with increasing the number of coils. To solve this problem, a single coil could be applied to replace the multi-coil array. Recent research findings suggested that optimization of coil array configurations offer some potential benefits in high image resolution, low-cost, and operating time. The multiple-input-multiple-output technique may also help to reduce the complexity of the hardware system. In the future, more investigations of EMT technique should be taken to improve the image

algorithm and hardware implementation system with particular focus on the development of low-cost and compact RF coils and coil arrays to produce high quality images.

Developing biosensors with implementation of biomarkers have attracted many attentions from researchers worldwide in the past few years. Up to date, cancer markers are still in discovery stage and the current evidences are too restricted for early lung cancer detection. Proteomic biomarkers have been applied within a panel of protein biomarkers but they are not recommended to be used as individual biomarkers for lung cancer detection. Applying individual marker does not helpful for clinicians to obtain enough information of cancer tissue such as the stage of cancer, treatment and state of subject. The major problem of biosensor-based techniques is related to integration of lung cancer detection in primary healthcare. QCM-based biosensors are more suitable and reliable for clinical surgery compared to other biosensors. The limitations of biosensors include small target size, marker levels, the possibility of high non-specific binding in the case of serum or real patient samples. Recent research trends of nano-biosensor techniques for diagnosis of molecules offer great potential for early lung cancer detection, however, these techniques are not mature for clinical trials. Future investigations should be address directly to improve the selectivity, sensitivity, accuracy, and multiplexing capacity of biosensors.

Acknowledgements

The author gratefully acknowledges the financial supports from the National Natural Science Foundation of China (Grant No. 61701159), the Natural Science Foundation of Anhui Province (Grant No. 101413246), the Foundation for Oversea Master Project from Ministry of Education of the People's Republic of China (Grant No. 2160311028), and the start-up funding from the Hefei University of Technology (Grant No. 407037164).

Author details

Lulu Wang[1,2]* and Jinzhang Xu[3]

*Address all correspondence to: luluwang2015@hfut.edu.cn

1 School of Instrument Science and Opto-electronics Engineering, Hefei University of Technology, Hefei, China

2 Institute of Biomedical Technologies, Auckland University of Technology, Auckland, New Zealand

3 School of Electrical Engineering and Automation, Hefei University of Technology, Hefei, China

References

[1] World Health Organization. Cancer fact sheet 2017. Available at: http://www.who.int/mediacentre/factsheets/fs297/en/ [Accessed 22.09.2017.]

[2] Reed MF, Molloy M, Dalton EL, Howington JA. Survival after resection for lung cancer is the outcome that matters. American Journal of Surgery. 2004;**188**(5):598-602

[3] Chiang TA, Chen PH, PF W, Wang TN, Chang PY, Ko AM, Huang MS, Ko YC. Important prognostic factors for the long-term survival of lung cancer subjects in Taiwan. BMC Cancer. 2008;**8**(1):324

[4] Journy N, Rehel JL, Pointe HDL, Lee C, Brisse H, Chateil JF, et al. Are the studies on cancer risk from CT scans biased by indication|[quest]| elements of answer from a large-scale cohort study in France. British Journal of Cancer. 2015;**112**(11):1841-1842

[5] Aberle DR, Adams AM, Berg CD, Black WC, Clapp JD, Fagerstrom RM, Gareen IF, Gatsonis C, Marcus PM, Sicks JD, et al. Reduced lung-cancer mortality with low-dose computed tomographic screening. The New England Journal of Medicine. 2011;**365**:395-409

[6] Asselin MC, O'Connor JPB, Boellaard R, Thacker NA, Jackson A. Quantifying heterogeneity in human tumours using MRI and PET. European Journal of Cancer. 2012;**48**:447-455

[7] Chicklore S, Goh V, Siddique M, Roy A, Marsden PK, Cook GJR. Quantifying tumour heterogeneity in F-18-FDG PET/CT imaging by texture analysis. European Journal of Nuclear Medicine and Molecular Imaging. 2013;**40**:133-140

[8] Ippolito D, Capraro C, Guerra L, De Ponti E, Messa C, Sironi S. Feasibility of perfusion CT technique integrated into conventional (18) FDG/PET-CT studies in lung cancer patients: Clinical staging and functional information in a single study. European Journal of Nuclear Medicine and Molecular Imaging. 2013;**40**:156-165

[9] Ghosal R, Kloer P, Lewis KE. A review of novel biological tools used in screening for the early detection of lung cancer. Postgraduate Medical Journal. 2009;**85**(1005):358-363

[10] Griffiths H. Magnetic induction tomography. Measurement Science & Technology. 2011; **12**(8):1126-1131

[11] Cheng BY. Development of a chemiluminescent immunoassay for cancer antigen 15–3. Labeled Immunoass. Clinical Medicine. 2016;**23**:1348-1351

[12] Sone K, Oguri T, Nakao M, Kagawa Y, Kurowaka R, Furuta H, et al. Cyfra 21-1 as a predictive marker for non-small cell lung cancer treated with pemetrexed-based chemotherapy. Anticancer Research. 2017;**37**(2):935

[13] Wang L. Early diagnosis of breast cancer. Sensor. 2017;**17**:1572

[14] Zhang Y, Yang D, Weng L, Wang L. Early lung cancer diagnosis by biosensors. International Journal of Molecular Sciences. 2013;**14**(8):15479-15509

[15] Jia JW, Li KL, Wu JX, Guo SL. Clinical significance of annexin ii expression in human non-small cell lung cancer. Tumour Biology the Journal of the International Society for Oncodevelopmental Biology & Medicine. 2013;**34**(3):1767-1771

[16] Uribarri M, Hormaeche I, Zalacain R, Lopezvivanco G, Martinez A, Nagore D, et al. A new biomarker panel in bronchoalveolar lavage for an improved lung cancer diagnosis.

Journal of Thoracic Oncology Official Publication of the International Association for the Study of Lung Cancer. 2014;**9**(10):1504-1512

[17] Dong Y, Zheng X, Yang Z, Sun M, Zhang G, An X, et al. Serum carcinoembryonic antigen, neuron-specific enolase as biomarkers for diagnosis of nonsmall cell lung cancer. Journal of Cancer Research & Therapeutics. 2016;**12**:34

[18] Gube M, Taeger D, Weber DG, Pesch B, Brand P, Johnen G, et al. Performance of biomarkers smrp, ca125, and cyfra 21-1 as potential tumor markers for malignant mesothelioma and lung cancer in a cohort of workers formerly exposed to asbestos. Archives of Toxicology. 2011;**85**(3):185-192

[19] Huang Z, Jiang Z, Zhao C, Han W, Lin L, Liu A, et al. Simple and effective label-free electrochemical immunoassay for carbohydrate antigen 19-9 based on polythionine-au composites as enhanced sensing signals for detecting different clinical samples. International Journal of Nanomedicine. 2017;**12**:3049-3058

[20] So HJ, Hong SI, Lee JK, Chang YH, Kang SJ, Hong YJ. Comparison of the serum fibrin-fibrinogen degradation products with cytokeratin 19 fragment as biomarkers in patients with lung cancer. Biomedical Reports. 2014;**2**(5):737-742

[21] Li B, Lin H, Fan J, Lan J, Zhong Y, Yang Y, et al. Cd59 is overexpressed in human lung cancer and regulates apoptosis of human lung cancer cells. International Journal of Oncology. 2013;**43**(3):850-858

[22] Ding H, Liu J, Xue R, Zhao P, Qin Y, Zheng F, et al. Transthyretin as a potential biomarker for the differential diagnosis between lung cancer and lung infection. Biomedical Reports. 2014;**2**(5):765

[23] Potprommanee L, Ma HT, Shank L, Juan YH, Liao WY, Chen ST, et al. Gm2-activator protein: A new biomarker for lung cancer. Journal of Thoracic Oncology. 2015;**10**(1):102-109

[24] Wang B, He YJ, Tian YX, Yang RN, Zhu YR, Qiu H. Clinical utility of haptoglobin in combination with cea, nse and cyfra21-1 for diagnosis of lung cancer. Asian Pacific Journal of Cancer Prevention. 2014;**15**(22):9611-9614

[25] Kormelink TG, Powe DG, Kuijpers SA, Abudukelimu A, Fens MHAM, Pieters EHE, et al. Immunoglobulin free light chains are biomarkers of poor prognosis in basal-like breast cancer and are potential targets in tumor-associated inflammation. Oncotarget. 2014;**5**(10):3159-3167

[26] Zhou Y, Chen WZ, Peng AF, Tong WL, Liu JM, Liu ZL. Neuron-specific enolase, histopathological types, and age as risk factors for bone metastases in lung cancer. Tumour Biology the Journal of the International Society for Oncodevelopmental Biology & Medicine. 2017;**39**(7):1010428317714194

[27] Martin Mateo MC, Bustamante BJ, Font AI. Serum copper, ceruloplasmin, lactic-dehydrogenase and alpha 2-globulin in lung cancer. Biomedicine/[publiée pour l'A.A.I.C.I.G.]. 1979; **31**(3):66-68

[28] Chee J, Naran A, Misso NL, Thompson PJ, Bhoola KD. Expression of tissue and plasma kallikreins and kinin b1 and b2 receptors in lung cancer. Biological Chemistry. 2008;**389**(9): 1225-1233

[29] Winther B, Reubsaet JL. Determination of the small cell lung cancer associated biomarker pro-gastrin-releasing peptide (progrp) using lc-ms. Journal of Separation Science. 2015;**30**(2): 234-240

[30] Wang T, Liang Y, Thakur A, Zhang S, Liu F, Khan H, et al. Expression and clinicopathological significance of s100 calcium binding protein a2 in lung cancer patients of chinese han ethnicity. Clinica Chimica Acta. 2017;**464**:118-122

[31] Wang T, Zhang L, Tian P, Tian S. Identification of differentially-expressed genes between early-stage adenocarcinoma and squamous cell carcinoma lung cancer using meta-analysis methods. Oncology Letters. 2017;**13**(5):3314

[32] Loftus TJ, Thomson AJ, Kannan KB, Alamo IG, Ramos HN, Whitley EE, et al. Effects of trauma, hemorrhagic shock, and chronic stress on lung vascular endothelial growth factor. Journal of Surgical Research. 2017;**210**:15

[33] Foa P, Fornier M, Miceli R, Seregni E, Santambrogio L, Nosotti M, et al. Tumour markers cea, nse, scc, tpa and cyfra 21.1 in resectable non-small cell lung cancer. Anticancer Research. 1999;**19**(4C):3613

[34] Liu J, Zhu H, Jiang H, Zhang H, Wu D, Hu X, et al. Tumor m2 pyruvate kinase in diagnosis of nonsmall cell lung cancer: A meta-analysis based on Chinese population. Journal of Cancer Research & Therapeutics. 2015;**11**(5):c104

[35] Indovina P, Marcelli E, Pentimalli F, Tanganelli P, Tarro G, Giordano A. Mass spectrometry-based proteomics: The road to lung cancer biomarker discovery. Mass Spectrometry Reviews. 2013;**32**(2):129-142

[36] Ye F, Shi MY, Zhao S. Noncompetitive immunoassay for carcinoembryonic antigen in human serum by microchip electrophoresis for cancer diagnosis. Clinica Chimica Acta. 2010;**411**:1058

[37] Schneider J, Philipp MVelcovsky HG, Morr H, Katz N. Pro-gastrin-releasing peptide (progrp), neuron specific enolase (NSE), carcinoembryonic antigen (CEA) and cytokeratin 19-fragments (cyfra 21-1) in patients with lung cancer in comparison to other lung diseases. Anticancer Research. 2003;**23**(2A):885

[38] Ho JA, Chang HC, Shih NY, Wu LC, Chang YF, Chen CC, et al. Diagnostic detection of human lung cancer-associated antigen using a gold nanoparticle-based electrochemical immunosensor. Analytical Chemistry. 2010;**82**(14):5944-5950

[39] Songnan Q, Mo H, Huan T, Yudong L, Min J, Lin W, et al. Autoantibodies to chromogranin a are potential diagnostic biomarkers for non-small cell lung cancer. Tumor Biology. 2015;**36**(12):9979-9985

[40] Holdenrieder S, Wehnl B, Hettwer K, Simon K, Uhlig S, Dayyani F. Carcinoembryonic antigen and cytokeratin-19 fragments for assessment of therapy response in non-small cell lung cancer: A systematic review and meta-analysis. British Journal of Cancer. 2017; **116**(8):1037

[41] Chu XY, Hou XB, Song WA, Xue ZQ, Wang B, Zhang LB. Diagnostic values of scc, cea, cyfra21-1 and nse for lung cancer in patients with suspicious pulmonary masses: A single center analysis. Cancer Biology & Therapy. 2011;**11**(12):995-1000

[42] Jr PE, Campa MJ, Gottlin EB, Kusmartseva I, Guan XR, Nd HJ. Panel of serum biomarkers for the diagnosis of lung cancer. Journal of Clinical Oncology Official Journal of the American Society of Clinical Oncology. 2007;**25**(35):5578

[43] Bennett WP, Hussain SP, Vahakangas KH, Khan MA, Shields PG, Harris CC. Molecular epidemiology of human cancer risk: Gene–environment interactions and p53 mutation spectrum in human lung cancer. Journal of Pathology. 1999;**187**(1):8-18

[44] Zereu M, Vinholes JJ, Zettler CG. P53 and bcl-2 protein expression and its relationship with prognosis in small-cell lung cancer. Clinical Lung Cancer. 2003;**4**(5):298-302

[45] Kim DH, Nelson HH, Wiencke JK, Zheng S, Christiani DC, Wain JC, et al. P16(ink4a) and histology-specific methylation of cpg islands by exposure to tobacco smoke in non-small cell lung cancer. Cancer Research. 2001;**61**(8):3419-3424

[46] Kondo K, Takahashi Y, Hirose Y, Nagao T, Tsuyuguchi M, Hashimoto M, et al. The reduced expression and aberrant methylation of p16(ink4a) in chromate workers with lung cancer. Lung Cancer. 2006;**53**(3):295

[47] Belinsky SA, Klinge DM, Liechty KC, March TH, Kang T, Gilliland FD, et al. Plutonium targets the p16 gene for inactivation by promoter hypermethylation in human lung adenocarcinoma. Carcinogenesis. 2004;**25**(6):1063

[48] Kovalchuk O, Naumnik W, Serwicka A, Chyczewska E, Niklinski J, Chyczewski L. K-ras codon 12 mutations may be detected in serum of patients suffering from adeno- and large cell lung carcinoma. A preliminary report. Folia Histochemica et Cytobiologica. 2001;**39**:70

[49] Iii HH, Cawthon R, He X, Chanock S, Lan Q. Genetic variation in telomere maintenance genes, telomere length, and lung cancer susceptibility. Lung Cancer. 2009;**66**(2):157-161

[50] Hu Z, Yang Z, Tian T, Liang J, Jin G, Shen H. Association between microrna polymorphisms, expressions, lung cancer development and prognosis. Biomedicine & Pharmacotherapy. 2009;**63**:322

[51] Schmitt MJ, Margue C, Behrmann I, Kreis S. Mirna-29: A microrna family with tumor-suppressing and immune-modulating properties. Current Molecular Medicine. 2013;**13**: 572-585

[52] Dacic S. Molecular prognostic markers of lung cancer. In: Molecular Pathology of Lung Cancer. New York: Springer; 2012

[53] JJ W, Yang T, Li X, Yang QY, Liu R, Huang JK, Li YQ, Yang CF, Jiang YG. Alteration of serum mir-206 and mir-133b is associated with lung carcinogenesis induced by 4-(methylnitrosamino)-1-(3-pyridyl)-1-butanone. Toxicology and Applied Pharmacology. 2013;**267**:238-2463

[54] Yanaihara N, Caplen N, Bowman E, Seike M, Kumamoto K, Yi M, et al. Unique microrna molecular profiles in lung cancer diagnosis and prognosis. Cancer Cell. 2006;**9**(3):189-198

[55] Miao LJ, Huang SF, Sun ZT, Gao ZY, Zhang RX, Liu Y, Wang J. Mir-449c targets C-myc and inhibits nsclc cell progression. FEBS Letters. 2013;**587**:1359-1365

[56] Sezginturk MK. A new impedimetric biosensor utilizing vegf receptor-1 (flt-1): Early diagnosis of vascular endothelial growth factor in breast cancer. Biosensors & Bioelectronics. 2011;**26**:4032-4039

[57] Nonaka Y, Abe K, Ikebukuro K. Electrochemical detection of vascular endothelial growth factor with aptamer sandwich. Electrochemistry. 2012;**80**:363-366

[58] Cho H, Yeh EC, Sinha R, Laurence TA, Bearinger JP, Lee LP. Single-step nanoplasmonic vegf(165) aptasensor for early cancer diagnosis. ACS Nano. 2012;**6**:7607-7614

[59] Remy-Martin F, El Osta M, Lucchi G, Zeggari R, Leblois T, Bellon S, Ducoroy P, Boireau W. Surface plasmon resonance imaging in arrays coupled with mass spectrometry (supra-ms): Proof of concept of on-chip characterization of a potential breast cancer marker in human plasma. Analytical and Bioanalytical Chemistry. 2012;**404**:423-432

[60] Altintas Z, Uludag Y, Gurbuz Y, Tothill IE. Surface plasmon resonance based immunosensor for the detection of the cancer biomarker carcinoembryonic antigen. Talanta. 2011;**86**:377-383

[61] Noah NM, Mwilu SK, Sadik OA, Fatah AA, Arcilesi RD. Immunosensors for quantifying cyclooxygenase 2 pain biomarkers. Clinica Chimica Acta. 2011;**412**:1391-1398

[62] Ladd J, Lu H, Taylor AD, Goodell V, Disis ML, Jiang S. Direct detection of carcinoembryonic antigen autoantibodies in clinical human serum samples using a surface plasmon resonance sensor. Colloids and Surfaces B. 2009;**70**:1-6

[63] Zhou Y, Wang Z, Yue W, Tang K, Ruan W, Zhang Q, Liu L. Label-free detection of p53 antibody using a microcantilever biosensor with piezoresistive readout. IEEE Sensors. 2009. DOI: 10.1109/ICSENS.2009.5398558

[64] Wang X, Zhang X, He P, Fang Y. Sensitive detection of p53 tumor suppressor gene using an enzyme-based solid-state electrochemiluminescence sensing platform. Biosensors & Bioelectronics. 2011;**26**:3608-3613

[65] Wang Y, Zhu X, Wu M, Xia N, Wang J, Zhou F. Simultaneous and label-free determination of wild-type and mutant p53 at a single surface plasmon resonance chip preimmobilized with consensus dna and monoclonal antibody. Analytical Chemistry. 2009;**81**:8441-8446

[66] Ilyas A, Asghar W, Allen PB, Duhon H, Ellington AD, Iqbal SM. Electrical detection of cancer biomarker using aptamers with nanogap break-junctions. Nanotechnology. 2012;**23**. DOI: 10.1088/0957-4484/23/27/275502

[67] Chung JW, Bernhardt R, Pyun JC. Additive assay of cancer marker ca 19–9 by spr biosensor. Sensors and Actuators B: Chemical. 2006;**118**:28-32

[68] Ladd J, Taylor AD, Piliarik M, Homola J, Jiang S. Label-free detection of cancer biomarker candidates using surface plasmon resonance imaging. Analytical and Bioanalytical Chemistry. 2009;**393**:1157-1163

[69] Yokotani T, Koizumi T, Taniguchi R, Nakagawa T, Isobe T, Yoshimura M, et al. Expression of α and β genes of human chorionic gonadotropin in lung cancer. International Journal of Cancer Journal International Du Cancer. 1997;**71**(4):539-544

[70] Piliarik M, Bockova M, Homola J. Surface plasmon resonance biosensor for parallelized detection of protein biomarkers in diluted blood plasma. Biosensors & Bioelectronics. 2010;**26**:1656-1661

[71] Carrascosa LG, Calle A, Lechuga LM. Label-free detection of DNA mutations by spr: Application to the early detection of inherited breast cancer. Analytical and Bioanalytical Chemistry. 2009;**393**:1173-1182

[72] Sato Y, Fujimoto K, Kawaguchi H. Detection of a k-ras point mutation employing peptide nucleic acid at the surface of a spr biosensor. Colloids and Surfaces B. 2003;**27**:23-31

[73] Piliarik M, Vaisocherova H, Homola J. Surface plasmon resonance biosensing. Methods in Molecular Biology. 2009;**503**:65-88

[74] Wang B, Liu JT, Luo JP, Wang MX, Shu-Xue QU, Cai XX. A three-channel high-precision optical detecting system for lung cancer marker cyfra21-1. Journal of Optoelectronics·Laser. 2013;**24**(9):1849-1854

[75] Ribaut C, Loyez M, Larrieu JC, Chevineau S, Lambert P, Remmelink M, Wattiez R, Christophe CC. Cancer biomarker sensing using packaged plasmonic optical fiber gratings: Towards in vivo diagnosis. Biosensors & Bioelectronics. 2016;**92**:449-456

[76] Sun W, Song W, Guo X, Wang Z. Ultrasensitive detection of nucleic acids and proteins using quartz crystal microbalance and surface plasmon resonance sensors based on target-triggering multiple signal amplification strategy. Analytica Chimica Acta. 2017;**978**:42

[77] Chen M, Hou C, Huo D, Yang M, Fa H. A highly sensitive electrochemical DNA biosensor for rapid detection of cyfra21-1, a marker of non-small cell lung cancer. Analytical Methods. 2015;**7**(22):9466-9473

[78] Marmugi L, Renzoni F. Optical magnetic induction tomography of the heart. Scientific Reports. 2016;**6**:23962

[79] Hu G, Cressman E, He B. Magnetoacoustic imaging of human liver tumor with magnetic induction. Applied Physics Letters. 2011;**98**(2):681

[80] Żywica AR. Magnetoacoustic tomography with magnetic induction for biological tissue imaging: Numerical modelling and simulations. Archives of Electrical Engineering. 2016; **65**(1):141-150

[81] Watson S, Williams RJ, Griffiths H, Gough W, Morris A. Magnetic induction tomography: Phase versus vector-voltmeter measurement techniques. Physiological Measurement. 2003;**24**(2):555

[82] Vauhkonen M, Hamsch M, Igney CH. A measurement system and image reconstruction in magnetic induction tomography. Physiological Measurement. 2008;**29**(6):S445

[83] Igney CH, Watson S, Williamson SJ, Griffiths H, Dössel O. Design and performance of a planar-array MIT system with normal sensor alignment. Physiological Measurement. 2005;**26**(2):S263-S278

[84] Patz R, Watson S, Ktistis C, Hamsch M, Peyton AJ. Performance of a FPGA-based direct digitising signal measurement module for MIT. Journal of Physics: Conference Series. 2010;**224**:1-4

[85] Scharfetter H, Kostinger A, Issa S. Hardware for quasi-single-shot multifrequency magnetic induction tomography (MIT): The Graz Mk2 system. Physiological Measurement. 2008;**29**:S431

[86] Wei H, Soleimani M. Electromagnetic tomography for medical and industrial applications: Challenges and opportunities. Proceedings of the IEEE. 2013;**101**(3):559-565

[87] Ma L, Soleimani M. Magnetic induction tomography methods and applications: A review. Measurement Science & Technology. 2017;**28**(7)

[88] Feldkamp JR, Quirk S. Optically tracked, single-coil, scanning magnetic induction tomography. Journal of Medical Imaging. 2017;**4**(2):023504

[89] Feldkamp JR. Single-coil magnetic induction tomographic three-dimensional imaging. Journal of Medical Imaging. 2015;**2**(1):013502

[90] Xiao Z, Tan C, Dong F. Effect of inter-tissue inductive coupling on multi-frequency imaging of intracranial hemorrhage by MIT. Measurement Science & Technology. 2017;**28**(8)

[91] Watson S, Wee HC, Griffiths H, Williams RJA. Highly phase-stable differential detector amplifier for magnetic induction tomography. Physiological Measurement. 2011;**32**:917

[92] Semenov S, Hopfer M, Planas R, Hamidipour A, Henriksson T. Electromagnetic tomography for brain imaging: 3D reconstruction of stroke in a human head phantom. IEEE Antenna Measurements & Applications. 2017:1-4

[93] Wang L, Al-Jumaily AM. Imaging of lung structure using holographic electromagnetic induction. IEEE Access. 2017;**PP**(99):1

[94] Wang L, Al-Jumaily AM, Simpkin R. Imaging of 3-D dielectric objects using far-field holographic microwave imaging technique. Progress in Electromagnetics Research B. 2014;**61**:135-147

[95] Levanda R, Leshem A. Synthetic aperture radio telescopes. IEEE Signal Process. 2010;**27**:14-29

Chapter 5

Research Status and Prospect for CT Imaging

Yi Liu

Additional information is available at the end of the chapter

http://dx.doi.org/10.5772/intechopen.73032

Abstract

Computed tomography (CT) is a very valuable imaging method and plays an important role in clinical diagnosis. As people pay more and more attention to radiation doses these years, decreasing CT radiation dose without affecting image quality is a hot direction for research of medical imaging in recent years. This chapter introduces the research status of low-dose technology from following aspects: low-dose scan implementation, reconstruction methods and image processing methods. Furthermore, other technologies related to the development tendency of CT, such as automatic tube current modulation technology, rapid peak kilovoltage (kVp) switching technology, dual-source CT technology and Nano-CT, are also summarized. Finally, the future research prospect are discussed and analyzed.

Keywords: low-dose CT, spectral CT, dual-source CT, nano-CT, image reconstruction, image enhancement

1. Introduction

Computed tomography (CT), also referred to as computerized axial tomography (CAT), is a noninvasive and high-tech medical examination that uses X-ray to produce cross-sectional images of the body. With these cross-sectional images, doctors can visualize anatomical structures and tissues inside the body, like small nodules or tumors, which they cannot see with a plain film X-ray. This does not violate the outer surface of the body, in other words, non-invasively. Since the first practical CT instrument developed in the 1970s by Godfrey N. Hounsfield (he received the Nobel Prize in 1979), X-ray CT technology has developed dramatically and become a standard imaging procedure for virtually all parts of the body in thousands of facilities throughout the world. Nowadays, CT scanners are used for a variety of reasons, for example, diagnostic and treatment planning, therapeutic and interventional purposes.

Generally, X-ray CT go through six generations [1]. The first generation, with parallel-beam geometry, only has single X-ray source and single X-ray detector cell to collect all the data for a single slice. The projection data were acquired in approximately 5 minutes, and the tomographic image was reconstructed in approximately 20 minutes. The second generation scanner uses fan-beam geometry and has multiple detectors, thus multiple projections obtained during each traversal past the patient with the acquisition time for one tomogram 1 minute. Both the first and second generation CT works in a translate/rotate model. In the third generation CT, a fan beam of X-rays is used and a curved detector array consisting of several hundred independent detectors is mechanically coupled to the X-ray source, and both rotate in synchrony, that is, rotate/rotate mode. The fourth generation CT also uses fan-beam geometry but with ring of stationary detections array. Only the X-ray tube revolves around the patient, namely, rotate/stationary mode. For third and fourth generation scanners, acquisition times are similar, less than 10 seconds for one tomogram. In the fifth-generation CT, the detector array remains stationary, while a high-energy electron beams is electronically swept along a semicircular tungsten strip anode. Its scanning time is about 50 ms, which is fast enough to image the beating heart without significant motion artifacts. The sixth generation CT is emerged due to the requirement for faster scan times, and in particular, for fast multiple scans for three-dimensional imaging. Both third and fourth generation fan-beam geometries achieve this using self-lubricating slip-ring technology to make the electrical connections with rotating components. It can produce one continuous volume set of data for entire region.

From the first generation to the sixth generation, CT pursues higher speed, spatial resolution and density resolution. At present, these three aspects are still goals of CT manufacturers, but beyond that low-dose scanning is the fourth aspect that CT manufacturers pay real attention to, and become the development direction of CT technology. Overall, the trend of X-ray CT now is mainly in low-dose CT, ultra-low-dose CT and spectral CT, to obtain clear positioning and qualitative diagnosis using the least X-ray radiation.

2. Low-dose CT

The application requirements for CT have almost covered all clinical departments, and have been commonly used in medical institutions. However, by the nature of CT scanning, larger radiation doses are involved compared to conventional X-ray imaging procedures, which may lead to adverse health effects. Many literatures show that X-ray radiation will increase radiation-induced cancer risks in adults and particularly in children. The research published in "New England Journal of Medicine" in 2007 shows that 1.5–2% of the tumors may be due to CT radiation. For example, when the effective dose is 10 mSv in an adult abdominal examination, the risk of cancer will increase 1/2000 [2]. And, more remarkable, children are particularly vulnerable to radiation dose damage [3, 4]. There is a growing concern on the significance of minimizing the radiation dose delivered to patients during X-ray CT. It is worth noting that the relative noise in CT images will increase as the radiation dose is decreased. And a tradeoff should be found between radiation dose and imaging quality. At international conferences on radiology in recent years, such as the radiological society of north American (RSNA), the

http://dx.doi.org/10.5772/intechopen.73032

topics of several speakers are related to dose protection. The International Commission on Radiation Protection (ICRP) also recommended that radiation doses should all be kept as low as reasonably achievable (ALARA). This means that radiation dose should be as little as possible on the premise that CT images can meet clinical requirement. "Low-dose" has emerged as one of the important direction of CT development.

Low-dose CT was first proposed by Naidich in 1990 and applied to the lung [5]. Their experiments showed that high-quality lung images could be obtained with less radiation doses. But, due to limitations of hardware and software, the image quality are not completely meet the requirements of clinical diagnosis at that moment. Fortunately, the developments of science and technology laid solid foundations for all kinds of low-dose CT technology, and more and more radiologists and researchers have applied themselves to low-dose CT imaging, for example, CT lung screening [6] and CT cardiac screening [7]. In addition, low-dose scan for children has received more attention [8]. On one hand, CT radiation dose reduction is partly dependent on the hardware optimization. On the other hand, it is related to personalized scan parameters, including the number of scans, the tube current and scanning time in milliampere-seconds (mAs), the tube voltage in the kilovolt peaks (kVp), the size of the patient, the axial scan range, the scan pitch (the degree of overlap between adjacent CT slices) and the specific design of the scanner being used.

For any CT scan, the most direct factors that affect the radiation dose are X-ray intensity and exposure time. The clinically common way to achieve the low-dose scan is to lower milliampere-seconds (mAs) or peak kilovoltage (kVp) setting in the scanning protocol, to reduce the intensity of X-ray. **Figure 1** shows a CT phantom reconstruction at standard dose, while lowering the mAs leads to a lower signal-to-noise ratio (SNR) and the decrease of density resolution due to the introduction of noise and streak artifacts [9], such as in **Figure 2**. Thus, it is difficult to distinguish similar density regions. Lowering the kVp causes a worse penetration, greatly reducing SNR. For example, if the tube voltage drops from 120 to 80 kVp, the tube current must be increased by four times to maintain the same SNR [10]. The differences between the two approaches therefore make them used in different applications, for instance, the way of

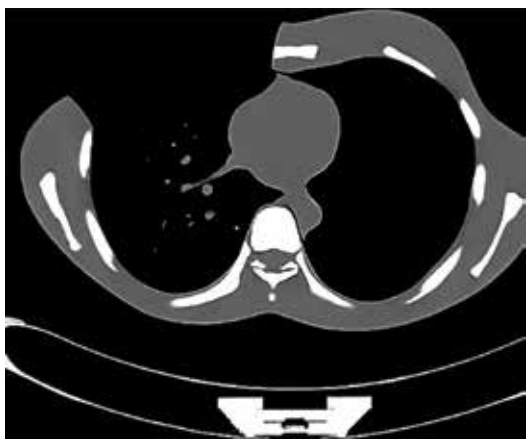

Figure 1. CT phantom reconstruction at standard dose (120 kV, 240 mAs).

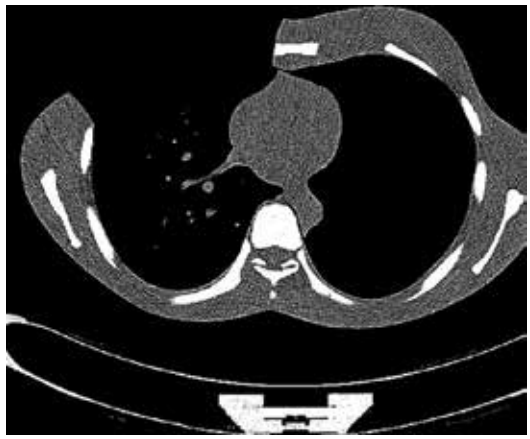

Figure 2. CT phantom reconstruction at low dose (120 kV, 30 mAs).

lowering tube current is often used for lesions with high contrast, such as calcifications, while the way of lowering tube voltage is often used for iodine-based contrast imaging [11].

In order to remove noise and artifacts mentioned above, researchers studied a lot of reconstruction algorithms based on the existing CT equipment, hoping to improve the image quality by designing the appropriate algorithm under the limited hardware conditions. Based on this, many techniques have been proposed to remove noise and artifacts in low-dose CT [12]. They are generally categorized into three major types such as projection restorations, iterative reconstruction (IR) and post-processing methods.

2.1. Projection restorations

Since the advent of the CT system, the analytic reconstruction algorithm, represented by filtered back projection (FBP), is the mainstream algorithm for two-dimensional CT system and the Feldkamp-Davis-Kress (FDK) algorithm is still the first selection of three-dimensional CT system. This is because the analytic algorithms are simple, thus fast and easy to realize. However, in a low-dose scanning, the projections are contaminated with excessive quantum noise, while the analytic algorithms lack effective ability for noise suppression; this makes the reconstructed images from a low-dose scan that are severely degraded with noise and artifacts. In order to solve this problem, some researchers treat the projection data as an image (called sinogram) and suppress excessive quantum noise in it by kinds of methods, making the projection data close to that at standard dose. Thus, reconstructions with suppressed noise and artifacts can be reconstructed from the denoised projections by analytical reconstruction methods. To cope with the excessive quantum noise in projection data, researchers have proposed different techniques to restore noise-corrupted projections. Hsieh modeled the noise in projection data and proposed an adaptive filtering to achieve streak artifact reduction in CT reconstruction [13]. In the study of Elbakri, the detected photon numbers are considered to follow a Poisson distribution plus a background Gaussian noise with zero mean, and then a penalized Poisson likelihood maximization algorithm was then proposed [14, 15]. Li statistically

analyzed the large sample of projection data and considered that noise in the low-dose CT sinogram after logarithm transform and calibration could be modeled as a signal-dependent variable and the sample variance depended on the sample mean by an exponential relationship [16]. Then Wang proposed several penalized weighted least-squares (PWLS) approaches on the noisy sinogram based on this model to adaptively remove non-stationary noise [17–19]. Ma designed a generalized Gibbs prior that exploited nonlocal information of the projection data and used the FBP method to finish the final CT reconstruction [20]. To obtain a more accurate model, Zhang studied the property of the projection data and found an important character that isolated noise points may exist in some areas of the sinogram [21]. Soon he proposed a noise reduction scheme which includes isolated data removal and segmentation-based filtering [22]. Denoising techniques based on wavelet transformation are also applied to projection restorations. Sahiner and Yagle showed how to restore noisy projections in wavelet domain (using wavelet transformation) [23]. Wang proposed wavelet coefficient local adaptive (WCLA) for the noisy sinogram and their method was proved to be effective in removing noise while maintaining the diagnostic image details [24]. Mahmood proposed a graph-based sinogram denoising method, which makes the sinogram as an ideal candidate for graph-based denoising since it generally has a piecewise smooth structure [25]. In addition, many sophisticated denoising techniques are used and improved for projection space denoising, for example, bilateral filtering [26–28], nonlocal means filtering [29, 30] and fuzzy filter [31, 32].

In this category, filtering process and reconstruction process are independent of each other, thus it is well facilitated for system integration. Furthermore, the calculation amount is usually far less than iterative reconstruction and advantages on computing speed is obvious. Projection denoising takes noise properties in projections into account, this makes filters restore the projection data effectively, yet has the potential disadvantage that the definition of edge in projection data is not definite, resulting in sharpness loss in image domain.

2.2. Iterative reconstruction

With rapid advances in computing power and the reduction in costs for that power, all the major CT vendors now offer iterative reconstruction (IR). It benefits from Shepp and Vardi who introduced maximum likelihood expectation maximization (MLEM) into the field of reconstruction [33]. Nowadays iterative reconstruction algorithm has been a hot issue in the field of CT reconstruction with one important reason that IR enables diagnostic image clarity on low-dose scans [34–36]. An IR algorithm first establishes a statistical model of Gaussian or Poisson distribution based on the physical model of the imaging system and statistical characteristics of projection data. Then, the corresponding energy equation is solved in the image space by an iterative algorithm. The reconstructed image quality is better than that reconstructed by the traditional analytic method. Another important algorithm, maximum a posterior (MAP) [37, 38], is very popular and frequently used in IR. MAP is based on Bayesian theory, and introduces the prior information of image space as a penalty term, thus can effectively suppress noise and keep the edge. MAP improves the quality of reconstruction obviously and is far superior to analytical reconstruction algorithms on scattering noise and artifacts elimination, so it is very suitable for low-dose CT reconstruction. How to design an efficient prior is the key point of MAP and has been one of the research hotspots of iterative reconstruction algorithm. The traditional iterative

reconstruction algorithm usually uses the neighborhood correlation of image space to construct a Markov field prior model [39, 40]. In this model, noise suppression is greatly affected by the noise level of projection data, and the constraint ability is declined when the projection data is seriously noisy. While some prior constructed by non-convex potential function may introduce additional staircase artifacts [41]. Bian proposed a total variation minimization low-dose CT reconstruction method based on a divergence constraint, which eliminates the block artifacts of the traditional total variation priors [42]. Chen considered the excellent denoising capability of nonlocal algorithm and proposed an adaptive-weighting nonlocal prior statistical reconstruction approach [43]. The proposed prior imposes an effective resolution-preserving and noise-removing regularization for reconstructions, and specially has a good recovery ability for region of gradated density. Zhang explored an adaptive Markov random field (MRF)-based penalty term which utilizes previous normal-dose scan to obtain the MRF coefficients and incorporated it into the PWLS image reconstruction framework [44]. Li proposed a hybrid nonlocal means regularization model for iterative reconstruction of low-dose CT perfusion to overcome the limitation of the conventional prior-image-induced penalty [45].

However, IR techniques such as algebraic reconstruction technique (ART) always have high computation loads (e.g., up to several hours per data set), which have prevented fast clinical applications. It is urgent to improve the reconstruction speed and researchers have proposed a variety of methods to speed up the convergence rate of IR algorithms, for example, ordered-subsets image reconstructions [46–48]. However, the practical application of IR is still limited by hardware level. Fortunately, the development of parallel computing technology has played an important role in the application of IR. The computation time of IR can be greatly reduced by using the graphics processing units (GPUs) [49–51]. It is worth noting that IR techniques require access to the raw projection data (projection restoration also has this problem) and are highly dependent on special scanner model, that is, requiring more detailed information such as scanning geometry, photon statistics, data-acquisition, correction physics, thus highly dependent on specific scanner models. Its limitation appeals a more broadly used denoising method that can perform on different systems, and leads us to think more about denoising after reconstruction.

2.3. Post-processing method

Image post-processing techniques, working on the image space alone, are retrospectively applied and relatively simple to implement without access to the raw projection data. Since post-processing methods directly enhance the existing CT images, they do not need to improve or replace the existing equipment, thus easy to be used and promoted. The main difficulty comes from the non-stationary mottle noise and streak-like artifacts, which often distribute over the whole CT image. These mottle noise and streak artifacts are caused by the back-projection process within the FBP algorithms, and are difficult to remove because they do not obey to specific distribution models. Various sophisticated techniques, considering the strong structural and statistical properties of objects in image space, have been proposed for improving the quality of low-dose CT images. In [52, 53], the low-dose CT reconstruction images are filtered by nonlinear or anisotropic filters, which can smooth the image effectively meanwhile preserve edges to some extent. But this kind of algorithms is easy to reduce the

image contrast and blur the image edge. Furthermore, since such filters are usually defined in small scale regions, it is impossible to suppress high-frequency noise in projection data, typically with almost no effect on metal artifacts. Wavelet-based method to a certain extent can remedy the defects of small scale spatial filtering, and effectively preserve the texture information while suppressing high-frequency noise [54, 55]. Zhong presented wavelet coefficient magnitude sum (WCMS) and experiments showed that 60% of the noise could be removed [56]. Borsdorf proposed a correlation-based wavelet method for noise reduction in low-dose CT images [57]. Large-scale nonlocal mean filter is another commonly used post-processing algorithm, which carry out the nonlinear filtering correction in the current position by searching the matching information according to the self-similarity of the tissues under various doses in a large scale. This method has good performance in noise elimination and edge preservation. Chen proposed a large-scale nonlocal means (LNLM) filter to improve abdomen low-dose CT images by exploiting large-scale structure similarity knowledge, which was further combined with a multiscale directional diffusion scheme to reduce the streak artifacts in thoracic CT images [58]. Ma proposed a new nonlocal mean algorithm by combining nonlocal mean and the results obtained from previous normal-dose scans to deal with low-dose CT, and the image artifacts are solved in a certain extent by means of image guidance techniques [59]. In [60], feature knowledge in available CT database is incorporated into weight update in LNLM strategy, and a notable image quality enhancement was reported. Dictionary learning and sparse representation were also used for reconstruction and enhancement for low-dose X-ray imaging [61–64]. The dictionary technique studies from normal-dose CT images (feature extraction) guide the low-dose CT image processing. Dictionary technology combines the advantages of large-scale nonlocal filtering and image guidance technology, and has very good extendibility. However, they have the limitation of computation time. Recently, the deep learning technology is popular and shows great potential in image denoising. Chen trained a deep convolutional neural network (CNN) to transform low-dose CT images toward normal-dose CT images, patch by patch and visual and quantitative evaluation demonstrates a competing performance of the proposed method [65]. Wu proposed a cascaded training network for low-dose CT image denoising, where the trained CNN was applied on the training dataset to initiate new trainings and remove artifacts [66]. Wolterink proposed to train a CNN jointly with an adversarial CNN to estimate routine-dose CT images from low-dose CT images and hence reduce noise [67]. Kang applied a CNN to wavelet coefficients of low-dose CT images and showed that wavelet domain CNN was efficient in removing the noises from low-dose CT compared to an image domain CNN [68, 69].

In addition to X-ray intensity, to shorten scanning time can also reduce the radiation dose dramatically, which can be achieved by reducing projection angles (sparse angles or incomplete angles) in acquisition process. Due to the projection, data of CT systems usually have high redundancy, under the condition of less sampling angles, the missing data can be repaired to get a complete projection data set, and the reconstruction quality can be improved using the repaired data. In the decade, dictionary learning and TV (total variance) constraint are two effective techniques to estimate the missing projection data [70–76]. Recently, the convolutional neural network was also performed in sparse-view reconstruction (down to 50 views) on parallel-beam X-ray CT [77].

2.4. ATCM technology

In addition to adjusting scanning parameters, GE, Philips, Siemens and Toshiba introduced automatic tube current modulation (ATCM) to realize low-dose CT scanning. ATCM is based on differences of attenuation characteristics of human anatomy structure, and adjusts the tube current automatically according to the X-ray attenuation change. ATCM controls the tube current by using a certain algorithm and an optimized mode in the X-Y plane or along the scanning direction (Z-axis), thereby radiation doses are reduced in unnecessary projection direction. Another way, ATCM can achieve imaging with the minimum radiation dose by setting the image quality that meets certain criteria in advance. For example, the anteroposterior diameter of the chest and pelvis is significantly smaller than its right-and-left diameter. The anteroposterior tissue is thinner and the X-ray attenuation is lower, while the side is thicker and the X-ray attenuation is higher. Studies have shown that the total radiation dose can be reduced by 29.4% by using the ATCM technique for full-body scan, and the abdominal radiation dose can be reduced by 29.7% [78]. At the annual conference on radiology in North America in 2008, some manufacturers introduced selective shielding techniques that would allow the closure of X-ray when it rotates to the direct irradiation position of sensitive organs, such as eyes, thyroid and breast, thereby to avoid direct exposure to sensitive organs [79]. In addition, an asymmetric shielding acquisition system, called adaptive dose shield (ADS), can shield the invalid X-ray at the beginning and end of the Z-axis scan. Furthermore, it reasonably distributes the irradiation area with a cardiac bowtie. The radiation doses of cardiac scan are therefore reduced without increasing noise.

3. Ultra low-dose CT

In the decades, ultra low-dose CT, defined as a radiation dose ≤1.9 mSv, was studied and used [80, 81]. Accordingly, researchers pay attention to the reconstruction algorithms for high-quality ultra low-dose CT. Yu proposed a previous scan-regularized reconstruction (PSRR) method for ultra low-dose CT of lung perfusion [82]. His study demonstrated that approximately 90% reduction in radiation dose is achievable using PSRR without compromising quantitative computed tomographic measurements of regional lung function. Xu compared the effect of different reconstruction algorithm applications for ultra low-dose CT on image quality improvement using a phantom study [83]. Rob investigated whether ultra low-dose CT and low-dose CT KUB (kidney, ureters and bladder) for acute renal colic impacted upon the specificity, sensitivity and detection of urolithiasis, and found that both ultra low-dose CT and low-dose CT yield comparable results against standard-dose CT KUB in detecting alternative diagnoses (they may not be as effective in detecting stones <3 mm in size or in patients with a body mass index of >30 kg/m^2) [84]. For the foreseeable future, ultra low-dose CT with the tendency of CT development and more commonly used in clinical, especially for several months baby, and pregnant female. In a word, CT technologies have entered into low-dose imaging times.

4. Spectral CT

CT manufacturers have tried their best to improve the hardware for the improvement of reconstructed image quality for low-dose CT. For example, they improved the detection efficiency to

increase the SNR of acquired data and sequentially reduced the noise in CT images. They also designed wide-detector CT to improve time resolution and improved the detector material. One study reported that the wide-detector revolution CTA with 70 Kv tube voltage and prospective ECG-gated technique can provide high accuracy for assessment of congenital heart disease (CHD) in infants and children, which can keep good image quality, with the low radiation dose [85]. More significantly, it is the appearance of spectral CT, which can achieve high time resolution and high intensity resolution.

Advances in multi-detector technology, photon counting energy dispersive detectors and computer-processing technology have made spectral CT imaging possible [86–94]. Spectral CT can convert the X-ray absorption coefficient of any material to absorption coefficient of any two base material and achieve the same attenuation effect. On the basis of the improvement of X-ray tubes and X-ray detectors, spectral CT can obtain two images at different levels of energy at the same time and at the same phase to reconstruct high-definition and monochromatic images from 40 to 140 keV and even generate three materials decomposition images, virtual non-contrast images and specific spectrum curve. Thanks to innovations on the tube ball and detectors, spectral CT not only achieves high resolution, high-definition images in the case of low radiation dose, but also uses the spectral imaging technology for the first time. Spectral CT uses different X-ray spectra and certain chemical elements to detect changes in the shape and function of the whole body, and can realize single photon imaging and physical separation, thus fundamentally changes the traditional way of CT imaging based on a single CT value and provides reliable information to diagnose disease earlier and more accurately, showing a great advantage in imaging. As a new method of clinical application, spectral CT can be developed rapidly in the qualitative, quantitative diagnosis and prognosis evaluation of systemic diseases. Nowadays, it is a promising technique with clinical application potential and has become another direction of CT technology. At present, there are two clinical kinds of spectral CT equipment. One takes the rapid kVp switching as the core technique and another is the dual-source CT (DSCT).

The rapid kVp switching technology is first launched by GE, that is, Discovery CT750 HD [95], it has a double energy system but only with a single source, as shown in **Figure 3**. This system is composed of a special X-ray source which can switch kVp in a very short time (0.5 ms) and detectors can detect the high-energy and low-energy photons, thus obtaining two projection data sets. Discovery CT750 HD adopt gemstone as the detector materials (that has more stability than traditional materials), rapid kVp switching and adaptive statistical iterative reconstruction (ASIR) technology, spectral grating imaging technology and so on, makes it has high resolution imaging with low radiation dose. Detectors made of gemstone ensure each image in a whole body scan reconstructed in a low-dose case from hardware. More importantly, ASIR is the key technology to achieve high resolution and low radiation dose at the same time. It can achieve the limit of 0.23 mm spatial resolution around the body, and find small lesions that cannot be found using a conventional CT scan, greatly improve the detection rate of the lesions and the identification of tumorous diseases [96]. Besides an approximate 50% reduction in radiation dose is achieved compare to routine dose.

DSCT is first launched by Siemens, at the moment, there are two clinical, commercially available DSCT scanners: the SOMATOM Definition (the first generation DSCT, launched in 2005) and the SOMATOM Definition Flash (the second generation DSCT, launched in 2019). Each of them contains two X-ray tubes and two detectors which are mounted so that the X-ray

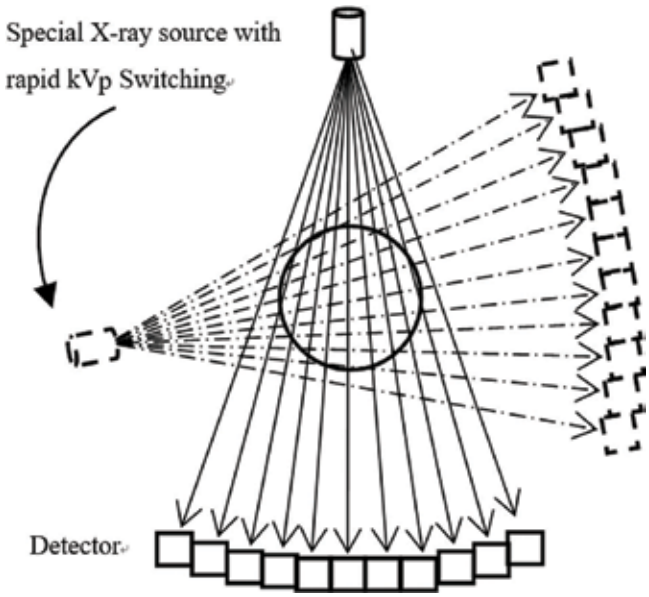

Figure 3. Diagram of discovery CT750 HD system.

beams are approximately perpendicular to each other, as shown in **Figure 4**. DSCT has two working model, that is, single source model and double source model. It works like an ordinary CT when using the single source model, while two acquisition systems work simultaneously when using the double source model. Thus one can obtain two independent sets of images, mainly used for separation of bones and calcification, tissue and collagen component,

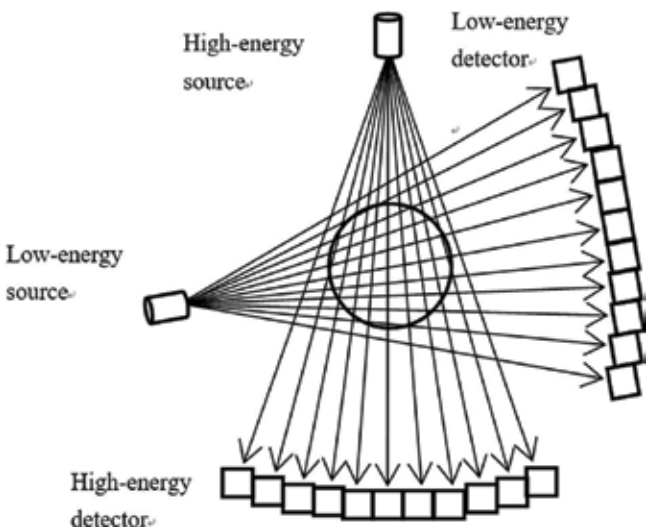

Figure 4. Diagram of DSCT system.

etc., or one set of fusion image reconstruction, mainly used for high time resolution requirements such as the cardiac workup. DSCT has advantages on time resolution, only 83 ms in SOMATOM Definition and 75 ms in SOMATOM Definition Flash, thus lead to a low radiation dose. In a word, DSCT provides faster scanning speed and lower radiation dose, and completely broke the traditional idea of CT technology, leading to a new revolution in CT history.

5. Nano-CT

In addition to technologies mentioned above, CT contrast agents that often used for distinguishing subtle changes of soft tissues with similar densities, also makes, or rather, requires a low kVp, that is, low-dose radiation. Studies have shown that a lower kVp can improve the enhancement degree of contrast agent and thus improve the contrast between different tissues [97]. Especially in turn, using this low-dose CT, one can obtain good images with a low contrast agent dose, because contrast agent is harmful to human health. For example, often used contrast agent in angiography imaging, iodinated compounds, have relatively short circulation times in vivo and its rapid renal clearance may lead to serious adverse effects. Therefore, a variety of CT contrast agents are required to be developed.

A long-sought-after CT contrast agent is the nanoparticle, which has tunable composition, shape and size, and can be readily attached to bioconjugates with interesting biofunctionalities on their surface [98, 99]. Nano-sized iodinated CT contrast agents have been developed that can increase the circulation time and decrease the adverse effects [100]. The classical nanoparticulate iodine-containing contrast agents include liposomal contrast agents, nanosuspensions, nanoemulsions, nanocapsules and polymeric nanoparticles [101]. Despite prolonged in vivo circulation time as compared to iodinated molecules, iodine-conjugated nanoparticles are still limited by iodine loading through surface covalent conjugation [102]. Moreover, iodinated agents cannot be used for those patients who are iodine hypersensitive. These appeals to new CT contrast agents using nanoparticles composed of other elements with higher X-ray attenuation. In 2006, Hainfeld first introduced gold nanoparticles (AuNPs) as CT contrast agent [103], and caused a lot of attention since gold has a higher atomic number than iodine, and thus, has a larger X-ray attenuation. Moreover, the size and shape of gold nanostructures can be easily controlled, and their surface can be modified with various functional groups [102]. Besides, it has good biotolerability and nontoxicity. All of these make AuNPs attract intense interest as CT contrast agents. Over the past few years, many studies on Au nanoparticle design techniques are reported and show good significant CT image enhancement [104–108]. In addition to iodine and gold, other nanoparticles based on heavy atoms such as lanthanides, Bismuth and tantalum Bismuth-based contrast agents, have been used as more efficient CT contrast agents [109, 110].

With the progress of micro-nano processing technology, nano-ray source, micron grade CCD with nanoscale resolution, precise optical focusing imaging device, synchronous radiation source with high brightness, CT is being extended to the nanoscale, that is, nano-CT, bringing us startlingly accurate pictures of objects [111]. Nano-CT is derived from micro-CT but with higher resolution. At present, it has been widely used in many fields such as biology imaging,

pathological examination, integrated circuit testing and so on, and it is believed to have broad application prospects. For example, the phoenix nanotom® m, which is a nanoCT® system, has been used in industry and realized a unique spatial and contrast resolution on a wide sample and application range. Nano-CT also has been developed at the European synchrotron radiation facility (ESRF) to image bone tissue at the nanoscale [112].

6. Summary

In recent years, CT has been developing steadily and the scope of clinical application has been continuously expanded. Now we pay more attention on utility-driven CT instead of algorithm-driven CT. Low-dose CT, ultra low-dose CT and spectral CT are representative directions of CT application, and the rapid development of the hardware provides substantial support. The future development of CT equipment is spectral CT, low-dose CT and even harmless CT. It is believed that with the progress of the ball tube and detector technology, the X-ray dose problem will be completely solved 1 day. The promotion of low-dose CT, combining the enhancement of time resolution, spatial resolution and density resolution, will make CT under the condition of safety and low-dose radiation, achieve more quickly in a clearer image display, making the disease more early and more clearly diagnosed. CT themselves will play an effective role clinical diagnosis and evaluation for more disease in such a high level of display. CT vendors shall stand to win in the fierce market competition if they step up such developments and win praise from the medical community and the whole people.

Acknowledgements

This work has been partially supported by the Shanxi Province Science Foundation for Youths (201601D021080), Research Project Supported by Shanxi Scholarship Council of China (2016-085), National Key Research and Development Program of China (2016YFC0101602) and Science Foundation of North University of China (XJJ2016019).

Author details

Yi Liu

Address all correspondence to: liuyi@nuc.edu.cn

Shanxi Provincial Key Laboratory for Biomedical Imaging and Big Data, North University of China, Taiyuan, China

References

[1] Cierniak R. X-Ray Computed Tomography in Biomedical Engineering. London: Springer; 2011

[2] Brenner DJ, Hall EJ. Computed tomography–An increasing source of radiation exposure. New England Journal of Medicine. 2007;**357**(22):2277-2284. DOI: 10.1056/NEJMra072149

[3] Brenner D, Elliston C, Hall E, Berdon W. Estimated risks of radiation-induced fatal cancer from pediatric CT. AJR American Journal of Roentgenology. 2001;**176**(2):289-296. DOI: 10.2214/ajr.176.2.1760289

[4] Shrimpton PC, Hillier MC, Lewis MA, Dunn M. National survey of doses from CT in the UK: 2003. British Journal of Radiology. 2006;**79**(948):968-980. DOI: 10.1259/bjr/93277434

[5] Naidich DP, Marshall CH, Gribbin C, et al. Low-dose CT of the lungs: Preliminary observations. Radiology. 1990;**175**(3):729-731. DOI: 10.1148/radiology.175.3.2343122

[6] Bach PB, Jett JR, Pastorino U, et al. Computed tomography screening and lung cancer outcomes. JAMA. 2007;**297**(9):953-961. DOI: 10.1001/jama.297.9.953

[7] Hausleiter J, Meyer T, Hermann F, et al. Estimated radiation dose associated with cardiac CT angiography. JAMA. 2009;**301**(5):500-507. DOI: 10.1001/jama.2009.54

[8] Stephen AE, Segev DL, Ryan DP, et al. The diagnosis of acute appendicitis in a pediatric population: To CT or not to CT. Journal of Pediatric Surgery. 2003;**38**(3):367-371. DOI: 10.1053/jpsu.2003.50110

[9] Wang Y, Shao Y, Gui Z, et al. A novel fractional-order differentiation model for low-dose CT image processing. IEEE Access. 2016;**4**(2):8487-8499. DOI: 10.1109/ACCESS.2016.2633272

[10] Nyman U, Ahl TL, Kristiansson M, et al. Patient-circumference-adapted dose regulation in body computed tomography. A practical and flexible formula. Acta Radiologica. 2005;**46**(4):396-406. DOI: 10.1080/02841850510021193

[11] Heneghan JP, Mcguire KA, Leder RA, et al. Helical CT for nephrolithiasis and ureterolithiasis: Comparison of conventional and reduced radiation-dose techniques. Radiology. 2003;**229**(2):575-580. DOI: 10.1148/radiol.2292021261

[12] Liu Y, Castro M, Lederlin M, et al. Edge-preserving denoising for intra-operative cone beam CT in endovascular aneurysm repair. Computerized Medical Imaging and Graphics. 2017;**56**:49-59. DOI: 10.1016/j.compmedimag.2017.01.004

[13] Hsieh J. Adaptive streak artifact reduction in computed tomography resulting from excessive x-ray photon noise. Medical Physics. 1998;**25**(11):2139-2147. DOI: 10.1118/1.598410

[14] Elbakri IA, Fessler JA. Statistical image reconstruction for polyenergetic X-ray computed tomography. IEEE Transactions on Medical Imaging. 2002;**21**(2):89-99. DOI: 10.1109/42.993128

[15] Elbakri IA, Fessler JA. Efficient and accurate likelihood for iterative image reconstruction in x-ray computed tomography. SPIE Medical Imaging. 2003;**5032**:1839-1850. DOI: 10.1117/12.480302

[16] Li T, Li X, Wang J, et al. Nonlinear sinogram smoothing for low-dose X-ray CT. IEEE Transactions on Nuclear Science. 2004;**51**(5):2505-2513. DOI: 10.1109/TNS.2004.834824

[17] Wang J, Li T, Lu H, et al. Penalized weighted least-squares approach to sinogram noise reduction and image reconstruction for low-dose X-ray computed tomography. IEEE Transactions on Medical Imaging. 2006;**25**(10):1272-1283. DOI: 10.1109/TMI.2006.882141

[18] Wang J, Li T, Lu H, et al. Noise reduction for low-dose single-slice helical CT sinograms. IEEE Transactions on Nuclear Science. 2006;**53**(3):1230-1237. DOI: 10.1109/TNS.2006.874955

[19] Wang J, Lu H, Wen J, et al. Multiscale penalized weightedleast-squares sinogram restoration for low-dose X-ray computed tomography. IEEE Transactions on Biomedical Engineering. 2008;**55**(3):1022-1031. DOI: 10.1109/TBME.2007.909531

[20] Ma J, Huang J, Chen Y. Generalized Gibbs prior based high quality low-dose X-CT reconstruction. Computer Engineering and Applications. 2008;**44**(16):4-7

[21] Zhang Y, Zhang J, Lu H. Noise analysis and noise reduction for low-dose CT sinogram. Journal of Optoelectronics Laser. 2010;**21**(7):1073-1107

[22] Zhang Y, Zhang J, Lu H. Statistical sinogram smoothing for low-dose CT with segmentation-based adaptive filtering. IEEE Transactions on Nuclear Science. 2010;**57**(5):2587-2598. DOI: 10.1109/TNS.2010.2060356

[23] Sahiner B, Yagle AE. Image reconstruction from projections under wavelet constraints. IEEE Transactions on Signal Processing. 1993;**41**(12):3579-3584. DOI: 10.1109/78.258101

[24] Wang D, Lu H, Zhang J, et al. Statistically-based wavelet denoising for low-dose CT sinogram. Journal of Image & Graphics. 2008;**13**(5):876-881

[25] Mahmood F, Shahid N, Vandergheynst P, et al. Graph-based sinogram denoising for tomographic reconstructions. In: IEEE Engineering in Medicine and Biology Society (EMBC'16); 16-20 August 2016; Orlando, FL, USA; 2016. DOI: 10.1109/EMBC.2016.7591594

[26] Yu L, Manduca A, Trzasko J D, et al. Sinogram smoothing with bilateral filtering for low-dose CT. In: Society of Photo-Optical Instrumentation Engineers; 18 March; 2008. pp. 69132-9-691329-8. DOI: 10.1117/12.772084

[27] Manduca A, Yu L, Trzasko JD, et al. Projection space denoising with bilateral filtering and CT noise modeling for dose reduction in CT. Medical Physics. 2009;**36**(11):4911-4919. DOI: 10.1118/1.3232004

[28] Zhang P, Zhang Q, Zhang F, et al. Combination of improved diffusion and bilateral filtering for low-dose CT reconstruction. Journal of Computer Applications. 2016;**36**(4):1100-1105. DOI: 10.11772/j.issn.1001-9081.2016.04.1100

[29] Chen Y, Chen W, Yin X, et al. Improving low-dose abdominal CT images by weighted intensity averaging over large-scale neighborhoods. European Journal of Radiology. 2011;**80**(2):42-49. DOI: 10.1016/j.ejrad.2010.07.003

[30] Li Z, Yu L, Trzasko JD, et al. Adaptive nonlocal means filtering based on local noise level for CT denoising. Medical Physics. 2014;**41**(011908). DOI: 10.1118/1.4851635

[31] Gui Z, Liu Y. Noise reduction for low-dose x-ray computed tomography with fuzzy filter. Optik-International Journal for Light and Electron Optics. 2012;**123**:1207-1211. DOI: 10.1016/j.ijleo.2011.07.052

[32] Liu Y, Zhang Q, Gui Z. Noise reduction for low-dose CT sinogram based on fuzzy entropy. Journal of Electronics and Information Technology. 2013;**35**:1421-1427. DOI: 10.3724/SP.J.1146.2012.01283

[33] Shepp LA, Vardi Y, Ra JB, et al. Maximum likelihood PET with real data. IEEE Transactions on Nuclear Science. 1984;**31**(2):910-913

[34] Geyer LL, Schoepf UJ, Meinel FG, et al. State of the art: Iterative CT reconstruction techniques. Radiology. 2015;**276**(2):339-357. DOI: 10.1148/radiol.2015132766

[35] Willemink MJ, de Jong PA, Leiner T, et al. Iterative reconstruction techniques for computed tomography part 1: Technical principles. European Radiology. 2013;**23**(6):1623-1631. DOI: 10.1007/s00330-012-2765-y

[36] Willemink, Martin J, Leiner, et al. Iterative reconstruction techniques for computed tomography part 2: Initial results in dose reduction and image quality. European Radiology. 2013;**23**(6):1632-1642. DOI: 10.1007/s00330-012-2764-z

[37] Sukovic P, Clinthorne NH. Penalized weighted least-squares image reconstruction for dual energy X-ray transmission tomography. IEEE Transactions on Medical Imaging. 2000;**19**:1075-1081. DOI: 10.1109/42.896783

[38] Thibault JB, Sauer KD, Bouman CA, et al. A three-dimensional statistical approach to improved image quality for multislice helical CT. Medical Physics. 2007;**34**:4526-4544. DOI: 10.1118/1.2789499

[39] Liu Y, Gui ZG, Zhang Q. Positron emission tomography image reconstruction algorithm based on an exponential Markov random field prior model. Journal of Clinical Rehabilitative Tissue Engineering Research. 2010;**14**(52):9760-9763. DOI: 10.3969/j.issn.1673-8225.20 10. 52.018

[40] Zhang R, Ye DH, Pal D, et al. A Gaussian mixture MRF for model-based iterative reconstruction with applications to low-dose X-ray CT. IEEE Transactions on Computational Imaging. 2016;**2**(3):359-374. DOI: 10.1109/TCI.2016.2582042

[41] Panin VY, Zeng GL, Gullberg GT. Total variation regulated EM algorithm. In: Nuclear Science Symposium; Toronto; 1999. pp. 1562-1566

[42] Bian Z, Ma J, Tian L, et al. Penalized weighted alpha-divergence approach to sinogram restoration for low-dose X-ray computed tomography. In: Nuclear Science Symposium and Medical Imaging; 2012. pp. 3675-3678

[43] Chen Y, Gao D, Nie C, et al. Bayesian statistical reconstruction for low-dose X-ray computed tomography using an adaptive-weighting nonlocal prior. Computerized Medical Imaging & Graphics the Official Journal of the Computerized Medical Imaging Society. 2009;**33**(7):495-500. DOI: 10.1016/j.compmedimag.2008.12.007

[44] Zhang H, Han H, Wang J, et al. Deriving adaptive MRF coefficients from previous normal-dose CT scan for low-dose image reconstruction via penalized weighted least-squares minimization. Medical Physics. 2014;**41**(4):041916. DOI: 10.1118/1.4869160

[45] Li B, Lyu Q, Ma J, et al. Iterative reconstruction for CT perfusion with a prior-image induced hybrid nonlocal means regularization: Phantom studies. Medical Physics. 2016;**43**(4):1688-1699. DOI: 10.1118/1.4943380

[46] Cho JH, Fessler JA. Accelerating ordered-subsets image reconstruction for x-ray CT using double surrogates. In: SPIE Medical Imaging International Society for Optics and Photonics; Washington; 2012. p. 65

[47] Kim D, Fessler JA. Accelerated ordered-subsets algorithm based on separable quadratic surrogates for regularized image reconstruction in X-ray CT. PRO. 2011;**7906**(1):1134-1137

[48] Wang AS, Stayman JW, Otake Y, et al. Accelerated statistical reconstruction for C-arm cone -beam CT using Nesterov's method. Medical Physics. 2015;**42**(5):2699. DOI: 10.1118 / 1.491 4378

[49] Scherl H, Keck B, Kowarschik M, et al. Fast GPU-based CT reconstruction using the common unified device architecture (CUDA). In: Nuclear Science Symposium Conference Record; Honolulu; 2008. pp. 4464-4466

[50] Tian Z, Jia X, Yuan K, et al. GPU-based low dose CT reconstruction via edge-preserving total variation regularization. Physics in Medicine and Biology. 2011;**56**(18):5949-5967. DOI: 10.1088/0031-9155/56/18/011

[51] Du Y, Yu G, Xiang X, et al. GPU accelerated voxel-driven forward projection for iterative reconstruction of cone-beam CT. Biomedical Engineering Online. 2017;**16**(1):2. DOI: 10.1186/ s12938-016-0293-8

[52] Buades A, Coll B, Morel JM. A review of image denoising algorithms, with a new one. Siam Journal on Multiscale Modeling & Simulation. 2010;**4**(2):490-530. DOI: 10.1137/040616024

[53] Kroon DJ, Slump CH, Maal TJJ. Optimized anisotropic rotational invariant diffusion scheme on cone-beam CT. In: International Conference on Medical Image Computing and Computer-Assisted Intervention; Springer-Verlag; 2010. pp. 221-228

[54] Liu QY. Application of wavelet analysis in denoising seismic data. Applied Mechanics and Materials. 2014;**530-531**:540-543. DOI: 10.4028/www.scientific.net/AMM.530-531.540

[55] Chen GY, Bui TD, Krzyzak A, 2004. Proceedings. IEEE, 2008:ii-917-20 vol.2. Image denoising using neighbouring wavelet coefficients. In: IEEE International Conference on Acoustics, Speech, and Signal Processing; 17-21 May 2004; Montreal, Que., Canada. 2008. pp. ii-917-20. DOI: 10.1109/ICASSP.2004.1326408

[56] Zhong J, Ning R, Conover D. Image denoising based on multiscale singularity detection for cone beam CT breast imaging. IEEE Transactions on Medical Imaging. 2004;**23**(6):696-703. DOI: 10.1109/TMI.2004.826944

[57] Borsdorf A, Raupach R, Flohr T, et al. Wavelet based noise reduction in CT-images using correlation analysis. IEEE Transactions on Medical Imaging. 2008;**27**(12):1685-1703. DOI: 10.1109/TMI.2008.923983

[58] Chen Y, Yang Z, Hu Y, et al. Thoracic low-dose CT image processing using an artifact suppressed large-scale nonlocal means. Physics in Medicine and Biology. 2012;**57**(9):2667. DOI: 10.1088/0031-9155/57/9/2667

[59] Ma J, Huang J, Feng Q, et al. Low-dose computed tomography image restoration using previous normal-dose scan. Medical Physics. 2011;**38**(10):5713-5731. DOI: 10.1118/1.3638125

[60] Xu W, Ha S, Mueller K. Database-assisted low-dose CT image restoration. Medical Physics. 2013;**40**(3):031109

[61] Bai T, Yan H, Shi F, et al. 3D dictionary learning based iterative cone beam CT reconstruction. International Journal of Cancer Therapy & Oncology. 2014;**2**(2):020240. DOI: 10.14319/ijcto.0202.40

[62] Ghadrdan S, Alirezaie J, Dillenseger JL, et al. Low-dose computed tomography image denoising based on joint wavelet and sparse representation. IEEE Engineering in Medicine and Biology Society; Chicago. 2014:3325-3328. DOI: 10.1109/EMBC.2014.6944334

[63] Chen Y, Liu J, Hu Y, et al. Discriminative feature representation: An effective postprocessing solution to low dose CT imaging. Physics in Medicine and Biology. 2017;**62**(6):2103-2131. DOI: 10.1088/1361-6560/aa5c24

[64] Zhang H, Zhang L, Sun Y, et al. Projection domain denoising method based on dictionary learning for low-dose CT image reconstruction. Journal of X-Ray Science and Technology. 2015;**23**(5):567-578. DOI: 10.3233/XST-150509

[65] Chen H, Zhang Y, Zhang W, et al. Low-dose CT denoising via convolutional neural network. Biomedical Optics Express. 2017;**8**(2):679-694. DOI: 10.1364/BOE.8.000679

[66] Wu D, Kim K, Fakhri GE, et al. A cascaded convolutional neural network for X-ray low-dose CT image denoising. Forthcoming. DOI: arXiv:1705.04267v2 [cs.CV]

[67] Wolterink JM, Leiner T, Viergever MA, et al. Generative adversarial networks for noise reduction in low-dose CT. IEEE Transactions on Medical Imaging. 2017;**36**(12):2536-2545. DOI: 10.1109/TMI.2017.2708987

[68] Kang E, Min J, Ye JC. A deep convolutional neural network using directional wavelets for low-dose X-ray CT reconstruction. Medical Physics. 2017;**44**(10):e360-e375. DOI: 10.1002/mp.12344

[69] Kang E, Min J, Ye JC. Wavelet Domain Residual Network (WavResNet) for Low-Dose X-ray CT Reconstruction. Forthcoming. DOI: arXiv:1703.01383v1 [cs.CV]

[70] Sidky EY, Kao CM, Pan X. Accurate image reconstruction from few-views and limited-angle data in divergent-beam CT. Journal of X-Ray Science and Technology. 2006;**14**(2):119-139

[71] Duan X, Zhang L, Xing Y, et al. Few-view projection reconstruction with an iterative reconstruction-reprojection algorithm and TV constraint. IEEE Transactions on Nuclear Science. 2009;**56**(3):1377-1382. DOI: 10.1109/TNS.2008.2009990

[72] Wang L, Li L, Yan B, et al. An algorithm for computed tomography image reconstruction from limited-view projections. Chinese Physics B. 2010;**19**(8):642-647. DOI: 10.1088/1674-1056/19/8/088106

[73] Zhang Y, Zhang WH, Chen H, et al. Few-view image reconstruct-ion combining total variation and a high-order norm. International Journal of Imaging Systems and Technology. 2013;**23**(3):249-255. DOI: 10.1002/ima.22058

[74] Li H, Chen X, Wang Y, et al. Sparse CT reconstruction based on multi-direction anisotropic total variation (MDATV). Biomedical Engineering Online. 2014;**13**(1):92. DOI: 10.1186/1475-925X-13-92

[75] Hu Z, Liu Q, Zhang N, et al. Image reconstruction from few-view CT data by gradient-domain dictionary learning. Journal of X-Ray Science and Technology. 2016;**24**(4):627-638. DOI: 10.3233/XST-160579

[76] Zhang C, Zhang T, Li M, et al. Low-dose CT reconstruction via L1 dictionary learning regularization using iteratively reweighted least-squares. Biomedical Engineering Online. 2016;**15**(1):66. DOI: 10.1186/s12938-016-0193-y

[77] Jin KH, Mccann MT, Froustey E, et al. Deep convolutional neural network for inverse problems in imaging. IEEE Transactions on Image Processing A Publication of the IEEE Signal Processing Society. 2017;**26**(9):4509-4522. DOI: 10.1109/TIP.2017.2713099

[78] Zhang Z. Development and clinical application of low dose computed technology. China Medical Equipment. 2016;**31**(9):87-89. DOI: 10.3969/j.issn.1674-1633.2016.09.022

[79] Zhang W, Xu J, et al. See development of low-dose CT from RSNA 2008. China Medica Device Information. 2009;**15, 7**:12-13. DOI: 10.15971/j.cnki.cmdi.2009.07.010

[80] Jakobs TF, Wintersperger BJ, Herzog P, et al. Ultra-low-dose coronary artery calcium screening using multislice CT with retrospective ECG gating. European Radiology. 2003;**13**(8):1923-1930. DOI: 10.1007/s00330-003-1895-7

[81] Vogt C, Cohnen M, Beck A, et al. Detection of colorectal polyps by multislice CT colonography with ultra-low-dose technique: Comparison with high-resolution videocolonoscopy. Gastrointestinal Endoscopy. 2004;**60**(2):201-209. DOI: 10.1016/S0016-5107(04)01684-0

[82] Yu H, Zhao S, Hoffman EA, et al. Ultra-low dose lung CT perfusion regularized by a previous scan. Academic Radiology. 2009;**16**(3):363-373. DOI: 10.1016/j.acra.2008.09.003

[83] Xu Y, He W, Chen H, et al. Impact of the adaptive statistical iterative reconstruction technique on image quality in ultra-low-dose CT. Clinical Radiology. 2013;**68**(9):902-908. DOI: 10.1016/j.crad.2013.03.024

[84] Rob S, Bryant T, Wilson I, et al. Ultra-low-dose, low-dose, and standard-dose CT of the kidney, ureters, and bladder: Is there a difference? Results from a systematic review of the literature. Clinical Radiology. 2017;**72**(1):11-15. DOI: 10.1016/j.crad.2016.10.005

[85] Zeng F, Xue Y, Liu Y, et al. Wide-detector revolution CT with 70 kV tube voltage and prospective ECG-gated technique in diagnosis of congenital heart disease in infants and children. Chinese Journal of Medical Imaging Technology. 2017;**33**(4):594-598. DOI: 10.13929/j.1003-3289.201611008

[86] Iwanczyk JS, Nygård E, Meirav O, et al. Photon counting energy dispersive detector arrays for x-ray imaging. IEEE Transactions on Nuclear Science. 2009;**56**(3):535-542. DOI: 10.1109/TNS.2009.2013709

[87] Symons R, Cork TE, Sahbaee P, et al. Low-dose lung cancer screening with photon-counting CT: A feasibility study. Physics in Medicine and Biology. 2017;**62**(1):202-213. DOI: 10.1088/1361-6560/62/1/202

[88] Taguchi K. Energy-sensitive photon counting detector-based X-ray computed tomography. Radiological Physics and Technology. 2017;**10**(1):8-22. DOI: 10.1007/s12194-017-0390-9

[89] Gutjahr R, Halaweish AF, Yu Z, et al. Human imaging with photon counting–based computed tomography at clinical dose levels: Contrast-to-noise ratio and cadaver studies. Investigative Radiology. 2016;**51**(7):421-429. DOI: 10.1097/RLI.0000000000000251

[90] Leng S, Gutjahr R, Ferrero A, et al. Ultra-high spatial resolution, multi-energy CT using photon counting detector technology. SPIE Medical Imaging. 2017:101320Y. DOI: 10.1117/12.2255589

[91] Katsuyuki T. Energy-sensitive photon counting detector-based X-ray computed tomography. Radiological Physics and Technology. 2017;**10**(1):8-22. DOI: 10.1007/s12194-017-0390-9

[92] Si-Mohamed S, Bar-Ness D, Sigovan M, et al. Review of an initial experience with an experimental spectral photon-counting computed tomography system. Nuclear Instruments and Methods in Physics Research Section A: Accelerators, Spectrometers, Detectors and Associated Equipment. 2017;**873**:27-35. DOI: 10.1016/j.nima.2017.04.014

[93] Morita H, Oshima T, Kataoka J, et al. Novel photon-counting low-dose computed tomography using a multi-pixel photon counter. Nuclear Instruments and Methods in Physics Research Section A: Accelerators, Spectrometers, Detectors and Associated Equipment. 2017;**857**:58-65. DOI: 10.1016/j.nima.2017.02.015

[94] Piccinelli M, Garcia EV. Advances in single-photon emission computed tomography hardware and software. Cardiology Clinics. 2016;**34**(1):1-11. DOI: 10.1016/j.ccl.2015.06.001

[95] Zhang D, Li X, Liu B. Objective characterization of GE discovery CT750 HD scanner: Gemstone spectral imaging mode. Medical Physics. 2011;**38**(3):1178-1188. DOI: 10.1118/1.3551999

[96] Xiang L. Current situation and development trends of dual energy CT. Science Mosaic. 2016;(9):87-90. DOI: 10.13838/j.cnki.kjgc.2016.09.021

[97] Deng Y, Ouyang Z, Luo J, et al. Clinical application of low-dose contrast agent combined with low-dose radiation CTU in urinary system diseases. Clinical Medicine & Engineering. 2015;**22**(5):532-534. DOI: 10.3969/j.issn.1674-46592015.05.0532

[98] Brannon-Peppas L, Blanchette JO. Nanoparticle and targeted systems for cancer therapy. Advanced Drug Delivery Reviews. 2004;**56**(11):1649-1659. DOI: 10.1016/j.addr.2004.02.014

[99] Park K, Lee S, Kang E, et al. New generation of multifunctional nanoparticles for cancer imaging and therapy. Advanced Functional Materials. 2009;**19**(10):1553-1566. DOI: 10.1002/adfm.200801655

[100] Longmire M, Choyke PL, Kobayashi H. Clearance properties of nano-sized particles and molecules as imaging agents: Considerations and caveats. Nanomedicine. 2008;**3**(5):703-717. DOI: 10.2217/17435889.3.5.703

[101] Lusic H, Grinstaff MW. X-ray-computed tomography contrast agents. Chemical Reviews. 2013;**113**(3):1641-1666. DOI: 10.1021/cr200358s

[102] Liu Y, Ai K, Lu L. Nanoparticulate X-ray computed tomography contrast agents: From design validation to in vivo applications. Accounts of Chemical Research. 2012;**45**(10):1817-1827. DOI: 10.1021/ar300150c

[103] Hainfeld JF, Slatkin DN, Focella TM, Smilowitz HM. Gold nanoparticles: A new X-ray contrast agent. The British Journal of Radiology. 2006;**79**(939):248. DOI: 10.1259/bjr/13169882

[104] Kim D, Park S, Lee JH, et al. Antibiofouling polymer-coated gold nanoparticles as a contrast agent for in vivo X-ray computed tomography imaging. Journal of the American Chemical Society. 2007;**129**(24):7661-7665. DOI: 10.1021/ja071471p

[105] Kojima C, Umeda Y, Ogawa M, et al. X-ray computed tomography contrast agents prepared by seeded growth of gold nanoparticles in PEGylated dendrimer. Nanotechnology. 2010;**21**(24):245104. DOI: 10.1088/0957-4484/21/24/245104

[106] Peng C, Zheng L, Chen Q, et al. PEGylated dendrimer-entrapped gold nanoparticles for in vivo blood pool and tumor imaging by computed tomography. Biomaterials. 2012;**33**(4):1107-1119. DOI: 10.1016/j.biomaterials.2011.10.052

[107] Wang H, Zheng L, Guo R, et al. Dendrimer-entrapped gold nanoparticles as potential CT contrast agents for blood pool imaging. Nanoscale Research Letters. 2012;**7**(1):190. DOI: 10.1186/1556-276X-7-190

[108] Park YS, Kasuya A, Dmytruk A, et al. Concentrated colloids of silica-encapsulated gold nanoparticles: Colloidal stability, cytotoxicity, and X-ray absorption. Journal of Nanoscience and Nanotechnology. 2007;**7**(8):2690-2695. DOI: 10.1166/jnn.2007.601

[109] Rabin O, Perez JM, Grimm J, et al. An X-ray computed tomography imaging agent based on long-circulating bismuth sulphide nanoparticles. Nature Materials. 2006;**5**(2):118-122. DOI: 10.1038/nmat1571

[110] Lee N, Choi SH, Hyeon T. Nano-sized CT contrast agents. Advanced Materials. 2013;**25**(19):2641-2660. DOI: 10.1002/adma.201300081

[111] Li G, Luo SH, Gu N. Research progress of Nano CT imaging. Chinese Science Bulletin. 2013;**58**(7):501-509. DOI: 10.1360/972012-714

[112] Yu B, Weber L, Pacureanu A, et al. Phase retrieval in 3D X-ray magnified phase nano CT: Imaging bone tissue at the nanoscale. In: 2017 IEEE 14th International Symposium on Biomedical Imaging (ISBI 2017); 18-21 April 2017; Melbourne, VIC, Australia; 2017. pp. 56-59. DOI: 10.1109/ISBI.2017.7950467

Chapter 6

Biocompatible Magic Sized Quantum Dots: Luminescent Markers and Probes

Anielle Christine Almeida Silva,
Lucas Ian Veloso Correia,
Marcelo José Barbosa Silva,
Mariana Alves Pereira Zóia,
Fernanda Van Petten Vasconcelos Azevedo,
Jéssica Peixoto Rodrigues, Luiz Ricardo Goulart,
Veridiana de Melo Ávila and Noelio Oliveira Dantas

Additional information is available at the end of the chapter

http://dx.doi.org/10.5772/intechopen.72841

Abstract

Nanoscience and nanobiotechnology have aroused great academic and technological interest. Works relating biomaterials at the nanoscale can reach new biotechnologies and help in the development and use of tools for bioimage and diagnosis applications. In this work we demonstrated the advantages of magic sized quantum dots as luminescent markers and probes to bioimage applications. The visualization of MSQDs bioconjugated with biological probes in cells were performed at periods greater than 2 h, and visualization with no commercial dye would not be possible. Therefore, we demonstrated that theses biocompatible nanocrystals are luminescent markers and probes to diagnosis.

Keywords: nanocrystals, biocompatibility, luminescence, bioconjugation, probes

1. Introduction

Nanotechnology in life sciences has as one of its objectives to diagnose diseases in a precise, fast and effective way, offering improvements to the existing diagnostic methods. In this sense, several nanomaterials have been studied and developed to benefit the biomedical technologies.

One of the nanomaterials with high potential for application in nanomedicine is the quantum dot, which is a semiconductor nanoparticle. This nanoparticle is a promising material for the diagnosis and understanding of cell biology, being used both for image generation and for detection of signals through [1–3].

Measures based on fluorescence have biochemical specificity and high sensitivity. There is considerable interest in the use of quantum dots as inorganic fluorophores because they have significant advantages over conventionally used fluorescent markers. For this, it is necessary that these nanoparticles are biocompatible so that they are conjugated properly to biological molecules, by means of bioconjugation techniques [4–7].

In cell biology it has been a practice to use fluorescent labels such as organic dyes, coordinating compounds of lanthanide ions and recombinant fluorescent proteins [8–12]. Organic fluorophores are used as molecular markers to identify structural compartments, molecules, or organelles. These fluorophores can be linked (conjugated) to the target directly or indirectly through conjugation with antibodies and other molecules that bind secondarily to the target. The fluorophore DAPI (4′6-diamidino-2-phenylindole), for example, has affinity for DNA molecules, and is commonly employed for labeling in cell nuclei.

Although they are widely used in the labeling of cellular structures, tissues and organisms, some limitations of these fluorophores should be considered. An irreversible photochemical reaction common to fluorophores is the photobleaching or photodegradation caused by the photochemical destruction of the fluorophore, causing them to irreversibly lose their fluorescence, either after being excited or after a few minutes, depending on the intensity of the source of excitation [13–15].

In this way, samples stained with such dyes need to be kept in dark environments and the microscopy section needs to be performed quickly, making it difficult to monitor a whole cellular process. In addition to photodegradation, other disadvantages involved in these types of labeling are: high toxicity and cell death using ultraviolet (UV) [16–18]. Fluorescent proteins such as GFP (Green Fluorescent Protein) are apparently non-toxic, but may induce undesired cellular processes, and it is a laborious technique.

Due to the disadvantages in the use of conventional fluorophores, several researches have been directed towards the development and reproducibility in the synthesis of nanocrystals for use in bio detection and bioimaging [19–21]. In particular, quantum dots (QDs) have been extensively studied because they exhibit high absorption and the absorption and emission spectra are easily controlled as a function of size, shape and crystalline phase [15, 19, 22], this enables tuning of the emission length as well as high efficiency. Like this, multicolored images can be obtained with the same material when it has different diameters [19, 21, 23, 24].

Unlike most conventional dyes which have a narrow absorption spectrum, the QDs have the additional advantage that a single laser can excite luminescence at different wavelengths while each organic dye must be excited over a long length of single wave and well defined [25–29].

The studies and applications of QDs reveal their efficacy as new luminescent probes for diagnostic purposes, enabling real-time acquisition of a single cell surface receptor, as well as the development of non-invasive models for the detection of small tumors [30]. Another highlight is the application of the QDs in living cells and tissues. Depending on the binder attached to

the quantum dots, they can be injected into cells by the micro injection technique. Once inside the cells, the QDs biochemical reaction [27, 31–33].

Recently, it has been shown that the magic-sized quantum dots (MSQDs) present great advantages in the medical and biological area. These MSQDs are quantum dots with extremely small sizes (<2 nm) and physical properties that are completely different from those presented by QDs [34, 35]. These MSQDs present thermodynamically stable structures, wide luminescence range, great size stability over time, relatively narrow absorption spectra, and heterogenic growth [36, 37]. The term magic size is related to a (magic) number of atoms in the structure that makes MSQDs extremely stable. The wide luminescence spectrum occurs because MSQDs have internal atomic defects [38].

The MSQDs can be important tools in the investigation of metastases and have been proposed as vehicles for administering drugs that can initiate certain photoactivated chemical reactions due to highly stable luminescence over time [39]. The cultures of cells marked with MSQDs continue to maintain their functions, remaining viable for analysis for prolonged periods of time [39–42].

In this chapter we highlight the advantages of MSQDs as a biocompatible luminescent marker and its use as a specific probe. In the biological labeling assays, we use CdSe/CdS MSQDs bioconjugated with Pepstatin A, BnSP-6, BthTx-II and a specific BC Fab antibody to allow its tracking within the cell and, in addition, to verify the specificity of this treatment for breast cancer cells.

2. Magic quantum dots luminescent markers and probes

Figure 1a shows the absorption and emission spectra of CdSe/CdSe MSQDs that observed a narrow band around 428 nm and a broad emission spectrum, respectively [41]. This broad emission is characteristics of the MSQDs and that is of great applicability in biological processes, enabling their visualization in different detection channels, varying from blue to red (**Figure 1a**) [43]. Using the three detection filters, the fluorescence images of the MSQDs in the cells were recorded (**Figure 1b–d**) [39–41].

One of the major problems of organic fluorophores besides cytotoxicity is the duration of luminescence, making it impossible to trace and observe biological assays as a function of time. Quantum dots present high intensity of luminescence compared to dyes and a monitoring time greater than 2 h, but after this time is observed a drastic decrease of luminescence intensity, that difficult of monitoring. This occurs because QDs interact with cellular proteins and decrease the luminescence intensity over time [17]. However, the high stability of MSQDS allows the highly stable luminescence, even after 36 h, (**Figure 2**) [39].

The fluorescence images of the CdSe MSQDs in HeLa cells after (a) 24 h and (b) 36 h are shown in **Figure 2**. It is verified that even after 36 h it is possible to visualize the luminescence of MSQDs. In **Figure 2(c)** it is shown that the observed luminescence is due to a set of MSQDs and that they were constructed with the CdSe core, a thin layer of CdS and functionalized with hydroxyl groups. These results show that the MSQDs can be used as biocompatible luminescent markers [39].

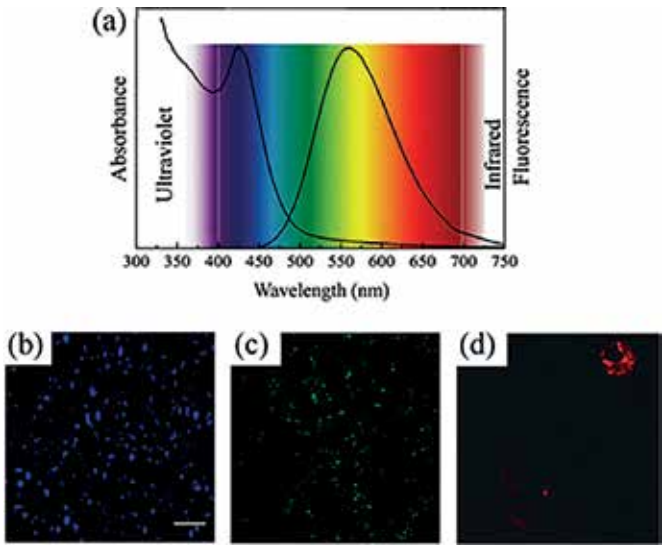

Figure 1. (a) Absorption and fluorescence spectra of CdSe/CdS MSQDs, (b)–(d) fluorescence images of MSQDS in cells using the blue, green and red detection filters, respectively [39–41].

Therefore, the photostable MSQDs allow researchers to investigate the distinct cellular process, in the form of experiments with phagocytosis and vesicles intracellular traffic [44]. Regarding in vivo experiments, stable luminescence MSQDs could be used for tumor cells migration since the monitoring could be done for days.

It is crucial the high biocompatibility of MSQDs, in other words, they cannot be harmful to the cells. It is well known that MSQDs have cadmium ions (Cd^{2+}) adsorbed in their superficies. The manipulation of the composition and diameter of core and shell of MSQDs reduce the cellular contact with Cd^{2+}. In this scenario, Cd^{2+} could stimulate various noxious effects as apoptosis, necrosis and DNA damage by the induction of reactive oxygen species production. Such effects extremely change the biology of the cells. For example, in an experiment with phagocytosis and intracellular traffic, apoptotic cells present a deficient phagocytose process which can infer misunderstand able results [39].

To investigate the true cause of the cytotoxic effect of cadmium chalcogenides QDs, we synthesized CdSe MSQDs with different amounts of Cd^{2+} adsorbed on their surface and have shown that this quantity is directly related to cytotoxicity (**Figure 3 a,b**). The biocompatibility is increased with decrease of Cd^{2+} adsorbed on MSQDs surface (**Figure 3b**). In addition, the decrease of Cd^{2+} is confirmed by the lower expression of the protein (**Figure 3c**). Thus, based on this, we developed new synthesis methodologies to develop a CdS shell using the Cd^{2+} adsorbed [45, 46]. Thus, we have shown in our recent studies that this shell increases biocompatibility and has no immunological effects [41].

Figure 4 shows fluorescence images of CdSe/CdSe MSQDs alone and bioconjugated Pepstatin A, BnSP-6, BthTx-II and a specific BC Fab antibody in the MDA-MB-23.1 [40, 41]. The fluorescence from MSQDs bioconjugated was detected inside the cells' nuclei compartment of MDA-MB-231. Notably, we verified that the MSQDs alone were not internalized in MDA-MB-231 (**Figure 4a**) [40].

http://dx.doi.org/10.5772/intechopen.72841

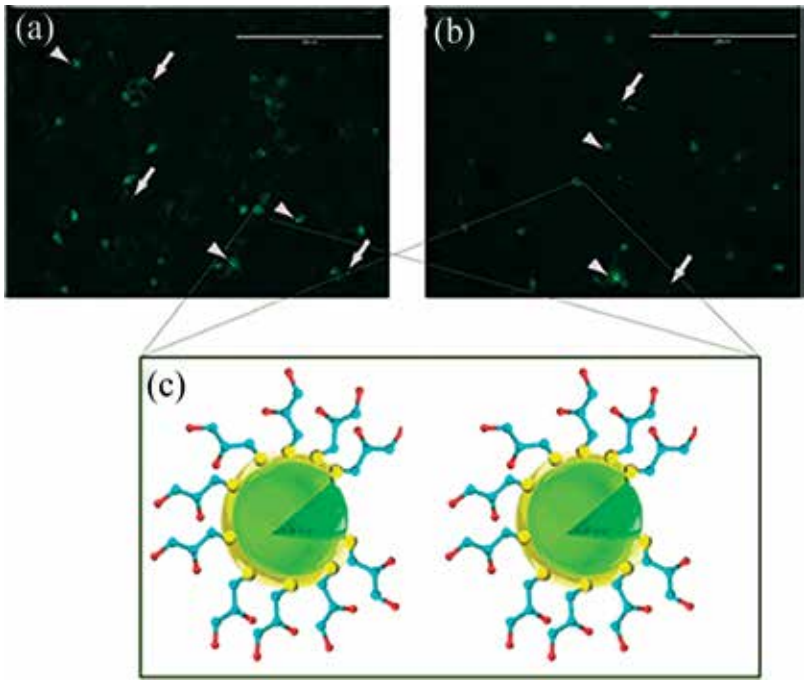

Figure 2. Fluorescent image of incubation with 0.05 M of MSQDs (a) after 24 h and (b) after 36 h. White arrow indicates MSQDs interacted to cellular membrane. Arrows head indicates MSQDs inside the cells. Scale bar = 200 μm. (c) Representation of a set of MSQDs [39].

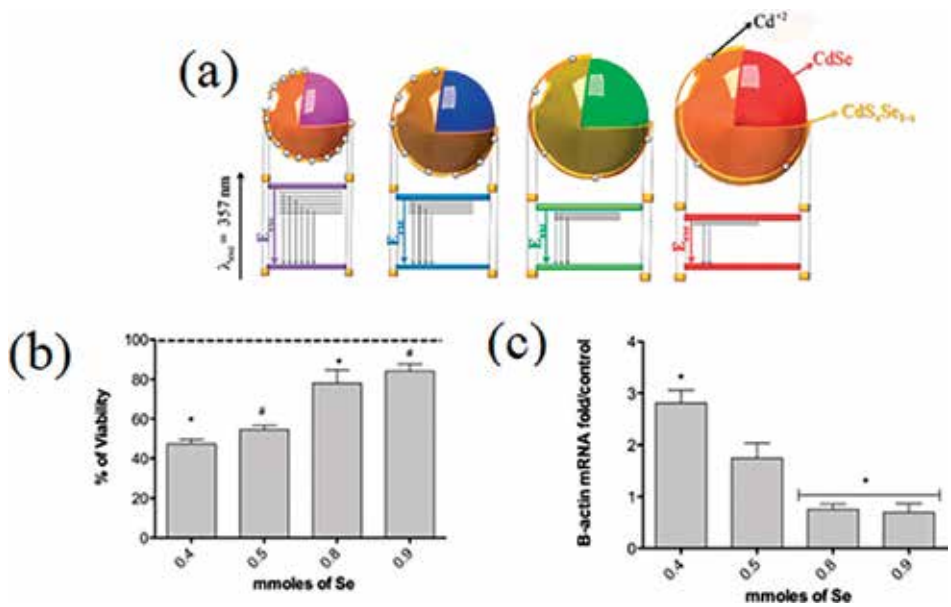

Figure 3. (a) Representation of CdSe MSQDs with different amounts of Cd^{2+} adsorbed on their surface, (b) Viability in function of diminution of Cd^{2+} and (c) B-action mRNA fold/control in function of diminution of Cd^{2+} (increase of Se).

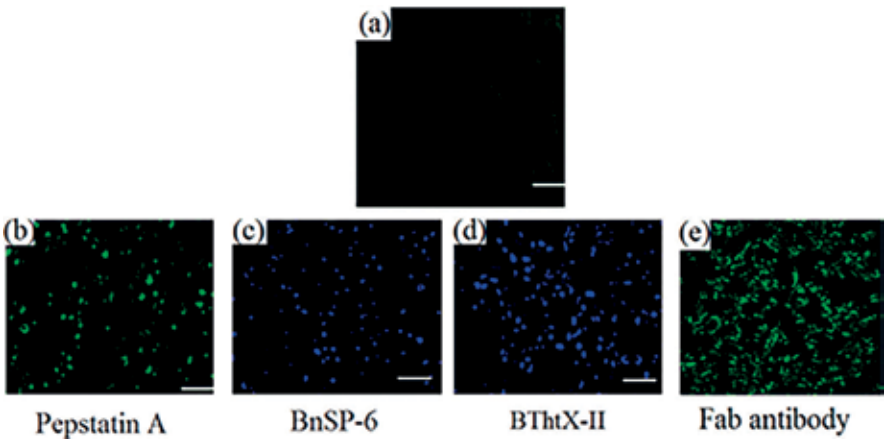

Figure 4. Fluorescence images of (a) CdSe/CdSe MSQDs, bioconjugated (b) Pepstatin in 6 h after treatment, (c) BnSP-6 in 3 h after treatment, (d) BthTx-II in 3 h after treatment and (e) a specific BC Fab antibody in the MDA-MB-23.1 [40, 41].

This result confirms the bioconjugation of the MSQDs with biological probes and in addition, all the assays were performed at periods greater than 2 h, and visualization with no commercial dye would not be possible. Therefore, the group presents experience in the development of new biocompatible luminescent markers specific to each type of treatment.

Author details

Anielle Christine Almeida Silva[1]*, Lucas Ian Veloso Correia[2], Marcelo José Barbosa Silva[3], Mariana Alves Pereira Zóia[4], Fernanda Van Petten Vasconcelos Azevedo[2], Jéssica Peixoto Rodrigues[4], Luiz Ricardo Goulart[4], Veridiana de Melo Ávila[2] and Noelio Oliveira Dantas[1]

*Address all correspondence to: aniellechristineas@gmail.com

1 Laboratory of New Insulation and Semiconductor Materials, Institute of Physics, Federal University of Uberlândia, Brazil

2 Laboratory of Biochemistry and Animal Toxins, Institute of Genetics and Biochemistry, Federal University of Uberlândia, Brazil

3 Laboratory of Immunoparasitology, Institute of Biomedical Sciences, Federal University of Uberlândia, Brazil

4 Laboratory of Nanobiotechnology, Institute of Genetics and Biochemistry, Federal University of Uberlândia, Brazil

References

[1] Du W, Liao L, Yang L, Qin A, Liang A. Aqueous synthesis of functionalized copper sulfide quantum dots as near-infrared luminescent probes for detection of Hg^{2+}, Ag^{+} and Au^{3+}. Scientific Reports. 2017;**7**(1):11451

[2] Liu J, Lv G, Gu W, Li Z, Tang A, Mei L. A novel luminescence probe based on layered double hydroxides loaded with quantum dots for simultaneous detection of heavy metal ions in water. Journal of Materials Chemistry C. 2017;**5**(20):5024-5030

[3] Ren D, Wang B, Hu C, You Z. Quantum dot probes for cellular analysis. Analytical Methods. 2017;**9**(18):2621-2632

[4] Yukawa H, Baba Y. *In vivo* fluorescence imaging and the diagnosis of stem cells using quantum dots for regenerative medicine. Analytical Chemistry. 2017;**89**(5):2671-2681

[5] Kim J, Biondi MJ, Feld JJ, Chan WCW. Clinical validation of quantum dot barcode diagnostic technology. ACS Nano. 2016;**10**(4):4742-4753

[6] Zhou S, Huo D, Hou C, Yang M, Fa H. Hyaluronan functionalizing QDs as turn-on fluorescent probe for targeted recognition CD44 receptor. Journal of Nanoparticle Research, 2017;**19**(9):319

[7] Tsuboi S, Sasaki A, Sakata T, Yasuda H, Jin T. Immunoglobulin binding (B1) domain mediated antibody conjugation to quantum dots for in vitro and in vivo molecular imaging. Chemical Communications, 2017;**9450**(53):9450-9453

[8] Liu J-J, Chang Q, Bao M-M, Yuan B, Yang K, Ma Y-Q. Silicon quantum dots delivered phthalocyanine for fluorescence guided photodynamic therapy of tumor. Chinese Physics B, 2017;**26**(9):98102

[9] Lv Y, Wu R, Feng K, Li J, Mao Q, Yuan H, Shen H, Chai X, Li LS. Highly sensitive and accurate detection of C-reactive protein by CdSe/ZnS quantum dot-based fluorescence-linked immunosorbent assay. Journal of Nanobiotechnology. 2017;**15**(1):35

[10] Jiang P, Zhu CN, Zhang ZL, Tian ZQ, Pang DW. Water-soluble Ag_2S quantum dots for near-infrared fluorescence imaging in vivo. Biomaterials. 2012;**33**:5130-5135

[11] Zhao P, Xu Q, Tao J, Jin Z, Pan Y, Yu C, Yu Z. Near infrared quantum dots in biomedical applications: Current status and future perspective. Wiley Interdisciplinary Reviews. Nanomedicine and Nanobiotechnology. 2017;1-16

[12] Zhu Z-J, Yeh Y-C, Tang R, Yan B, Tamayo J, Vachet RW, Rotello VM. Stability of quantum dots in live cells. Nature Chemistry. 2011;**3**(12):963-968

[13] Zhou J, Yang Y, Zhang CY. Toward biocompatible semiconductor quantum dots: From biosynthesis and bioconjugation to biomedical application. Chemical Reviews. 2015;**115**(21):11669-11717

[14] Pelaz B, Alexiou C, Alvarez-Puebla RA, Alves F, Andrews AM, Ashraf S, Balogh LP, Ballerini L, Bestetti A, Brendel C, Bosi S, Carril M, Chan WCW, Chen C, Chen X, Chen X, Cheng Z, Cui D, Du J, Dullin C, Escudero A, Feliu N, Gao M, George M, Gogotsi Y, Grünweller A, Gu Z, Halas NJ, Hampp N, Hartmann RK, Hersam MC, Hunziker P, Jian J, Jiang X, Jungebluth P, Kadhiresan P, Kataoka K, Khademhosseini A, Kopeček J, Kotov NA, Krug HF, Lee DS, Lehr CM, Leong KW, Liang XJ, Ling Lim M, Liz-Marzán LM, Ma X, Macchiarini P, Meng H, Möhwald H, Mulvaney P, Nel AE, Nie S, Nordlander P, Okano T, Oliveira J, Park TH, Penner RM, Prato M, Puntes V, RotelloVM, Samarakoon A, Schaak RE, Shen Y, Sjöqvist S, Skirtach AG, Soliman MG, Stevens MM, Sung HW, Tang BZ, Tietze R, Udugama BN, VanEpps JS, Weil T, Weiss PS, Willner I, Wu Y, Yang L, Yue Z, Zhang Q, Zhang Q, Zhang XE, Zhao Y, Zhou X, Parak WJ. Diverse applications of nanomedicine. ACS Nano. 2017;**11**(3):2313-2381

[15] Wegner KD, Hildebrandt N. Quantum dots: Bright and versatile in vitro and in vivo fluorescence imaging biosensors. Chemical Society Reviews. 2015;**44**(14):4792-4834

[16] Panchuk-Voloshina N, Haugland R, Bishop-Stewart J, Bhalgat M, Millard P, Mao F, Leung W, Haugland R. Alexa dyes, a series of new fluorescent dyes that yield exceptionally bright, photostable conjugates. Journal of Histochemistry and Cytochemistry. 1999;**47**:1179-1188

[17] Resch-Genger U, Grabolle M, Cavaliere-Jaricot S, Nitschke R, Nann T. Quantum dots versus organic dyes as fluorescent labels. Nature Methods. 2008;**5**:763-75

[18] Akinfieva O, Nabiev I, Sukhanova A. New directions in quantum dot-based cytometry detection of cancer serum markers and tumor cells. Critical Reviews in Oncology/ Hematology. 2013;**86**(1):1-14

[19] Bera D, Qian L, Tseng TK, Holloway PH. Quantum dots and their multimodal applications: A review. Materials (Basel). 2010;**3**(4):2260-2345

[20] Biju V, Mundayoor S, Omkumar RV, Anas A, Ishikawa M. Bioconjugated quantum dots for cancer research: Present status, prospects and remaining issues. Biotechnology Advances. 2010;**28**(2):199-213

[21] Matea CT, Mocan T. Quantum dots in imaging , drug delivery and sensor applications. International Journal of Nanomedicine. 2017;**12**:5421-5431

[22] McBride JR, Dukes AD, Schreuder MA, Rosenthal SJ. On ultrasmall nanocrystals. Chemical Physics Letters. 2010;**498**(1-3):1-9

[23] Xing Y, Rao J. Quantum dot bioconjugates for in vitro diagnostics & in vivo imaging. Cancer Biomarkers. 2008;**4**(6):307-319

[24] Petryayeva E, Algar WR, Medintz IL. Quantum dots in bioanalysis: A review of applications across various platforms for fluorescence spectroscopy and imaging. Applied Spectroscopy. 2013;**67**(3):215-252

[25] Alivisatos AP. Semiconductor clusters, quantum nanocrystals, quantum dots. Science (80-.). 1996;**271**(5251):933-937

[26] Sagar D, Cooney R, Sewall S, Dias E, Barsan M, Butler I, Kambhampati P. Size dependent, state-resolved studies of exciton-phonon couplings in strongly confined semiconductor quantum dots. Physical Review B. 2008;**77**(23):235321

[27] Sukhanova A, Nabiev I. Fluorescent nanocrystal quantum dots as medical diagnostic tools. Expert Opinion on Medical Diagnostics. 2008;**2**(4)

[28] Deerinck TJ. The application of fluorescent quantum dots to confocal, multiphoton, and electron microscopic imaging. Toxicologic Pathology. 2008;**36**(1):112-116

[29] Banyai L, Koch SW. Semiconductor Quantum Dots. Singapore: World Scientific; 1993

[30] Goldman ER, Balighian ED, Mattoussi H, Kuno MK, Mauro JM, Tran PT, Andersont GP. Avidin: A natural bridge for quantum dot-antibody conjugates. Journal of the American Chemical Society. 2002;**124**(22):6378-6382

[31] Alivisatos AP, Gu W, Larabell C. Quantum dots as cellular probes. Annual Review of Biomedical Engineering. 2005;**7**(1):55-76

[32] Revon LB, Chiang H-J, Huang Y-W, Chan M-H, Chen H-H, Lee H-J. Cellular internalization of quantum dots mediated by cell-penetrating peptides. Pharmaceutical Nanotechnology. 2013;**1**(2):151-161

[33] Parak WJ, Gerion D, Pellegrino T, Zanchet D, Micheel C, Williams SC, Boudreau R, Le Gros MA, Larabell CA, Alivisatos AP. Biological applications of colloidal nanocrystals. Nanotechnology. 2003;**14**:R15-R27

[34] Bowers MJ, McBride JR, Rosenthal SJ. White-light emission from magic-sized cadmium selenide nanocrystals. Journal of the American Chemical Society. 2005;**127**(44):15378-15379

[35] Kudera S, Zanella M, Giannini C, Rizzo A, Li Y, Gigli G, Cingolani R, Ciccarella G, Spahl W, Parak WJ, Manna L. Sequential growth of magic-size CdSe nanocrystals. Advanced Materials. 2007;**19**(4):548-552

[36] Dukes AD, McBride JR, Rosenthal SJ. Synthesis of magic-sized CdSe and CdTe nanocrystals with diisooctylphosphinic acid. Chemistry of Materials. 2010;**22**(23):6402-6408

[37] Nguyen KA, Day PN, Pachter R. Understanding structural and optical properties of nanoscale CdSe magic-size quantum dots: Insight from computational prediction. Journal of Physical Chemistry C. 2010;**114**(39):16197-16209

[38] Ouyang J et al. Multiple families of magic-sized CdSe nanocrystals with strong bandgap photoluminescence via noninjection one-pot syntheses. Journal of Physical Chemistry C. 2008;**112**:13805-13811

[39] Silva ACA, de Deus SLV, Silva MJB, Dantas NO. Highly stable luminescence of CdSe magic-sized quantum dots in HeLa cells. Sensors & Actuators, B: Chemical. 2014;**191**:108-114

[40] Silva ACA, Azevedo FVPV, Zóia MAP, Rodrigues JP, Dantas NO, Melo VRÁ, Goulart LR. Magic sized quantum dots as a theranostic tool for breast cancer. In: Recent Studies & Advances in Breast Cancer. Wilmington: Open Access eBooks; 2017. pp. 1-10

[41] Silva ACA, Freschi APP, Rodrigues CM, Matias BF, Maia LP, Goulart LR, Dantas NO. Biological analysis and imaging applications of CdSe/CdSxSe1−x/CdS core-shell magic-sized quantum dot. Nanomedicine: Nanotechnology, Biology, and Medicine. 2016;**12**(5):1421-1430

[42] Silva ACA, Dantas NO, Silva MJB, Spanó MA, Goulart LR. Functional nanocrystals: Towards biocompatibility , nontoxicity and biospecificity. In: Advances in Biochemistry & Applications in Medicine. 1st ed. Wilmington: Open Access eBooks; 2017. pp. 1-27

[43] Harrell SM, McBride JR, Rosenthal SJ. Synthesis of ultrasmall and magic-sized CdSe nanocrystals. Chemistry of Materials. 2013;**25**(8):1199-1210

[44] Kosaka N, McCann TE, Mitsunaga M, Choyke PL, Kobayashi H. Real-time optical imaging using quantum dot and related nanocrystals. Nanomedicine (London). 2010;**5**(5):765-776

[45] Silva ACA, Neto ESF, da Silva SW, Morais PC, Dantas NO. Modified phonon confinement model and its application to CdSe/CdS core-shell magic-sized quantum dots synthesized in aqueous solution by a new route. Journal of Physical Chemistry C. 2013;**117**(4):1904-1914

[46] Silva ACA, da Silva SW, Morais PC, Dantas NO. Shell thickness modulation in ultrasmall CdSe/CdSxSe1−x/CdS core/shell quantum dots via 1-thioglycerol. ACS Nano. 2014;**8**(2):1913-1922

Edited by Morteza Sasani Ghamsari

Nano-bioimaging is a real-time observation method for the study of biological processes in subcellular structures and entire cells. This technique aims to interfere as little as possible with life processes using nanoscale materials and probes. In this method, nanoscale photon source is often used for imaging, and 3D structure of the observed specimen is studied in detail without physical interference. Over the last decade, further boost in bioimaging has led to increase the nano-bioimaging impact that includes many improvements in the data analysis method, image processing, and molecular imaging technology. However, to increase the usage of nano-bioimaging, several developments in the field of diagnosis accuracy, photobleaching prevention, and controlling of the fluorescence resonance energy transfer (FRET) must be achieved. The purpose of this book is to provide a perspective on the current status of nano-bioimaging technologies.

Published in London, UK

IntechOpen

ISBN 978-1-83881-453-3